The Hong Kong Polytechnic University
Department of Electrical Engineering

VOLTAGE STABILITY ANALYSIS BASED ON PROBABILITY THEORY

ZHANG Jianfen

A thesis submitted in partial fulfilment of the requirements for the degree of Doctor of Philosophy

May 2009

CERTIFICATE OF ORIGINALITY

I hereby declare that this thesis is my own work and that, to the best of my knowledge and belief, it reproduces no material previously published or written, nor material that has been accepted for the award of any other degree or diploma, expect where due acknowledgement has been made in the text.

_____(Signed)

ZHANG Jianfen (Name of student)

Abstract

In the last decades, several blackouts have occurred due to the voltage instability and led to huge economic losses. Voltage stability becomes an increasingly concerned problem. Many methods have been developed for voltage stability analysis. However, most of the computational tools developed so far are based on predetermined set of severe but credible situations. The essential weakness of such deterministic techniques is that they do not and cannot account for the probabilistic or stochastic nature of system behavior. However, there are uncertainties such as measurement errors, forecast inaccuracy and outages of system elements in power systems. To carry out deterministic voltage stability analysis for every possible or probable combination is impractical because of an extremely large computational requirement.

Therefore, the present research attempts to apply probability theory to study voltage stability problem and to improve the voltage stability of power system considering uncertainties of load forecasts and load parameters. Similar to the prevailed deterministic approaches, voltage stability will be examined via ‘static’ and ‘dynamic’ system behaviors under probabilistic environment. The static voltage stability analysis based on power flow will regard the maximum load point as the critical point, where the Jacobian matrix of power flow equation is singular. The ‘dynamic’ voltage stability analysis based on small disturbance and using eigenvalue

analyses will consider Hopf bifurcation or saddle node bifurcation as critical point, where system state matrix has one or a pair of eigenvalues with zero real part.

In deterministic studies, the degree of voltage stability is often quantified in terms of stability margin, which is the distance between the normal operating point and the critical operating point. Static voltage stability analysis based on power flow is a common tool to assess stability margin index due to its simplicity and fast calculation. Under probabilistic studies, however, system loads are random variables such that the stability margin is also random variable. In the present study, probabilistic power flow technique combined with point of collapse method will be used to obtain probabilistic characteristics of stability margin and nodal voltages at the maximum load points. Maximum entropy will be employed to determine the probabilistic distribution of stability margin according to these probabilistic characteristics.

After static study, voltage instability will be investigated using probabilistic eigenvalue approach by considering the dynamic behaviors of system components. With load assumed to be normal distribution, the characteristics of nodal voltages are obtained through probabilistic power flow. Probabilistic eigenvalues are used to determine probabilistic stability margin, taking into account the random load variations.

The probabilistic studies will then be extended to examine the impact of the load parameter characteristics on voltage stability. With loads represented by exponential recovery load model, and with the assumption that the load parameters are normal distribution, the eigenvalues are also approximated by normal distribution. Expectation and standard deviation of eigenvalues that determine the distribution of eigenvalues are obtained from probabilistic characteristics of load parameters. The distribution of critical eigenvalue is used to determine the stability probability of power system. Effect of uncertainties of load parameters on probabilistic stability margin will be investigated.

In all the above stability studies, probabilistic results will be compared by Monte Carlo approaches, using 10000 deterministic samples for each result, and effectiveness of the proposed techniques (static and eigenvalue) will be demonstrated.

Finally, power system voltage stabilizer (PSVS) is adopted to improve voltage stability of power system considering the random variations of loads. Modal participation factor is used to locate power system voltage stabilizer; instability modal coefficient and probabilistic sensitivity index are employed to determine the input signal of PSVS. Then the Quasi-Newton method will be used to adjust the parameters of PSVS. Subsequently, voltage stability of power system under wide range of operation can be enhanced by the present systematic PSVS design.

Acknowledgements

The work presented in this thesis was carried out under the supervision of Dr. C.T. TSE, Department of Electrical Engineering, the Hong Kong Polytechnic University. The author wishes to expression her sincerest gratitude to her chief supervisor, Dr. C.T. TSE, for his invaluable guidance, advice and encouragement.

The author would like to take this opportunity to acknowledge the co-supervisor Prof. K. W. WANG of Department of Electrical Engineering, Zhengzhou University, for his academic advice and kind help.

The author is also grateful to Dr. Zhen WANG for many academic discussions and helps.

The financial support provided by the Research Grants Council of Hong Kong under project PolyU 5212/03E and the Research Committee of the Hong Kong Polytechnic University through the award of scholarships is also appreciated. The helpful assistance from the Research Office is appreciated.

Finally but not the least, the author would like to thank all members of her family for their support and encouragement, especially thank her husband Dr. Xinzheng ZHANG. He has contributed more to this thesis than he can imagine.

Table of Contents

Chapter 1 Introduction **1**

1.1 What is voltage stability 1

1.2 Literature review 4

1.2.1 Voltage instability mechanism 4

1.2.2 Voltage stability analysis 5

1.2.3 Probabilistic analysis in voltage stability analysis 17

1.2.4 Probabilistic eigenvalue used in power system dynamic stability studies 19

1.3 Motivation of this research work 20

1.4 Outline of the thesis 23

1.5 Publications 24

Chapter 2 Voltage stability analysis based on probabilistic power flow and maximum entropy **27**

2.1 Introduction 27

2.2 The foundation of probability theory 31

2.2.1 Numerical attributes of random variables 31

2.2.2 Normal distribution 33

2.3 Point of collapse method for voltage stability analysis 34

2.4 Stability margin assessment by probabilistic approach 35

2.4.1 $\boldsymbol{B} = \overline{\boldsymbol{S}_0}$ 36

2.4.2 $\boldsymbol{B} = \boldsymbol{S}_0$ 39

2.5 The maximum entropy method 41

2.6 Applications of probabilistic approach and maximum entropy 44

2.6.1 Case study on 39-bus system 45

2.6.2 Case study on 57-bus system 51

2.7 Summary 55

Chapter 3 Determination of probabilistic stability margin considering the uncertainty of loads **57**

3.1 Introduction 57

3.2 Probabilistic power flow calculation 58

3.3 Plug-in modeling technique 60
3.3.1 Multimachine system representation technique 61
3.3.2 State space equation 63
3.4 Eigenvalue sensitivities 65
3.4.1 General formulas of eigenvalue sensitivities 65
3.4.2 Derivatives of matrix $\boldsymbol{A}$ with regard to zero order block parameters 66
3.4.3 Derivatives of matrix $\boldsymbol{A}$ with regard to first order block parameters 66
3.5 Probabilistic stability analyses 67
3.5.1 Probabilistic characteristics of eigenvalue 67
3.5.2 Assessment criterion of stability probability 70
3.5.3 Load margin for probabilistic voltage stability 71
3.5.4 Probabilistic load characteristics 73
3.6 Case studies 74
3.6.1 Test system I 74
3.6.2 Test system II 79
3.7 Conclusion 81
Chapter 4 Voltage stability analysis considering the uncertainties of dynamic load parameters 83
4.1 Introduction 83
4.2 Exponential recovery load model 84
4.3 Probabilistic eigenvalue 86
4.4 Determination of probabilistic critical load level 88
4.5 Case studies 88
4.5.1 Test system I 89
4.5.2 Test system II 94
4.5.3 Test system III 96
4.5.4 Observation of results 98
4.6 Conclusion 98
Chapter 5 Probabilistic power system voltage stabilizer design considering uncertainties of loads 101
5.1 Introduction 101

5.2 Probability of stability 103
5.3 Power system voltage stabilizers 104
5.4 Design of PSVS 105
5.4.1 Location of PSVS 105
5.4.2 Selection of PSVS input signal 106
5.4.3 PSVS parameter optimization 109
5.5 Case studies 111
5.5.1 9-bus system 111
5.5.2 39-bus system 115
5.6 Conclusion 119
Chapter 6 Conclusions and future work 121
6.1 Conclusions 121
6.2 Recommended future work 124
Appendix 1 Machine models 127
Appendix 2 Representation of voltage dependent load 129
Appendix 3 Test system data 131
Reference 143

List of Figures

Fig. 1. 1 Classifications of power system stability..... 2
Fig. 2. 1 Interpretations of load margin in the load power space..... 28
Fig. 2. 2 Hyper-cone loading model and its worst conditions 30
Fig. 2. 3 Two cases for load increase direction..... 35
Fig. 2. 4 PDF of exponential distribution..... 44
Fig. 2. 5 39-bus system 45
Fig. 2. 6 Probabilistic distributions of stability margin with different load variance in 39-bus system with $\boldsymbol{B} = \overline{\boldsymbol{S}_0}$ 49
Fig. 2. 7Probabilistic distributions of stability margin with different load variance in 39-bus system with $\boldsymbol{B} = \boldsymbol{S}_0$ 50
Fig. 2. 8 Probabilistic distributions of stability margin with different load variance in 57-bus system with $\boldsymbol{B} = \overline{\boldsymbol{S}_0}$ 53
Fig. 2. 9 Probabilistic distributions of stability margin with different load variance in 57-bus system with $\boldsymbol{B} = \boldsymbol{S}_0$ 54
Fig. 3. 1 Two types of elementary transfer blocks..... 62
Fig. 3. 2 Overall view of PMT connection..... 62
Fig. 3. 3 Probabilistic density function of a critical eigenvalue for σ_L=0.0389μ 73
Fig. 3. 4 Distribution of stability margin of 9-bus system for σ_L=0.0389μ (without reactive limit of generator)..... 73
Fig. 3. 5 9-bus system 75
Fig. 3. 6 Distribution of critical α with load variance σ_L 77
Fig. 3. 7 Distribution of stability margin of 9-bus system for σ_L=0.0775μ (without reactive limit of generator)..... 77
Fig. 3. 8 39-bus system 79
Fig. 3. 9 Distribution of stability margin of 39-bus system for σ_L=0.0389μ (without reactive limit of generator)..... 80
Fig. 3. 10 Distribution of stability margin of 39-bus system for σ_L=0.0775μ (without reactive limit of generator)..... 81
Fig. 4. 1 Exponential recovery load representation..... 86

Fig. 4. 2 Flowchart to obtain critical load level 89
Fig. 4. 3 Loci of the critical eigenvalues 92
Fig. 4. 4 Distribution of stability margin of 9-bus system for σ_P=0.0389μ 93
Fig. 4. 5 Distribution of stability margin of 9-bus system for σ_P=0.0606μ 94
Fig. 4. 6 14-bus system 95
Fig. 4. 7 Distribution of stability margin of 14-bus system for σ_P=0.0389μ 96
Fig. 4. 8 Distribution of stability margin of 14-bus system for σ_P=0.0775μ 96
Fig. 4. 9 Distribution of stability margin of 39-bus system for σ_P=0.0389μ 97
Fig. 4. 10 Distribution of stability margin of 39-bus system for σ_P=0.0775μ 97
Fig. 5. 1 Distribution of eigenvalue with $\bar{\alpha} = -0.0618$ and $\sigma_\alpha = 0.1131$ 104
Fig. 5. 2 Symbolic representation of the excitation system of a generator including PSVS 105
Fig. 5. 3 Distribution of probabilistic stability margin of 9-bus system without PSVS . 112
Fig. 5. 4 Voltage instability mode coefficient in 9-bus system 113
Fig. 5. 5 PSI corresponding to residue with input signals of nodal voltage of 9-bus system 113
Fig. 5. 6 Distribution of probabilistic stability margin of 9-bus system with optimized PSVS 115
Fig. 5. 7 Distribution of probabilistic stability margin of 39-bus system without PSVS 116
Fig. 5. 8 Voltage instability mode coefficient of 39-bus system 117
Fig. 5. 9 PSI with input signals of nodal voltage of 39-bus system 118
Fig. 5. 10 Distribution of probabilistic stability margin of 39-bus system with optimized PSVS 119
Fig. A1. 1 The GMT/PMT representation of the third-order generator model 127
Fig. A1. 2 The GMT/PMT representation of the fourth-order generator model 128
Fig. A2. 1 Voltage dependant load module 130
Fig. A3. 1 IEEE Type 1 rotating excitation system model adopted for 39-bus sysem ... 133
Fig. A3. 2 Exciter model adopted for 9-bus system 138
Fig. A3. 3 Exciter model adopted for 14-bus system 140
Fig. A3. 4 Turbine governor model adopted for 14-bus system 141

List of Tables

Table 2. 1 Functions and their expectation of random variable 43
Table 2. 2 Stability margin for 39-bus system with $\boldsymbol{B} = \overline{\boldsymbol{S}_0}$ 46
Table 2. 3 Stability margin for 39-bus system with $\boldsymbol{B} = \boldsymbol{S}_0$ 47
Table 2. 4 Stability margin for 57-bus system with $\boldsymbol{B} = \overline{\boldsymbol{S}_0}$ 51
Table 2. 5 Stability margin for 57-bus system with $\boldsymbol{B} = \boldsymbol{S}_0$ 52
Table 3. 1 Probabilistic stability margin with different probability requirement 72
Table 3. 2 Probabilistic stability margin with different load variance σ_L of 9-bus system (without reactive power limit of generator) 77
Table 3. 3 Probabilistic stability margin with different load variance σ_L of 9-bus system (with reactive power limit of generator of Qmax=1) 78
Table 3. 4 Probabilistic stability margin with different load variance σ_L of 39-bus system (without reactive power limit of generator) 80
Table 3. 5 Probabilistic stability margin with different load variance σ_L of 39-bus system (with reactive power limit of generator of Qmax=3) 80
Table 4. 1 Critical eigenvalues at different load levels with σ_P=0.0389μ 91
Table 4. 2 Stability margin with different variances σ_P of load parameters for 9-bus system 93
Table 4. 3 Stability margin with different variances σ_P of load parameters for 14-bus system 95
Table 4. 4 Stability margin with different variances σ_P of load parameters for 39-bus system 97
Table 4. 5 The computational time for I_{SM} of different test systems 98
Table 5. 1 The critical eigenvalue at a critical load level without PSVS 112
Table 5. 2 Probabilistic stability margin of 9-bus system without PSVS 112
Table 5. 3 Voltage stability without and with PSVS 114
Table 5. 4 Probabilistic stability margins with PSVS 114
Table 5. 5 Critical eigenvalues at critical load level without PSVS 115
Table 5. 6 Probabilistic stability margins of 39-bus system without PSVS 116
Table 5. 7 Voltage stability without and with PSVS 118

Table 5. 8 Probabilistic stability margins of 39-bus system with PSVS..... 118
Table A3. 1 Bus data of 39-bus system..... 131
Table A3. 2 Line data for 39-bus system..... 132
Table A3. 3 Detailed model unit data of 39-bus system..... 133
Table A3. 4 Detailed model generator excitation system data of 39-bus system..... 133
Table A3. 5 Bus data of 57-bus system..... 134
Table A3. 6 Line data of 75-bus system..... 135
Table A3. 7 Load-flow results of 9-bus system..... 137
Table A3. 8 Line data of 9-bus system..... 137
Table A3. 9 Generator data of 9-bus system..... 137
Table A3. 10 Exciter data of 9-bus system..... 137
Table A3. 11 Bus data of 14-bus system..... 138
Table A3. 12 Line data of 14-bus system..... 139
Table A3. 13 Generator data of 14-bus system..... 139
Table A3. 14 Exciter data of 14-bus system..... 140
Table A3. 15 Turbine governor data of 14-bus system..... 140

Chapter 1 Introduction

1.1 What is voltage stability

Power system stability has been and continues to be an important problem for secure system operation since 1920s. It is the ability of an electric power system, for a given initial operating condition, to regain a state of operating equilibrium after being subjected to a physical disturbance, with most system variables bounded so that practically the entire system remains intact (Kundur et al., 2004). The classification of power system stability is proposed by IEEE/CIGRE task force (Kundur et al., 2004) shown in Fig. 1.1.

Voltage stability, one category of power system stability, has attracted increasing attention in last decades. It refers to the ability of a power system to maintain steady voltages at all buses in the system after being subjected to a disturbance from a given initial operating condition (Kundur et al., 2004). When voltage instability occurs, voltages at some buses may progressively fall or rise. The main factor causing this problem is the inability of the power system to meet the demand for reactive power (Kundur, 1994). It is essentially a local phenomenon, but its consequences may have a widespread impact. A possible outcome of voltage instability is loss of load in an area, or tripping of transmission lines and other

elements by their protective systems leading to cascading outages (Kundur et al., 2004), which may lead to loss of synchronism of some generators.

The incidents of power systems due to voltage instability or voltage collapse in different countries all over the world have been reported by Taylor (1994) and Ajjarapu (2006). The west region (WECC) of the United States experienced voltage collapse on July 2, 1996. The blackout due to voltage collapse of Chilean power system in May 1997 resulted in a loss of 80% of its loads. Voltage collapse in Athens on July 12, 2004 led to the blackout of the entire Athens and Peloponnese peninsula. These incidents resulted in huge economic losses, life thereat and inconvenience to people. Therefore, voltage stability study has attracted increasing attention of researchers and engineers.

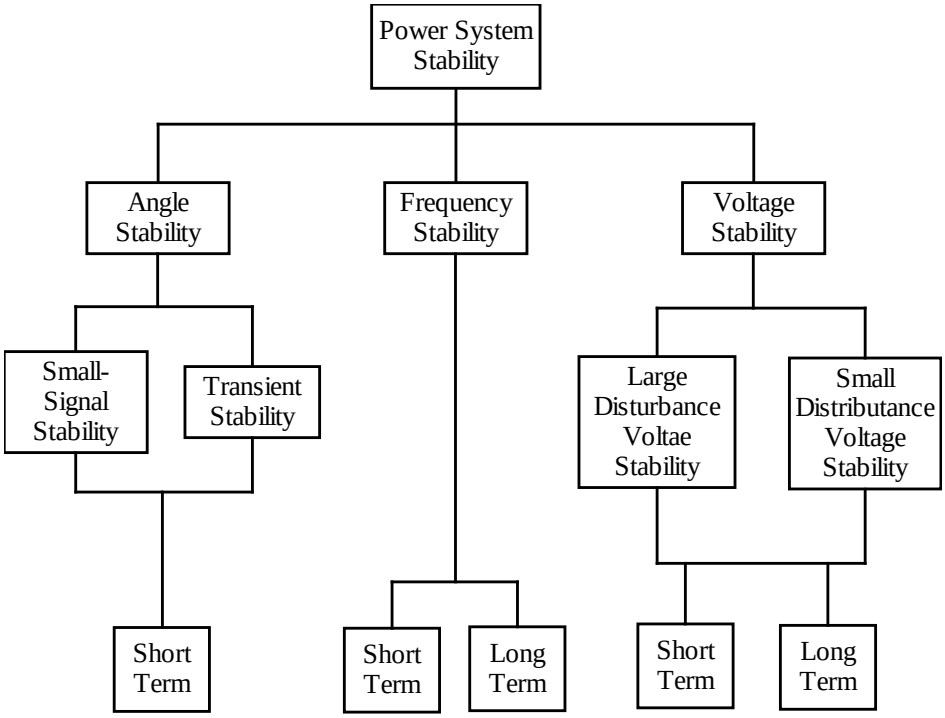

Fig. 1. 1 Classifications of power system stability

For convenience in analysis and for gaining useful insight into the nature of voltage stability problem, IEEE/CIGRE task force classified voltage stability into four categories: large-disturbance voltage stability, small-disturbance voltage stability, short-term voltage stability and long-term voltage stability (Kundur et al., 2004).

Large-disturbance voltage stability refers to the system's ability to maintain steady voltages following large disturbances such as system faults, loss of generation, or circuit contingencies.

Small-disturbance voltage stability refers to the system's ability to maintain steady voltages when subjected to small perturbations such as incremental changes in system load.

Short-term voltage stability involves dynamics of fast acting load components such as induction motors, electronically controlled loads, and HVDC converters. The study period of interest is in the order of several seconds and analysis requires solution of appropriate system differential equations.

Long-term voltage stability involves slower acting equipment such as tap-changing transformers, thermostatically controlled loads, and generator current limiters. The study period of interest may extend to several or many minutes, and long-term simulations are required for analysis of system dynamic performance. Stability is usually determined by the resulting outage of equipment, rather than the severity of the initial disturbance.

1.2 Literature review

There are two aspects in voltage stability analysis: one is voltage instability mechanism analysis, including identifying factors that lead to voltage instability and the weak area and buses that are most susceptible to voltage instability; the other is voltage stability assessment, including estimating whether the power system is voltage stable and calculating the voltage stability margin (Gao, Morison, & Kundur, 1992).

1.2.1 Voltage instability mechanism

Great progress has been made in voltage stability studies. However, in comparison with rotor angle stability theory, the theory of voltage stability is far away from mature. Even the wide agreement on the mechanism of voltage instability has not been reached.

During early period, voltage stability was regarded as static problem. As a result, the existence of the equilibrium points of power system was the major criterion for voltage stability. This voltage collapse mechanism is mainly interpreted by multiple solutions of power flow equations (Tamura, Mori, & Iwamoto, 1983) and the existence of the intersection of system and load curves (Begovic et al., 1995). With the further development of voltage stability studies, the complexity of voltage instability and the effect of dynamic elements of power system have been recognized, such as dynamic characteristic of load, generators, exciter systems, on-load tap changer, reactive compensators and converter of high voltage direct current devices.

Consequently, the dynamic mechanism for voltage collapse draws more attention (Bao, Duan, & He, 2000; Dahlgren, 1994). The restoration characteristic of dynamic load is important research interest.

1.2.2 Voltage stability analysis

Voltage stability is a complex problem. Many methods have been developed. According to the models used, they can be divided into three types: static analysis based on power flow equations, small disturbance analysis based on linearized system differential-algebraic equations, and dynamic time domain simulations based on nonlinear system differential-algebraic equations.

1.2.2.1 Static analysis

Static voltage stability study focuses on the existence of power system equilibrium points. It requires that the disturbance is so small and the evolvement of power system is so slow that the dynamic characteristics can be ignored. It regards power system transmission limit as the stability limit. There are many static analysis methods developed in literature. Most of them are based on the characteristic at the critical point, such as V-Q sensitivity analysis, Q-V modal analysis, singular value decomposition etc, some are based on multi-solutions of load flow equations, and others are originally derived from a two bus network and are extended to complex power system (Kessel & Glavitsch, 1986; Smon, Verbic, & Gubina, 2006; Vu, Begovic, Novosel, & Saha, 1999).

➢ ***V-Q sensitivity analysis*** (Kundur, 1994)

The network constraints may be expressed in the following linearized form (Kundur, 1994):

$$\begin{bmatrix} \Delta \boldsymbol{P\theta} \\ \Delta \boldsymbol{Q} \end{bmatrix} = \begin{bmatrix} \boldsymbol{J}_{P\theta PV} & \boldsymbol{J} \\ \boldsymbol{J}_{Q\theta QV} & \boldsymbol{J} \end{bmatrix} \begin{bmatrix} \Delta \\ \Delta \boldsymbol{V} \end{bmatrix} \tag{1.1}$$

where $\Delta \boldsymbol{P}$ and $\Delta \boldsymbol{Q}$ are incremental changes in bus real power and reactive power injections. $\Delta \boldsymbol{\theta}$ is incremental change in bus voltage angle, and $\Delta \boldsymbol{V}$ is incremental change in bus voltage magnitude.

In order to analyze the incremental relationship between $\boldsymbol{Q}$ and $\boldsymbol{V}$, let $\Delta \boldsymbol{P} = \boldsymbol{0}$, the following equation is given,

$$\Delta \boldsymbol{Q} = \boldsymbol{J}_{\boldsymbol{R}} \Delta \boldsymbol{V} \tag{1.2}$$

where

$$\boldsymbol{J}_{\boldsymbol{R}} = [\boldsymbol{J}_{\theta PQV} - \boldsymbol{J}_{\boldsymbol{Q}} \ \boldsymbol{J}^{-1} \boldsymbol{J} \quad] \tag{1.3}$$

$\boldsymbol{J}_{\boldsymbol{R}}$ is the reduced Jacobian matrix of the system. From equation (1.2), equation (1.4) is given

$$\Delta \boldsymbol{V} = \boldsymbol{J}_{\boldsymbol{R}}^{-1} \Delta \boldsymbol{Q} \tag{1.4}$$

The *i*th diagonal element of the matrix $\boldsymbol{J}_{R}^{-1}$ is the V-Q sensitivity at bus *i*. It represents the change in bus voltage magnitude with respect to the change in reactive power injection at the same bus, and is used as indication of the proximity of the bus to voltage instability. If the V-Q sensitivity for every bus is positive, the system is stable; if the V-Q sensitivity for at least one bus is negative, the system is unstable. Because of the nonlinear nature of the V-Q relationships, the magnitudes

of the sensitivities for different system conditions do not provide a direct measure of the relative degree of stability.

- ***Q-V modal analysis*** (Gao et al., 1992; Kundur, 1994; Morison, Gao, & Kundur, 1993)

The eigenvalues and the eigenvectors of the reduced Jacobian matrix $\boldsymbol{J_R}$ defined in (1.3) can be used to identify voltage stability characteristic of the system. For practical purposes, $\boldsymbol{J_R}$ can be taken as a symmetric matrix and therefore, the eigenvalues of $\boldsymbol{J_R}$ are close to being purely real (Gao et al., 1992) . If all eigenvlues are positive, the system is voltage stable; if at least one eigenvalue is negative, the system is voltage unstable. The magnitude of eigenvalue determines the degree of stability. Although this magnitude of the eigenvalues can provide a relative measure of the proximity to instability, they do not provide an absolute measure due to the nonlinearity of the problem. Participations obtained from right and left eigenvectors corresponding to the smallest eigenvalue can provide the information of concerned variable associated with the critical mode, and can be used to determine weak buses (Gao et al., 1992).

- ***Singular value decomposition***

The Jacobian matrix of power flow equations is singular at the critical point of the power system. The smallest singular value of a matrix is the shortest distance between the matrix and its corresponding singular matrix. If the minimum singular value of Jacobian matrix of power flow equal to zero, then the studied matrix is

singular and no power flow solution can be obtained (Lof, Andersson, & Hill, 1993). Therefore, the minimum singular value of Jacobian matrix of power flow has been used as a static voltage stability index (Hong, Pan, & Lin, 1997; Lof et al., 1993; Lof, Smed, Andersson, & Hill, 1992; Tiranuchit & Thomas, 1988). Fast and highly efficient algorithms to get the minimum singular value of Jacobian matrix of load flow equations have been presented (Hong et al., 1997; Lof et al., 1992). Due to the nonlinear relationship, the minimum singular value cannot supply information for the margin (the distance between the current operating point and the point of voltage collapse).

- ***Continuation power flow***

Continuation power flow can trace the power flow solution curve with respect to a varying parameter in concern. From the solution curve, the voltage collapse point, i.e. the critical point or steady-state voltage stability limit, and stability margin can be obtained. To get these power flow solutions, the iterative calculation starts from a known solution, and the predictor and corrector technique is used to get the subsequent solution at different load levels. As the Jacobian matrix of power flow equations is singular at voltage collapse point, it is difficult to get the solution of power flow near the critical point. The difficulty is overcome by introducing other parameter and equation (Ajjarapu & Christy, 1992; Canizares & Alvarado, 1993; Chiang, Flueck, Shah, & Balu, 1995; Iba, Suzuki, Egawa, & Watanabe, 1991; Li & Chiang, 2008; Mori & Yamada, 2002), which make the power flow Jacobian nonsingular at the voltage collapse point.

Continuation power flow provides a robust numerical solution technique to obtain the voltage stability critical point, and it can take different inequality constrains into account. Nevertheless, this method only obtains an approximate solution other than an exact solution of collapse voltage and it is time-consuming.

- ***Point of collapse method***

A salient characteristic of voltage collapse point is that the Jacobian matrix $\boldsymbol{J}$ of power flow equations is singular, i.e. $\boldsymbol{J}$ has a zero eigenvalue but the corresponding eigenvectors (left and right) are non-zero. Employing this characteristic, point of collapse method have been proposed to obtain the critical point of power system by solving the expanded power flow equations as follow (Canizares & Alvarado, 1993; Chiang & Jean-Jumeau, 1995; Lu, Liu, & Thorp, 1995)

$$\begin{aligned} &\boldsymbol{f}(\boldsymbol{x},\lambda)=\boldsymbol{0} \\ &\boldsymbol{f}_x(x,\lambda)\cdot\boldsymbol{v}=\boldsymbol{0} \text{ (or } \boldsymbol{w}\cdot\boldsymbol{f}_x(\boldsymbol{x},\lambda)=\boldsymbol{0}) \\ &\boldsymbol{v}^T\boldsymbol{v}-1=0 \text{ (}or\ \boldsymbol{w}\boldsymbol{w}^T-1=0\text{)} \end{aligned} \tag{1.5}$$

where $\boldsymbol{v}$ ($\boldsymbol{w}$) is the right (left) eigenvector corresponding to the zero eigenvalue of Jacobian matrix $\boldsymbol{f}_x(\boldsymbol{x},\lambda)$. In general, a set of $2n+1$ nonlinear equations have to be solved when this method is used.

The point of collapse method can obtain the critical points quickly. However, it is restricted by the initial solution. If the initial solution is not appropriate, it may fail to get the critical point. Furthermore, it is difficult for this method to consider reactive power limit of generator and other inequality constrains.

- ***Nonlinear programming technique***

As the critical point corresponds to the maximum load power, the determination of critical point can be expressed as an optimization problem (Obadina & Berg, 1988; Cutsem, 1991; Zarate, Castro, Ramos, & Ramos, 2006). Optimal solution is solved by nonlinear programming technique and the stability margin can be obtained from the optimal solution. Nonlinear programming optimization technique (Ajjarapu, Lau, & Battula, 1994; Hwachang, Byongjun, Sae-Hyuk, & Ajjarapu, 2003; Song, Lee, & Moon, 2005) has been used to enhance the voltage stability margin of power system.

Nonlinear programming technique can calculate the critical point accurately and quickly. It can also take different inequality constrains into account.

- ***Closest critical point***

Voltage stability margin is a useful index for power system planning and operation. Usually, it is assumed that loads increase along a predefined direction until the system's maximum load point is reached. An unexpected load increase at some buses or area may result in smaller voltage stability margin. The closest critical point, which is defined as the point on the loadability boundary having minimum Euclidean distance from an operating point, represents the worst case scenario for a power system. The corresponding load increase direction can provide useful information to operators to take measures against voltage collapse. Different methods (Alvarado, Dobson, & Yi, 1994; Bedoya, Castro, & da Silva, 2008; Dobson, 1992; Dobson & Lu, 1993; Mori & Iizuka, 1998; Nam, Song, Kim, Moon, & Lee,

1999; Yorino, Harada, & Cheng, 1997) have been developed to estimate the closest critical point and the corresponding load increase direction.

- ***Multiple power flow solutions***

Load flow equations are a set of nonlinear equations, and they may have multiple solutions. The multiple solutions have been used to estimate the voltage stability of power system. The relationship between voltage instability and multiple load flow solutions in electrical power system has been examined in the work of Tamura et al (Tamura et al., 1983), which stated that the individual solutions of the solution pair have different features from each other even through they are close to each other. Since a pair of near solutions is indispensable for estimating a critical load condition accurately, a method for finding a pair of multiple load flow solutions in bulk power system has been proposed (Iba, Suzuki, Egawa, & Watanabe, 1990). An efficient algorithm to solve all load flow solutions have been presented (Ma & Thorp, 1993). Tamura, Sakamoto, & Tayama (1988) proposed a voltage instability proximity index based on multiple load flow solutions which can be used for monitoring the system state. Liu, Chang, Jiang, & Yeh (2005) described an algorithm to compute all the type-1 load-flow solutions based on continuation power flow method, which can provide more complete information for voltage stability assessment.

- ***Local method***

In this method, different indicators for voltage collapse are first derived from simple two-bus system (El-Kateb, Abdelkader, & Kandil, 1997; Kessel & Glavitsch, 1986;

Musirin & Rahman, 2002; Smon et al., 2006; Vu et al., 1999), and then these indicators are extended to complex power system. One way that these indices are used to determine the stability of complex system is using the Thevenin's equivalent which is obtained from original power system as seen from the load bus. The other way is to evaluate the index for every line or every load bus in the system. A local method (Vu et al., 1999) is proposed based on the power transfer impedance-matching principle. The measured data are used to obtain the Thevenin's equivalent of the system and the apparent impedance of the load. Voltage collapse occurs when load impedance and the equivalent apparent impedance are equal. The indicator L which varies between 0 (no load of system) and 1 (voltage collapse) is defined to detect voltage instability (Kessel & Glavitsch, 1986). El-Kateb et al.(1997) developed a linear indicator for voltage collapse, and the indicator was extended to a multinode power system. Smon et al. (2006) used the Tellegen's theorem to simplify the determination of the Thevenin's parameters and proposed a new index to determine the voltage-stability margin.

The local methods use the local information to directly evaluate voltage stability. In addition to the benefits of small computation effort and simplicity, local methods also give a good insight into the voltage-collapse process and can easily be used for online system monitoring.

In summary, static voltage analysis techniques are still attractive because its calculation is simple and fast. Furthermore, the static analysis techniques can

provide much insight into the nature of the problem and identify the key contributing factor if appropriately used.

1.2.2.2 Small disturbance analysis

Small disturbance analysis is used to estimate the stability of power system under small perturbation. This method is a rigorous mathematic method and determines whether the system is stable by eigenvalues of state matrix, which is obtained by eliminating algebraic variables of linearized differential-algebraic equations at their equilibrium operating points. If all eigenvalues have negative real parts, the system is asymptotically stable.

This method has been used for voltage stability analysis along the P-V curve (Byongjun & Ajjarapu, 1995; Rajagopalan, Lesieutre, Sauer, & Pai, 1992). With system parameter variations, different bifurcations, such as saddle-node bifurcation, Hopf bifurcation and singularity-induced bifurcation, may occur (Byongjun & Ajjarapu, 1995). The dynamic aspects of operation on a typical P-V curve were examined with a typical system model of machines with voltage regulators, constant impedance and constant power loads (Rajagopalan et al., 1992). Besides generator dynamics and associated control devices, the load dynamics were also taken into account (Byongjun & Ajjarapu, 1995). Small disturbance analysis has been used to analyze structural stability related to bifurcation phenomena and the effect of different load models was investigated (Pai, Sauer, Lesieutre, & Adapa, 1995). Vournas, Pai, & Sauer (1996) studied the relationship between types of bifurcation in power systems and their expected occurrence for voltage regulated and

unregulated synchronous machines on a single machine infinite bus system. Zeng, Berizzi, & Marannino (1997) used small-signal voltage stability analysis to study the influence of the various model parameters on the voltage stability limits. Su, Cheng, Wen, & Zhang (2006) examined the dynamic stability using small signal analysis and identified the stability type by mode participation factors of the state variables. A fast algorithm was proposed to identify and trace both saddle node bifurcation and Hopf bifurcation and to estimate the stability margin without calculating any eigenvalues (Zhou & Ajjarapu, 2005). The integration-based eigenvalue tracing was presented to trace any specified eigenvalue of interest (Wen & Ajjarapu, 2006). This method was used to identify Hopf bifurcation and determine the stability margin. The relationship between a detailed power system dynamic model and a standard load flow model has been discussed (Sauer & Pai, 1990). Only under very drastic assumptions about the synchronous machines and their control systems, the determinant of the standard load flow Jacobian provides information about the steady-state stability of a dynamic model.

In a realistic power system, there are many dynamic elements and time constants of these dynamic elements can range from seconds to ten minutes. It is crucial to establish the appropriate system model, which is simple and can reflect the dynamic nature of power system.

1.2.2.3 Dynamic analysis

Dynamic method based on non-linear differential algebraic equations is often regarded as time domain simulation. Time domain simulation is a powerful measure

to explore the mechanism and process of voltage collapse, to verify voltage stability study findings and to investigate the effectiveness of control measure in voltage stability enhancement. The results of time simulation are clear and intuitional. Simulation was employed to demonstrate the mechanism of the voltage collapse on 39-bus 10-generator system when suffering a very small increase of loads near the static bifurcation point (Begovic & Phadke, 1990). To reduce the oscillation and enhance dynamic voltage stability, time simulation was used to investigate the effectiveness of the proposed parameter optimization method (Lee & Lee, 1993). Simulation was used to demonstrate voltage oscillatory instability caused by the induction motor loads interacting with automatic voltage regulators and to show the control effectiveness of an appropriate lead/lag compensation in the automatic voltage regulator (de Mello & Feltes, 1996). Static and simulation programs have been developed for voltage stability studies, and their practicality were verified by Nagao, Tanaka, & Takenaka (1997). Borghetti, Caldon, Mari, & Nucci (1997) have used time simulation method to study the effect of different simplified-dynamic load models on voltage stability analysis. Morison et al (1993) have presented time domain simulation to demonstrate voltage instability and to clarify the influence of ULTCs, generator MXLs, and voltage dependent loads.

According to the different responding time of different dynamic elements, voltage stability analysis can be classified into long term and short term analysis (Cutsem, 1998; Kundur et al., 2004). With modern computer technology, it is quite feasible to handle the whole set of differential-algebraic, discrete-continuous time equations in

digital simulations. However, for the purposes of understanding voltage instability mechanisms as well as devising faster analysis methods, it is advantageous to exploit the time separation which exists between the short and long term phenomena. Therefore, time-scale decomposition was introduced and discussed (Cutsem, 1998). The idea of time-scale decomposition is described as follow. The fast subsystem is assumed infinitely fast and can be replaced by its equilibrium equations when dealing with the slow subsystem. Conversely, the fast dynamics can be approximated by considering the slow variables as practically constant during the fast transients. The Quasi Steady-State (QSS) approximation for slow subsystem has been used to simulate the voltage behavior of a power system beyond the transient period (Cutsem & Mailhot, 1997). The QSS approximation for mid term simulation was combined with small signal analysis to analyze the transient and mid-term dynamics of power system voltage stability (Cutsem & Vournas, 1996). Van Cutsem, Moisse, & Mailhot (1999) combined QSS simulation and binary search to form an efficient tool suitable for off-line security limit determination.

Time domain simulations, in which appropriate modeling is included, capture the events and their chronology leading to instability. However, such simulations are time-consuming and do not readily provide sensitivity information and the degree of stability.

1.2.2.4 Summary of deterministic voltage stability analysis

In summary, different research methods for voltage stability have been reviewed. Most of the computational methods for voltage stability analysis developed so far

are based on the analysis of a predetermined set of severe but credible situations. However, there are uncertainties such as measurement errors, forecast inaccuracy and outages of system elements in power systems. To carry out deterministic voltage stability analysis for every possible or probable combination of bus loads and generating unit outages is completely impractical because of an extremely large computational requirement. Therefore, probabilistic methods have been introduced to power system stability analysis taking these uncertainties.

1.2.3 Probabilistic analysis in voltage stability analysis

The probabilistic theory has been successfully used in many aspects of power system analysis (Anders, 1990), such as the reliability evaluation, production simulation, power network loss analysis, load flow studies and transient stability analysis. Probabilistic method has been used in voltage stability analysis considering different uncertainties such as element forced outages (Aboreshaid & Billinton, 1999; Arya, Titare, & Kothari, 2007; Billinton & Aboreshaid, 1998; Sharaf & Berg, 1991), load uncertainty (Hatziargyriou & Karakatsanis, 1998; Kataoka, 2003; Nwankpa & Hassan, 1993; Schellenberg, Rosehart, & Aguado, 2006; Sobierajski & Fulczyk, 2004) and load parameters (Indulkar & Viswanathan, 1983) etc. Indulkar & Viswanathan (1983) described a probabilistic approach for evaluation of voltage stability of Extra High Voltage lines with series compensation, where the uncertainties of the coefficients of the load polynomials relating the complex power of the loads with the load voltage were considered. Sharaf & Berg (1991) proposed a probabilistic voltage stability indexes based on sensitivity, the expected voltage instability proximity, which takes into account the probabilistic nature of system

elements' forced outages. Voltage stability considerations have been included in the reliability assessment (Amjady, 2004; Billinton & Aboreshaid, 1998; Momoh, Makarov, & Mittelstadt, 1999). Aboreshaid & Billinton (1999) proposed a probabilistic evaluation approach of voltage stability based on contingency enumeration. Probabilistic load flow for assessment of voltage instability has been presented taking into account the random variation of loads, generation uncertainties, dispatching effects and outages (Hatziargyriou & Karakatsanis, 1998). Kataoka (2003) proposed a nodal loading model, called the "hyper-cone" model, for use in voltage stability assessment of electric power systems and determined the worst cases based on this model. The "vertex" of the hyper-cone is taken to be the current operating point, and the uncertainty of future loading is represented by the "thickness" of the hyper-cone. Schellenberg et al (2006) describes a probabilistic voltage stability analysis based on cumulant-based stochastic nonlinear programming to get the probabilistic distributions of maximum load levels and bus voltages. A security measure has been presented by De Marco & Bergen (1987). It indicated vulnerability to voltage collapse which accounts for random load disturbances in electric power system. A voltage collapse indicator has been defined (Nwankpa & Hassan, 1993) which considers the effects of random fluctuations at various load buses by using a stochastic approach. Sobierajski and Fulczyk (2004) developed P-Q curve method to estimate the probability of the critical voltage violation under the assumption that active and reactive power at a given load bus are uniformly distributed.

However, most of the previous probabilistic voltage stability analysis methods are based on static analysis and do not consider the effects of dynamic elements in power systems. Indeed, voltage instability or collapse is dynamic process (Taylor, 1994). The probabilistic method should be incorporated with dynamic voltage stability analysis to obtain more accurate and reliable results.

1.2.4 Probabilistic eigenvalue used in power system dynamic stability studies

Probabilistic theory was introduced for power system dynamic stability studies (Burchett & Heydt, 1978). The sensitivities of eigenvalues are used to calculate the statistics of eigenvalues from the known statistic nature of system stochastic parameters. Under the assumption that system parameters are multivariable normal distribution, the probabilistic densities of real parts of eigenvalues are determined. The stability probability of entire power system is then computed from joint normal distribution. With the development of eigenvalue sensitivities with regard to arbitrary system parameters (Wang, Chung, Tse, & Tsang, 2000b), probabilistic eigenvalue have been used to analyze the angular stability of power system and to determine the probabilistic stability considering the multiple operation conditions (Wang, Chung, Tse, & Tsang, 2000a; Wang, Tse, & Tsang, 1998). Probabilistic eigenvalue method has been also used for robust PSS site selection (Wang, Chung, Tse, & Tsang, 2001) and the parameter optimization of robust PSSs (Chung, Wang, Tse, Bian, & David, 2003; Chung, Wang, Tse, & Niu, 2002; Tse, Wang, Chung, & Tsang, 2000).

1.3 Motivation of this research work

Probabilistic voltage stability analysis methods have been presented in literatures. Most of them use probabilistic index to assess the voltage stability of power system, and indicate which buses are weak and most susceptible to instability. Few of them indicate the probabilistic voltage stability margin. Furthermore, few of them consider effect of dynamic elements of power systems.

Small disturbance method has been used for voltage stability analysis. But most of them are based on deterministic situations. The uncertainties of loads are not taken into account. Although dynamic loads have been included in small disturbance voltage stability analysis, the uncertainties of load model parameters have not been considered.

Probabilistic eigenvalue analysis has been developed for dynamic stability studies of power system. The first order and second sensitivities of eigenvalues with regard to arbitrary system parameters have been systematically determined. This provides the foundation for small disturbance voltage stability studies using probabilistic eigenvalues considering the uncertainties of load and load parameters.

Similar to robust Power System Stabilizers (PSS) for rotor angle stability under multiple operating conditions, the voltage stability should be improved by designing some robust voltage stability stabilizers.

This thesis aims to incorporate the probability theory with voltage stability analysis, to determine probabilistic stability margin and to design voltage stability controller for improvement of voltage stability. The objectives of this project can be defined as:

- to determine the probabilistic distribution of static voltage stability margin considering the random variations of loads;

- to determine the probabilistic stability margin considering uncertainties in loads by using probabilistic eigenvalue method;

- to extend probabilistic eigenvalue technique to include uncertainties of load parameters in voltage stability analysis;

- to design power system voltage stabilizer to improve voltage stability taking into account random load variations.

Probabilistic distribution of voltage stability margin

Voltage stability margin is a useful index to quantify the degree of stability, which indicates how far the current operating point is to the collapse point. The technique based on power flow is often used to determine voltage stability margin because it is simple and fast. In practice, loads in power system are random so that the stability margin is random variable. In the present study, the probabilistic characteristics of stability margins and critical points can be obtained from those of loads through

probabilistic point of collapse method, and then the distribution of stability margin and other variables at critical point can be determined by maximum entropy. The effect of load uncertainty degree on stability margin will be examined.

Probabilistic stability margin considering load uncertainties

In small disturbance voltage stability analysis, different bifurcations have been regarded as the critical point for voltage stability. In this study, Hopf bifurcation is regarded as the critical point of voltage stability. In order to obtain Hopf bifurcation, one has to form state matrix $\boldsymbol{A}$ firstly. Elements of the state matrix $\boldsymbol{A}$ are functions of system parameters which are assumed to have known statistics. Therefore, the stability margin determined by Hopf bifurcation is non-deterministic. As probabilistic eigenvalue analysis has been systematically developed, the stability probability of power system is easy to determine at any load level. In this research work, the probabilistic critical point which is the maximal load point meeting stability requirements, and the probabilistic stability margin will be determined by probabilistic eigenvalue technique considering the uncertainties of loads.

Probabilistic stability margin considering uncertainties of load parameters

With the advancement of voltage stability study, load dynamics have been recognized. After exponential recovery load model (Karlsson & Hill, 1994) and adaptive load model (Xu & Mansour, 1994) proposed according to the results from the measurement of actual power system load, dynamic load models have been introduced to voltage stability analysis (Byongjun & Ajjarapu, 1995; Zeng et al., 1997). There is always some uncertainty associated with load parameters due to the

dynamic load variation. Dynamic parameter variation will affect the assessment of voltage stability margin. Therefore, in this research work, the probabilistic eigenvalue is extended to study the effect of uncertainties of load parameter on probabilistic stability margin.

Power system voltage stabilizer design and parameter optimization

Similar to Power System Stabilizer used for angular stability, Power System Voltage Stabilizer has been presented for dynamic voltage stability enhancement of power systems or prevention of fast voltage stability (Radman, Pama, Powell, & Gao, 2007). Considering the random variations of loads, the present study will adopt probabilistic eigenvalue to design power system voltage stabilizer to enhance voltage stability. The location, design and parameters optimization of power system voltage stabilizer will be presented.

1.4 Outline of the thesis

The remaining chapters of the thesis are arranged as follows.

Chapter 2 determines the probabilistic distribution of voltage stability margin based on probabilistic point of collapse method and maximum entropy. The effect of uncertainty degree of loads will be investigated.

Chapter 3 examines the probabilistic eigenvalue methods for determination of probabilistic stability margin considering the uncertainties of loads.

Chapter 4 extends the probabilistic eigenvalue technique to take into account uncertainties of dynamic load parameters in voltage stability analysis.

Chapter 5 presents a probabilistic method for power system voltage stabilizer design and parameter optimization to improve voltage stability of power system.

Chapter 6 encapsulates the main finding and contribution of this research work and points out some suggestions for future work on probabilistic voltage stability studies.

1.5 Publications

Journal paper published

Zhang, J.F.; Tse C.T.; Wang K.W.; Chung C. Y., 'Voltage stability analysis considering the uncertainties of dynamic load parameters', IET Generator, Transmission & Distribution, 2009, Vol. 3, Iss. 10, pp. 941–948.

Journal paper accepted

Zhang, J.F.; Tse C.T. ; Wang K.W. ; Chung C. Y., 'Voltage stability analysis based on probabilistic power flow and maximum entropy', to IET Generator, Transmission and Distribution.

Conference paper

Zhang, J.F.; Tse, C.T.; Wang, K.W.; Chung, C.Y., 'Small disturbance voltage stability analysis considering the effect of dynamic load parameters', International Power Engineering Conference, Singapore, 2007, 3-6 Dec. 2007, pp. 371-375.

Paper under review

Zhang, J.F.; Tse, C.T.; Wang, K.W.; Bian X.Y., 'Determination and enhancement of probabilistic stability margin with load uncertainties', submitted to IEEE Transaction on power systems.

Chapter 2 Voltage stability analysis based on probabilistic power flow and maximum entropy

2.1 Introduction

Static voltage stability analysis based on power flow attracts researchers because of its simplicity and fast calculation. It regards the maximum load point as the critical point, where the Jacobian matrix of the power flow equations becomes singular. Static voltage stability analysis can provide margin index which is the distance between the current operating point and the maximum load point for power system operators.

The stability margin is also called load margin. Two types of load margins have been proposed for voltage stability analysis (Ajjarapu & Christy, 1992; Canizares & Alvarado, 1993; Dobson & Lu, 1993). As illustrated in Fig. 2.1, one is obtained by increasing loads and generations from the current operating point S_0 along a predefined direction $\boldsymbol{B}$ (Ajjarapu & Christy, 1992; Canizares & Alvarado, 1993; Zarate, Castro, Ramos, & Ramos, 2006) until the system maximum load point S_* is reached (Fig. 2.1(a)). Since the direction of loads and generations is predefined, the load coefficient λ can describe the load margin. The other is the distance between current operating point S_0 and the closest critical point S_{cr} which is on the critical super surface $\boldsymbol{\Sigma}$ and has the smallest Euclidean distance from the current operating

point S_0 (Fig. 2.1(b)) (Alvarado, Dobson, & Yi, 1994; Dobson & Lu, 1993). S_{cr} represents the worst case scenario for a given power system. In general, these two types of load margins are often applied for deterministic voltage stability analysis.

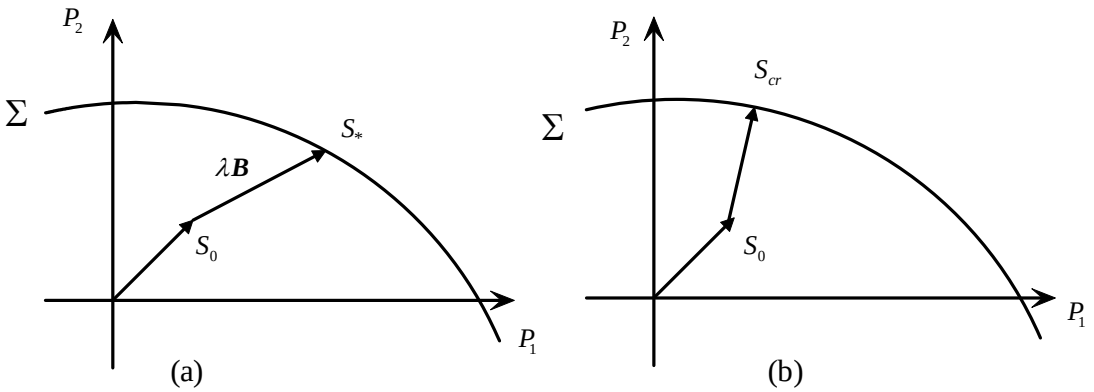

Fig. 2. 1 Interpretations of load margin in the load power space

Deterministic voltage stability analysis requires specific values for loads. In reality, the loads vary from time to time. It is impossible to carry out conventional voltage stability study for every possible or probable combination of bus loads because of the requirements on extremely large computational effort. Probabilistic method may be the best technique to a wide range operation of load variations/uncertainties. Various probabilistic methods have been used for voltage stability analyses (Aboreshaid & Billinton, 1999; Haesen, Bastiaensen, Driesen, & Belmans, 2009; Hatziargyriou & Karakatsanis, 1998; Kataoka, 2003; Schellenberg, Rosehart, & Aguado, 2006; Sharaf & Berg, 1991). Sharaf and Berg (1991) presented expected voltage instability proximity index at all load buses based on sensitivity which took into account the element forced outages. According to voltage instability index, the weakest bus close to voltage instability or collapse is identified. Sharaf & Berg (1991) also determined the worst scenario of voltage stability and distinguished the

critical system elements as well as the probability of the worst scenario. Hatziargyriou & Karakatsanis (1998) used the results of the probabilistic load flow to appraise voltage instability considering random variation of loads, generation uncertainties, dispatching effects and outages. The standard deviation of voltage and reactive injection sensitivities have been applied as probabilistic voltage collapse indices. A hyper-cone nodal loading model (Kataoka, 2003) whose thickness represents the uncertainty of future loading, has been developed for voltage stability assessment of electric power system. The worst case S_2 is determined on the intersection of the transfer limit surface and the loading hyper-cone (Fig. 2.2). S_1 and S_3 respectively represent the minimum total load critical point and the on-scenario critical point. Sobierajski and Fulczyk (2004) employed the P-Q curve to estimate the probability of the critical voltage violation under the assumption that active and reactive power at given load buses are uniformly distributed. Schellenberg et al. (2006) suggested a cumulant-based method to solve a maximum loading problem incorporating a constraint on the maximum variance of the loading parameters. They took advantage of some properties regarding saddle node bifurcations to create a linear mapping relationship between random bus loading variables and all other system variables to evaluate the cumulants of system variables, and obtained the probabilistic density function of stability margin. Stochastic response surface method (Haesen et al., 2009) has been employed for a probabilistic load margin considering stochastic generation source.

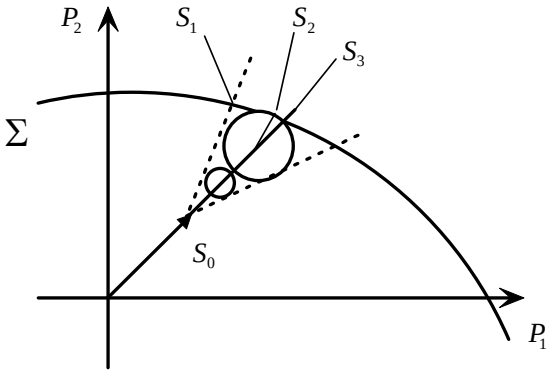

Fig. 2. 2 Hyper-cone loading model and its worst conditions

Although probabilistic methods have been adopted for voltage stability studies, most of them are used to assess the voltage stability and to identify the weak buses or area. Only a few papers (Haesen et al., 2009; Schellenberg et al., 2006) can provide the probabilistic distribution of stability margin taking into account random variations of the loads or generations. This chapter combines the probabilistic technique and point of collapse approach to determine the probabilistic characteristics of stability margin and nodal voltages at the maximum load point, and then applies the maximum entropy technique to study the distribution of stability margin considering the load variations.

Entropy, a concept in information theory, is a measure of uncertainty. An entropy application is to deal with problems involving the determination of unknown distributions but with available information such as expected values or other statistical functions (Papoulis, 2002; Zellner & Highfield, 1988). Similar to the cumulant method, maximum entropy method is a general method and is not restricted to a special distribution. With the moments of random variable of stability

margin obtained in terms of probabilistic point of collapse approach, the distribution can be determined by maximum entropy.

2.2 The foundation of probability theory

2.2.1 Numerical attributes of random variables

In many practical problems, the characteristic of random variables can be described by the numerical attributes such as expected value, variance, and moment.

a) Expected value (Bartoszyński, 1996)

If X is a discrete random variables that assumes values $x_1,x_2,\ldots$with probabilities $P\{X=x_i\}$, $i=1,2,\ldots n,\ldots$, then the expected value of X is defined as

$$E(X)=\sum_i x_i P\{X=x_i\} \tag{2.1}$$

provided that

$$\sum_i |x_i| P\{X=x_i\}<\infty \tag{2.2}$$

If X is a continuous random variable with density function $f(x)$, then the expected value of the variable X is defined as

$$E(X)=\int_{-\infty}^{+\infty} xf(x)dx \tag{2.3}$$

provided that

$$\int_{-\infty}^{+\infty} |x| f(x)dx<\infty \tag{2.4}$$

The reason for introducing conditions (2.2) and (2.4) is connected with the possibility that the value of an infinite sum may depend on the order of summation (and a similar phenomenon may occur for an integral). The absolute convergence

(respectively absolute integrability) guarantees that the expected value is unambiguously defined.

b) Moments (Bartoszyński, 1996)

Given random variable X, the expectation of X^n, if it exists, will be called nth moment (or moment of the order n) of X, denoted as m_n,

$$m_n = E(X^n) \tag{2.5}$$

and m_n exists if $E|X|^n<\infty$.

Clearly, the moment of the order zero always exists and equals one, while m_1 is simply the expectation of X.

Ordinary moments of the random variable $Y = X - E(X)$ are called central moments of X, so that

$$\gamma_n = E[(X - m_1)^n] \tag{2.6}$$

where $m_1 = E(X)$.

Obviously, the first central moment γ_1 is always zero.

c) Variance (Bartoszyński, 1996)

If $E(X^2) < \infty$, then the second central moment of X is called the variance of X:

$$\sigma^2 = E[(X - m_1)^2] \tag{2.7}$$

where $m_1 = E(X)$. The positive square root of variance σ^2 is called the standard deviation of X.

d) Covariance (Bartoszyński, 1996)

The covariance between X and Y is defined as

$$\mathrm{Cov}(X,Y)=E(XY)-E(X)E(Y)=E[(X-E(X))(Y-E(Y))] \tag{2.8}$$

If Cov(X,Y)=0, the random variables X, Y are called uncorrelated or orthogonal.

The coefficient of correlation between X and Y is defined as

$$\rho=\rho_{X,Y}=\frac{\mathrm{Cov}(X,Y)}{\sqrt{\sigma_X\sigma_Y}} \tag{2.9}$$

2.2.2 Normal distribution

The normal distribution is perhaps the most important distribution in statistical paradigms since many measurements approximate normal distributions (Hogg, 1983). X is a normal random variable (Hogg, 1983; Ross, 1993) (or X is normally distributed) with parameters μ and σ^2 if the density of X is given by

$$f(x)=\frac{1}{\sqrt{2\pi}\sigma}e^{-(x-\mu)^2/2\sigma^2},\quad -\infty<x<\infty \tag{2.10}$$

In fact μ and σ^2 are the mean and the variance of this distribution. The normal distribution is denoted as $N(\mu, \sigma^2)$.

Let $Y=(X-\mu)/\sigma$, the density of Y is

$$f(y)=\frac{1}{\sqrt{2\pi}}e^{-y^2/2},\quad -\infty<y<\infty \tag{2.11}$$

Y is a standard normal random variable. The mean and the variance of the standard normal distribution are respectively zero and one.

2.3 Point of collapse method for voltage stability analysis

Because of its simple calculation and intuition, voltage stability analysis based on power flow is still attractive. Many methods such as continuation power flow (Ajjarapu & Christy, 1992; Iba, Suzuki, Egawa, & Watanabe, 1991), non-linear programming method (Irisarri, Wang, Tong, & Mokhtari, 1997; Parker, Morrison, & Sutanto, 1996) and point of collapse method (Canizares & Alvarado, 1993; Chiang & Jean-Jumeau, 1995), have been used to obtain the saddle-node bifurcation and stability margin. In order to incorporate with probabilistic method conveniently, point of collapse is adopted to compute the stability margin in this chapter.

A salient characteristic of the voltage collapse point is that the Jacobian matrix $\boldsymbol{J}$ of power flow equations is singular; $\boldsymbol{J}$ has a zero eigenvalue but the corresponding eigenvectors (left and right) are non-zero. Based on this property, the exact critical point of power system is directly obtained by solving the extended power flow equations as follows,

$$\boldsymbol{f}(\boldsymbol{V}) - \lambda \boldsymbol{B} - \boldsymbol{S}_0 = \boldsymbol{0} \tag{2.12a}$$

$$\boldsymbol{J}_V^T \boldsymbol{w} = \boldsymbol{0} \tag{2.12b}$$

$$\boldsymbol{w}^T \boldsymbol{w} - 1 = 0 \tag{2.12c}$$

where $\boldsymbol{B}$ describes the load increase; $\boldsymbol{S}_0$=$\boldsymbol{S}_{G0}$-$\boldsymbol{S}_{L0}$, is the initial injections; $\boldsymbol{S}_{G0}$ and $\boldsymbol{S}_{L0}$ are power vectors of generations and loads respectively in the base case. $\boldsymbol{V}$ stands for vector of voltage; $\boldsymbol{w}$ is the left eigenvector of $\boldsymbol{J}$ with respect to zero eigenvalue; λ stands for stability margin; T stands for transpose. (2.12a) describes the power flow; (2.12b) and (2.12c) ensure $\boldsymbol{J}$ is singular at the critical point.

2.4 Stability margin assessment by probabilistic approach

With the equation (2.12), if the initial loads, generations and the direction of load increase are predefined, the critical point and the stability margin λ are easy to obtain. There definitely exist uncertainties in power systems, such as the variations of loads and the generator outputs. In this chapter, loads $\boldsymbol{S}_{\mathrm{L0}}$ are regarded as random variables and the generations $\boldsymbol{S}_{\mathrm{G0}}$ are not random variable. Therefore, the injections $\boldsymbol{S}_0 = \boldsymbol{S}_{G0} - \boldsymbol{S}_{L0}$ are random variables, and the possible injection values are $\boldsymbol{S}_{01}$, $\boldsymbol{S}_{02}$,..., $\boldsymbol{S}_{0\mathrm{n}}$. Two cases of load increase directions are considered. In one case shown in Fig. 2.3(a), the load increase directions are predefined and equal to the expectation of $\boldsymbol{S}_0$, i.e. $\boldsymbol{B} = \overline{\boldsymbol{S}_0}$. The critical points corresponding to $\boldsymbol{S}_{01}$, $\boldsymbol{S}_{02}$,..., $\boldsymbol{S}_{0\mathrm{n}}$ are $\boldsymbol{S}_{*1}$, $\boldsymbol{S}_{*2}$,..., $\boldsymbol{S}_{*\mathrm{n}}$ with the relationship $\boldsymbol{S}_{01} + \lambda_1 \overline{\boldsymbol{S}_0} = \boldsymbol{S}_{*1}$, …, $\boldsymbol{S}_{0n} + \lambda_n \overline{\boldsymbol{S}_0} = \boldsymbol{S}_{*n}$. λ_1,…, λ_{n} are random margins corresponding to $\boldsymbol{S}_{01}$, $\boldsymbol{S}_{02}$,..., $\boldsymbol{S}_{0\mathrm{n}}$. In other case shown in Fig. 2.3(b), the load increase directions are random as $\boldsymbol{S}_0$, i.e. $\boldsymbol{B} = \boldsymbol{S}_0$. The critical points corresponding to $\boldsymbol{S}_{01}$, $\boldsymbol{S}_{02}$, ..., $\boldsymbol{S}_{0\mathrm{n}}$ are $\boldsymbol{S}_{*1}$, $\boldsymbol{S}_{*2}$,..., $\boldsymbol{S}_{*\mathrm{n}}$ with the relationship $\boldsymbol{S}_{01} + \lambda_1 \boldsymbol{S}_{01} = \boldsymbol{S}_{*1}$,…, $\boldsymbol{S}_{0n} + \lambda_n \boldsymbol{S}_{0n} = \boldsymbol{S}_{*n}$. This chapter aims to determine the probabilistic stability margin λ taking into the random load variations.

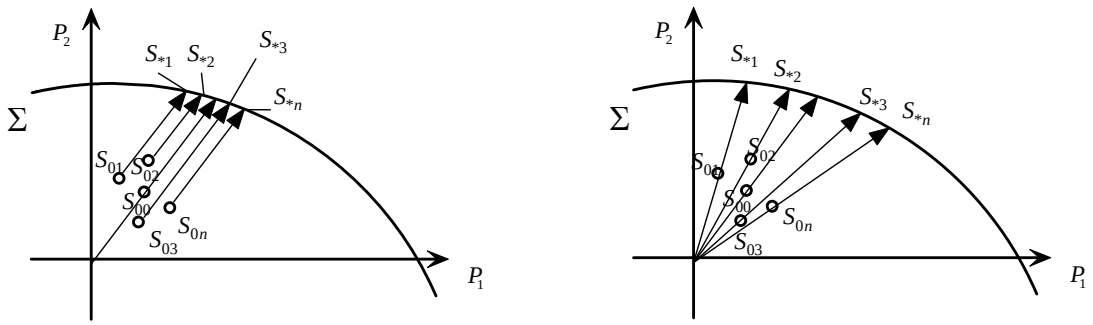

(a) **(b)**

Fig. 2. 3 Two cases for load increase direction

In equation (2.12), if the voltages are expressed with rectangular coordinates, every expression is the second order function of nodal voltage and left eigenvector. Equation (2.12) can be represented as,

$$\boldsymbol{F}_1(V_1V_1,\cdots,V_1V_n,\cdots,V_nV_1,\cdots,V_nV_n)-\lambda\boldsymbol{B}-(\boldsymbol{S}_{G0}-\boldsymbol{S}_{L0})=\boldsymbol{0} \tag{2.13a}$$

$$\boldsymbol{F}_2(V_1w_1,\cdots,V_1w_n,\cdots,V_nw_1,\cdots,V_nw_n)=\boldsymbol{0} \tag{2.13b}$$

$$F_3(w_1w_1,\cdots,w_nw_n)-1=0 \tag{2.13c}$$

where, V_i and w_i, for i=1 to n, respectively stand for the elements of voltage vector and left eigenvector. $\boldsymbol{B}$ describes direction of load increase. λ stands for stability margin. Since the direction of load increase $\boldsymbol{B}$ will affect the stability margin, the calculation of probabilistic stability margin will be divided into two parts as follows.

2.4.1 $\boldsymbol{B}=\overline{\boldsymbol{S}_0}$

For $\boldsymbol{B}=\overline{\boldsymbol{S}_0}=\boldsymbol{S}_{G0}-\overline{\boldsymbol{S}_{L0}}$, if equation (2.13) is expanded at the means of nodal voltages, stability margin, the left eigenvector and nodal loads, it can be represented as

$$\begin{aligned}
&\boldsymbol{F}_1(\overline{V}_1\overline{V}_1,\cdots,\overline{V}_1\overline{V}_n,\cdots,\overline{V}_n\overline{V}_1,\cdots,\overline{V}_n\overline{V}_n)\\
&+\boldsymbol{F}_1(\Delta V_1\overline{V}_1,\cdots,\Delta V_1\overline{V}_n,\cdots,\Delta V_n\overline{V}_1,\cdots,\Delta V_n\overline{V}_n)\\
&+\boldsymbol{F}_1(\overline{V}_1\Delta V_1,\cdots,\overline{V}_n\Delta V_1,\cdots,\overline{V}_1\Delta V_n,\cdots,\overline{V}_n\Delta V_n)\\
&+\boldsymbol{F}_1(\Delta V_1\Delta V_1,\cdots,\Delta V_1\Delta V_n,\cdots,\Delta V_n\Delta V_1,\cdots,\Delta V_n\Delta V_n)\\
&-\overline{\lambda}(\boldsymbol{S}_{G0}-\overline{\boldsymbol{S}_{L0}})-\Delta\lambda(\boldsymbol{S}_{G0}-\overline{\boldsymbol{S}_{L0}})-(\boldsymbol{S}_{G0}-\overline{\boldsymbol{S}_{L0}}-\Delta\boldsymbol{S}_{L0})=\boldsymbol{0}
\end{aligned} \tag{2.14a}$$

$$\begin{aligned}
&\boldsymbol{F}_2(\overline{V}_1\overline{w}_1,\cdots,\overline{V}_1\overline{w}_n,\cdots,\overline{V}_n\overline{w}_1,\cdots,\overline{V}_n\overline{w}_n)\\
&+\boldsymbol{F}_2(\Delta V_1\overline{w}_1,\cdots,\Delta V_1\overline{w}_n,\cdots,\Delta V_n\overline{w}_1,\cdots,\Delta V_n\overline{w}_n)\\
&+\boldsymbol{F}_2(\overline{V}_1\Delta w_1,\cdots,\overline{V}_1\Delta w_n,\cdots,\overline{V}_n\Delta w_1,\cdots,\overline{V}_n\Delta w_n)\\
&+\boldsymbol{F}_2(\Delta V_1\Delta w_1,\cdots,\Delta V_1\Delta w_n,\cdots,\Delta V_n\Delta w_1,\cdots,\Delta V_n\Delta w_n)\\
&=\boldsymbol{0}
\end{aligned} \tag{2.14b}$$

$$
\begin{aligned}
&F_3(\overline{w}_1\overline{w}_1,\cdots,\overline{w}_n\overline{w}_n)+F_3(\overline{w}_1\Delta w_1,\cdots,\overline{w}_n\Delta w_n)\\
&+F_3(\Delta w_1\overline{w}_1,\cdots,\Delta w_n\overline{w}_n)+F_3(\Delta w_1\Delta w_1,\cdots,\Delta w_n\Delta w_n)\\
&-1=0
\end{aligned}
\tag{2.14c}
$$

Since $\overline{\Delta\lambda}=0$, $\overline{\Delta \boldsymbol{S}_{L0}}=\boldsymbol{0}$, $\overline{\Delta \boldsymbol{V}}=\boldsymbol{0}$ and $\overline{\Delta \boldsymbol{w}}=\boldsymbol{0}$, the expectation of equation (2.14) is expressed as equation (2.15)

$$
\begin{aligned}
&\boldsymbol{F}_1(\overline{V}_1\overline{V}_1,\cdots,\overline{V}_1\overline{V}_n,\cdots,\overline{V}_n\overline{V}_1,\cdots,\overline{V}_n\overline{V}_n)\\
&+\boldsymbol{F}_1(\overline{\Delta V_1\Delta V_1},\cdots,\overline{\Delta V_1\Delta V_n},\cdots,\overline{\Delta V_n\Delta V_1},\cdots,\overline{\Delta V_n\Delta V_n})\\
&-\overline{\lambda}(\boldsymbol{S}_{G0}-\overline{\boldsymbol{S}_{L0}})-(\boldsymbol{S}_{G0}-\overline{\boldsymbol{S}_{L0}})=\boldsymbol{0}
\end{aligned}
\tag{2.15a}
$$

$$
\begin{aligned}
&\boldsymbol{F}_2(\overline{V}_1\overline{w}_1,\cdots,\overline{V}_1\overline{w}_n,\cdots,\overline{V}_n\overline{w}_1,\cdots,\overline{V}_n\overline{w}_n)\\
&+\boldsymbol{F}_2(\overline{\Delta V_1\Delta w_1},\cdots,\overline{\Delta V_1\Delta w_n},\cdots,\overline{\Delta V_n\Delta w_1},\cdots,\overline{\Delta V_n\Delta w_n})=\boldsymbol{0}
\end{aligned}
\tag{2.15b}
$$

$$
F_3(\overline{w}_1\overline{w}_1,\cdots,\overline{w}_n\overline{w}_n)+F_3(\overline{\Delta w_1\Delta w_1},\cdots,\overline{\Delta w_n\Delta w_n})-1=0
\tag{2.15c}
$$

As $\overline{\Delta V_i\Delta V_j}=C_{V_iV_j}$, $\overline{\Delta V_i\Delta w_j}=C_{V_iw_j}$, $\overline{\Delta w_i\Delta w_j}=C_{w_iw_j}$, equation (2.15) can also be represented with covariance of random variances of nodal voltages and left eigenvector. With the covariances, the means of nodal voltages, left eigenvector at critical point and stability margin can be obtained by solving equation (2.15) via Newton-Raphson method.

Omitting the second order terms of equation (2.14) and (2.15), the linearized relationships among nodal voltage $\boldsymbol{V}$, stability margin λ, left eigenvector $\boldsymbol{w}$ and the nodal load $\boldsymbol{S}_{L0}$ are shown as equation (2.16),

$$
\boldsymbol{J}\begin{bmatrix}\Delta\boldsymbol{V}\\ \Delta\boldsymbol{w}\\ \Delta\boldsymbol{\lambda}\end{bmatrix}=\begin{bmatrix}-\Delta\boldsymbol{S}_{L0}\\ \boldsymbol{0}\\ \boldsymbol{0}\end{bmatrix}
\tag{2.16}
$$

$$\text{where } \boldsymbol{J} = \begin{bmatrix} \left.\frac{\partial \boldsymbol{F}_1}{\partial \boldsymbol{V}}\right|_{\boldsymbol{V}=\bar{\boldsymbol{V}}} & \boldsymbol{0} & -(\boldsymbol{S}_{G0} - \overline{\boldsymbol{S}_{L0}}) \\ \left.\frac{\partial \boldsymbol{F}_2}{\partial \boldsymbol{V}}\right|_{\boldsymbol{V}=\bar{\boldsymbol{V}}} & \left.\frac{\partial \boldsymbol{F}_2}{\partial \boldsymbol{w}}\right|_{\boldsymbol{w}=\bar{\boldsymbol{w}}} & \boldsymbol{0} \\ \boldsymbol{0} & \left.\frac{\partial F_3}{\partial \boldsymbol{w}}\right|_{\boldsymbol{w}=\bar{\boldsymbol{w}}} & \boldsymbol{0} \end{bmatrix} \tag{2.17}$$

The deviations of random variables nodal voltage, left eigenvector and stability margin from their means are obtained by rearranging equation (2.16) as:

$$\begin{bmatrix} \Delta \boldsymbol{V} \\ \Delta \boldsymbol{w} \\ \Delta \boldsymbol{\lambda} \end{bmatrix} = \boldsymbol{J}^{-1} \begin{bmatrix} -\Delta \boldsymbol{S}_{L0} \\ \boldsymbol{0} \\ \boldsymbol{0} \end{bmatrix} \tag{2.18}$$

The covariances of random variables nodal voltage, left eigenvector and stability margin are

$$\boldsymbol{C} = \begin{bmatrix} \boldsymbol{C}_{VV} & \boldsymbol{C}_{Vw} & \boldsymbol{C}_{V\lambda} \\ \boldsymbol{C}_{wV} & \boldsymbol{C}_{ww} & \boldsymbol{C}_{w\lambda} \\ \boldsymbol{C}_{\lambda V} & \boldsymbol{C}_{\lambda w} & \boldsymbol{C}_{\lambda\lambda} \end{bmatrix} = \boldsymbol{J}^{-1} E\left(\begin{bmatrix} -\boldsymbol{\Delta S}_{L0} \\ \boldsymbol{0} \\ \boldsymbol{0} \end{bmatrix} \begin{bmatrix} -\boldsymbol{\Delta S}_{L0}{}^{T} & \boldsymbol{0} & \boldsymbol{0} \end{bmatrix} \right) (\boldsymbol{J}^{-1})^{T}$$

$$= \boldsymbol{J}^{-1} \begin{bmatrix} \boldsymbol{C}_{S_{L0}S_{L0}} & \boldsymbol{0} & \boldsymbol{0} \\ \boldsymbol{0} & \boldsymbol{0} & \boldsymbol{0} \\ \boldsymbol{0} & \boldsymbol{0} & \boldsymbol{0} \end{bmatrix} (\boldsymbol{J}^{-1})^{T} \tag{2.19}$$

The *n*th moment for $[\Delta V \quad \Delta w \quad \Delta\lambda]^T$ is computed from equation (2.18). As a result, the *n*th moment for $[V \quad w \quad \lambda]^T$ can be obtained using following equation

$$E(X^n) = (\overline{X})^n + \overline{(\Delta X)^n} + \sum_{r=1}^{n-1} C_n^r \overline{X}^r \overline{(\Delta X)^{n-r}} \tag{2.20}$$

2.4.2 $\boldsymbol{B} = \boldsymbol{S}_0$

Since $\boldsymbol{B}=\boldsymbol{S}_0=\boldsymbol{S}_{G0}-\boldsymbol{S}_{L0}$, $\boldsymbol{B}$ is random vector like $\boldsymbol{S}_0$, the expended equation of (2.13) at the means of nodal voltages, stability margin, the left eigenvector and nodal loads can be represented as

$$\begin{aligned}
&\boldsymbol{F}_1(\overline{V}_1\overline{V}_1,\cdots,\overline{V}_1\overline{V}_n,\cdots,\overline{V}_n\overline{V}_1,\cdots,\overline{V}_n\overline{V}_n)\\
&+\boldsymbol{F}_1(\Delta V_1\overline{V}_1,\cdots,\Delta V_1\overline{V}_n,\cdots,\Delta V_n\overline{V}_1,\cdots,\Delta V_n\overline{V}_n)\\
&+\boldsymbol{F}_1(\overline{V}_1\Delta V_1,\cdots,\overline{V}_n\Delta V_1,\cdots,\overline{V}_1\Delta V_n,\cdots,\overline{V}_n\Delta V_n)\\
&+\boldsymbol{F}_1(\Delta V_1\Delta V_1,\cdots,\Delta V_1\Delta V_n,\cdots,\Delta V_n\Delta V_1,\cdots,\Delta V_n\Delta V_n)\\
&-\overline{\lambda}(\boldsymbol{S}_{G0}-\overline{\boldsymbol{S}_{L0}})+\overline{\lambda}\Delta\boldsymbol{S}_{L0}-\Delta\lambda(\boldsymbol{S}_{G0}-\overline{\boldsymbol{S}_{L0}})+\Delta\lambda\Delta\boldsymbol{S}_{L0}\\
&-(\boldsymbol{S}_{G0}-\overline{\boldsymbol{S}_{L0}}-\Delta\boldsymbol{S}_{L0})=\boldsymbol{0}
\end{aligned} \tag{2.21a}$$

$$\begin{aligned}
&\boldsymbol{F}_2(\overline{V}_1\overline{w}_1,\cdots,\overline{V}_1\overline{w}_n,\cdots,\overline{V}_n\overline{w}_1,\cdots,\overline{V}_n\overline{w}_n)\\
&+\boldsymbol{F}_2(\Delta V_1\overline{w}_1,\cdots,\Delta V_1\overline{w}_n,\cdots,\Delta V_n\overline{w}_1,\cdots,\Delta V_n\overline{w}_n)\\
&+\boldsymbol{F}_2(\overline{V}_1\Delta w_1,\cdots,\overline{V}_1\Delta w_n,\cdots,\overline{V}_n\Delta w_1,\cdots,\overline{V}_n\Delta w_n)\\
&+\boldsymbol{F}_2(\Delta V_1\Delta w_1,\cdots,\Delta V_1\Delta w_n,\cdots,\Delta V_n\Delta w_1,\cdots,\Delta V_n\Delta w_n)\\
&=\boldsymbol{0}
\end{aligned} \tag{2.21b}$$

$$\begin{aligned}
&F_3(\overline{w}_1\overline{w}_1,\cdots,\overline{w}_n\overline{w}_n)+F_3(\overline{w}_1\Delta w_1,\cdots,\overline{w}_n\Delta w_n)\\
&+F_3(\Delta w_1\overline{w}_1,\cdots,\Delta w_n\overline{w}_n)+F_3(\Delta w_1\Delta w_1,\cdots,\Delta w_n\Delta w_n)\\
&-1=0
\end{aligned} \tag{2.21c}$$

Similar to (2.15), the expectation of equation (2.21) is expressed as equation (2.22)

$$\begin{aligned}
&\boldsymbol{F}_1(\overline{V}_1\overline{V}_1,\cdots,\overline{V}_1\overline{V}_n,\cdots,\overline{V}_n\overline{V}_1,\cdots,\overline{V}_n\overline{V}_n)\\
&+\boldsymbol{F}_1(\overline{\Delta V_1\Delta V_1},\cdots,\overline{\Delta V_1\Delta V_n},\cdots,\overline{\Delta V_n\Delta V_1},\cdots,\overline{\Delta V_n\Delta V_n})\\
&-\overline{\lambda}(\boldsymbol{S}_{G0}-\overline{\boldsymbol{S}_{L0}})+\overline{\Delta\lambda\Delta\boldsymbol{S}_{L0}}-(\boldsymbol{S}_{G0}-\overline{\boldsymbol{S}_{L0}})=\boldsymbol{0}
\end{aligned} \tag{2.22a}$$

$$\begin{aligned}
&\boldsymbol{F}_2(\overline{V}_1\overline{w}_1,\cdots,\overline{V}_1\overline{w}_n,\cdots,\overline{V}_n\overline{w}_1,\cdots,\overline{V}_n\overline{w}_n)\\
&+\boldsymbol{F}_2(\overline{\Delta V_1\Delta w_1},\cdots,\overline{\Delta V_1\Delta w_n},\cdots,\overline{\Delta V_n\Delta w_1},\cdots,\overline{\Delta V_n\Delta w_n})=\boldsymbol{0}
\end{aligned} \tag{2.22b}$$

$$F_3(\overline{w}_1\overline{w}_1,\cdots,\overline{w}_n\overline{w}_n)+F_3(\overline{\Delta w_1\Delta w_1},\cdots,\overline{\Delta w_n\Delta w_n})-1=0 \tag{2.22c}$$

Due to the difficulty of determining $\overline{\Delta\lambda\Delta \boldsymbol{S}_{L0}}$, the means of voltage $\boldsymbol{V}$, stability margin λ and left eigenvector $\boldsymbol{w}$ are calculated from (2.22) by neglecting $\overline{\Delta\lambda\Delta \boldsymbol{S}_{L0}}$. Omitting the second order terms of equation (2.21) and (2.22), the linearised relationships among nodal voltage $\boldsymbol{V}$, stability margin λ, left eigenvector $\boldsymbol{w}$ and the nodal load $\boldsymbol{S}_{L0}$ are shown as equation (2.23),

$$\boldsymbol{J}\begin{bmatrix}\Delta \boldsymbol{V}\\ \Delta \boldsymbol{w}\\ \Delta \boldsymbol{\lambda}\end{bmatrix}=\begin{bmatrix}-(1+\overline{\lambda})\Delta \boldsymbol{S}_{L0}\\ \boldsymbol{0}\\ \boldsymbol{0}\end{bmatrix} \tag{2.23}$$

The Jacobian matrix $\boldsymbol{J}$ in (2.23) is the same as that in (2.16). The deviations from means of random variables nodal voltage, left eigenvector and stability margin is obtained by rearranging equation (2.23) as:

$$\begin{bmatrix}\Delta \boldsymbol{V}\\ \Delta \boldsymbol{w}\\ \Delta \boldsymbol{\lambda}\end{bmatrix}=\boldsymbol{J}^{-1}\begin{bmatrix}-(1+\overline{\lambda})\Delta \boldsymbol{S}_{L0}\\ \boldsymbol{0}\\ \boldsymbol{0}\end{bmatrix} \tag{2.24}$$

The covariances of random variables nodal voltage, left eigenvector and stability margin are obtained as,

$$\boldsymbol{C}=\begin{bmatrix}\boldsymbol{C}_{VV} & \boldsymbol{C}_{Vw} & \boldsymbol{C}_{V\lambda}\\ \boldsymbol{C}_{wV} & \boldsymbol{C}_{ww} & \boldsymbol{C}_{w\lambda}\\ \boldsymbol{C}_{\lambda V} & \boldsymbol{C}_{\lambda w} & \boldsymbol{C}_{\lambda\lambda}\end{bmatrix}=\boldsymbol{J}^{-1}E\left(\begin{bmatrix}-(1+\overline{\lambda})\boldsymbol{\Delta S}_{L0}\\ \boldsymbol{0}\\ \boldsymbol{0}\end{bmatrix}\begin{bmatrix}-(1+\overline{\lambda})\boldsymbol{\Delta S}_{L0}{}^{T} & \boldsymbol{0} & \boldsymbol{0}\end{bmatrix}\right)(\boldsymbol{J}^{-1})^{T}$$

$$=\boldsymbol{J}^{-1}\begin{bmatrix}(1+\overline{\lambda})^{2}\boldsymbol{C}_{\boldsymbol{S}_{L0}\boldsymbol{S}_{L0}} & \boldsymbol{0} & \boldsymbol{0}\\ \boldsymbol{0} & \boldsymbol{0} & \boldsymbol{0}\\ \boldsymbol{0} & \boldsymbol{0} & \boldsymbol{0}\end{bmatrix}(\boldsymbol{J}^{-1})^{T} \tag{2.25}$$

The *n*th moment for $[\Delta V \quad \Delta w \quad \Delta\lambda]^{T}$ is computed from equation (2.24). As a result, the *n*th moment for $[V \quad w \quad \lambda]^{T}$ can be obtained by using equation (2.20).

The probabilistic characteristics of critical points can be described by probabilistic characteristics of stability margins and nodal voltages. Taking the first case ($\boldsymbol{B} = \overline{\boldsymbol{S}_0}$) for example, the procedure of probabilistic critical point calculation is:

Step 1 Calculate the probabilistic power flow at a load level, and get the initial voltages and covariances of voltages $\boldsymbol{C_V}$;

Step 2 Calculate the eigenvalues and eigenvectors of Jacobian matrix of power flow equations. The left eigenvector corresponding to minimum real eigenvalue is the initial left eigenvector;

Step 3 Compute the mismatches in equation (2.15); if the mismatches meet the error requirement, go to step 6; otherwise continue;

Step 4 Form the Jacobian matrix $\boldsymbol{J}$ of extended power flow equations (2.15) with respect to the means of nodal voltage, stability margin and left eigenvector;

Step 5 Calculate the corrections of the means of nodal voltage, stability margin and left eigenvector and correct them; go to step 3;

Step 6 Calculate the covariances of nodal voltage, left eigenvector and stability margin according to equation (2.19). Substitute the covariances in equations (2.15) and calculate the mismatches. If the mismatches meet the error requirement, stop, otherwise go to step 4.

Consequently, the means and covariances of both nodal voltages and stability margin can be determined from the probabilistic computation. The moments of stability margin can be obtained in terms of (2.18) and (2.20).

2.5 The maximum entropy method

Entropy is a measure of uncertainty of a random variable. The entropy H of a discrete random variable X is defined by (Cover, 1991)

$$H = -\sum P(X = x)\ln(P(X = x)) \tag{2.26}$$

For a continuous random variable, the entropy of a probabilistic density function (PDF) $p(x)$ is defined as (Zellner & Highfield, 1988)

$$H = -\int p(x)\ln p(x)dx \tag{2.27}$$

An application of entropy is to determine an unknown distribution based on the principle of maximum entropy, provided that expected values and its other statistical functions are given. The solution by maximum entropy, in its general form(Mohammad-Djafari, 1991), is

$$\begin{aligned} &\max \quad H = -\int p(x)\ln p(x)dx \\ &\text{s.t.} \quad \mathrm{E}\{\varphi_{\mathrm{n}}(x)\} = \int \varphi_{\mathrm{n}}(x)\,p(x)dx = \mu_{\mathrm{n}}, \quad \mathrm{n} = 0,\cdots,N \end{aligned} \tag{2.28}$$

where $\mu_0 = 1, \varphi_0(x) = 1$ and $\varphi_{\mathrm{n}}(x), \mathrm{n} = 1,...N$ are N known functions, and $\mu_{\mathrm{n}}, \mathrm{n} = 1,\cdots,N$ are N given expectation data. The classical solution of this problem is given by

$$p(x) = \exp\left[-\sum_{\mathrm{n}=0}^{N}\lambda_{\mathrm{n}}\varphi_{\mathrm{n}}(x)\right] \tag{2.29}$$

The $N+1$ Lagrange parameters $\boldsymbol{\lambda} = [\lambda_0,\cdots,\lambda_N]$ are obtained by solving the following $N+1$ nonlinear equations,

$$\int \varphi_{\mathrm{n}}(x)\exp\left[-\sum_{\mathrm{n}=0}^{N}\lambda_{\mathrm{n}}\varphi_{\mathrm{n}}(x)\right]dx = \mu_{\mathrm{n}}, \quad \mathrm{n} = 0,\cdots,N \tag{2.30}$$

For example, the maximum entropy is applied to a simple exponential distribution with a PDF of

$$f(x) = \lambda e^{-\lambda x} \tag{2.31}$$

where $x \geq 0, \lambda > 0$. If $\lambda = 4,\ 0 \leq x \leq 4$.

With the PDF, expectations of random variable functions, for example the geometrical moments, can be calculated as listed in Table 2.1. The objective is to determine the distribution of random variable only with known function $\varphi_n(x)$, n=1,…, 4 and expectations of random variable functions $E\{\varphi_n(x)\}=\mu_n$ in Table 2.1. By solving the five nonlinear equations like equation (2.30), the five Lagrange parameters $\boldsymbol{\lambda}= [\lambda_0, \lambda_1, \lambda_2, \lambda_3, \lambda_4]$ in equation (2.29) are obtained. The PDF of random variable x can be obtained as form of equation (2.29) with five known Lagrange parameters $\boldsymbol{\lambda}=[\lambda_0 , \lambda_1, \lambda_2, \lambda_3, \lambda_4]$.

Table 2. 1 Functions and their expectation of random variable

n	0	1	2	3	4
$\varphi_n(x)$	1	x	x^2	x^3	x^4
μ_n	1	0.25	0.125	0.09374	0.09371

The PDF obtained by maximum entropy is then compared with known PDF of exponential distribution in Fig. 2.4. Note that for this simple case, the derived curve and the actual exponential curve almost coincide, and accurate result can be obtained for N=4. This shows that maximum entropy method can determine any unknown distribution with enough available information of random variables.

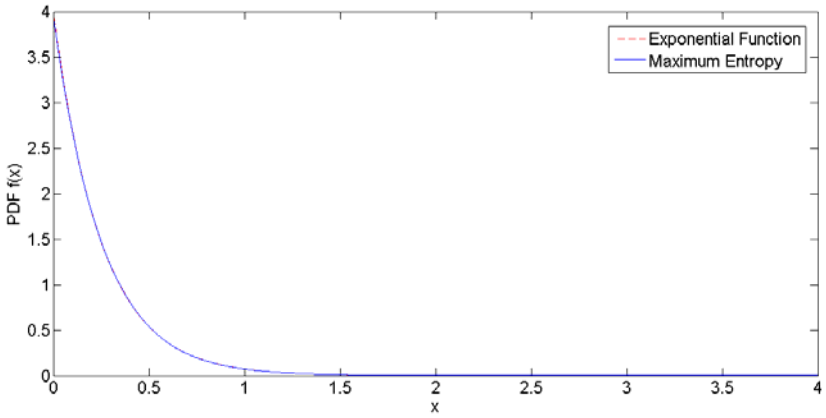

Fig. 2. 4 PDF of exponential distribution

2.6 Applications of probabilistic approach and maximum entropy

The proposed method is investigated on two test systems: a 39-bus (Fig. 2.5) and a 57-bus system. The bus data and line data of these two systems are listed in appendices 3A and 3B respectively. Normal distribution is one of the most common random distributions. In this chapter all active and reactive loads are assumed to be Gaussian random variables. The loads are independent random variables with means at the expected values of bus loading from the original system. The variance of each load (Schellenberg et al., 2006) has been chosen such that the 99% confidence is within ±10% of the normal loading value. The load standard deviation $\sigma_L=0.04\mu$ (μ is expected valued of load) has been used (Aboreshaid, Billinton, & Fotuhi-Firuzabad, 1996) for probabilistic transient stability analysis. In order to study the effect of uncertainty of load on stability margin here, the variance of each load is chosen such that the 99%, 95%, 90%, 85%, 80% confidence are within ±10% of the normal loading value. In other words, the standard deviations of loads are respectively 0.0389μ, 0.0510μ, 0.0606μ, 0.0694μ and 0.0755μ. For simplicity, no

limitations for reactive power of generation or bus voltage levels are assumed first. All the loads are constant power models. The probabilistic stability margin and its distribution are determined by applying probabilistic point of collapse method (section 2.4) and maximum entropy (section 2.5). Monte Carlo simulations, consisting of 10,000 samples, are used to validate the proposed method.

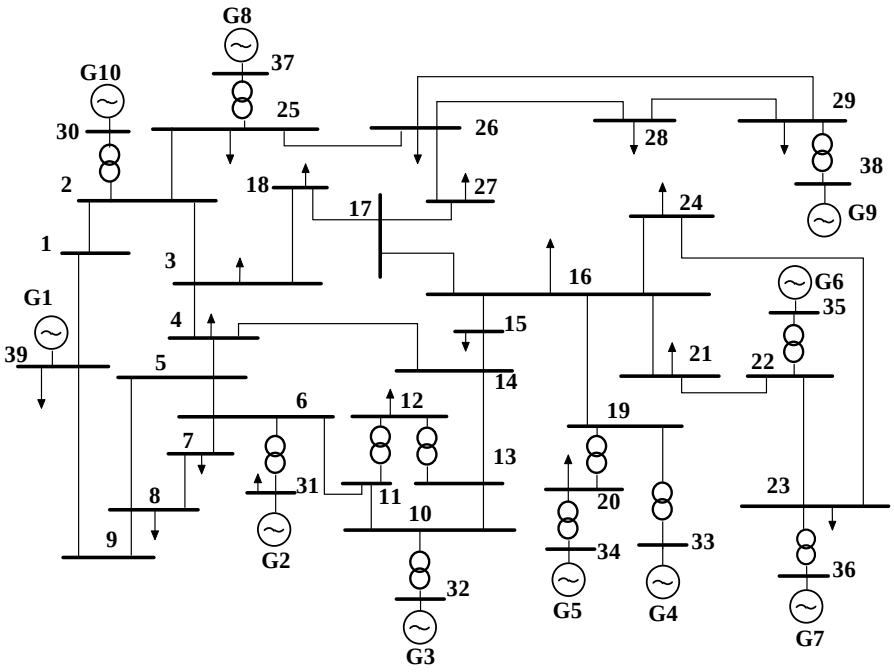

Fig. 2. 5 39-bus system

2.6.1 Case study on 39-bus system

The 39-bus system shown in Fig. 2.5 includes ten generators and 19 loads. As mentioned in section 2.4, two cases of load increase directions are considered.

First, when direction $\boldsymbol{B}$ of load increase is equal to $\overline{\boldsymbol{S}_0}$, with different variances of loads, the means and variances of stability margins listed in Table 2.2 are calculated from equations (2.15) and (2.19) using probabilistic point of collapse method. From Table 2.2, it is observed that when the mean of stability margin has insignificant

changes, the variance of stability margin increases with load variances as expected. Additionally, a stability margin index I_{SM} of, say, 99% is introduced in Table 2.2. For example, I_{SM}=1.2974 in row (a) implies that if the system load is increased by 1.2974$\boldsymbol{B}$ ($\boldsymbol{B} = \overline{\boldsymbol{S}_0}$), 99% of the PDF in Fig. 2.6a has a margin greater than 1.2974 for a system load variance σ_L=0.0389μ. Of course, if the load variance increases, I_{SM} will be reduced.

Table 2. 2 Stability margin for 39-bus system with $\boldsymbol{B} = \overline{\boldsymbol{S}_0}$

	σ_L	Probabilistic Method			Monte Carlo		Difference (%)	
		Mean	Variance (10^{-3})	I_{SM}	Mean	Variance (10^{-3})	Mean	Variance
(a)	0.0389μ	1.3507	0.5232	1.2974	1.3504	0.5249	0.022	0.324
(b)	0.0510μ	1.3500	0.8995	1.2798	1.3495	0.9043	0.037	0.531
(c)	0.0606μ	1.3492	1.2694	1.2658	1.3487	1.2783	0.037	0.696
(d)	0.0694μ	1.3485	1.6667	1.2527	1.3479	1.6815	0.045	0.880
(e)	0.0775μ	1.3476	2.0770	1.2406	1.3470	2.0993	0.045	1.062

To validate the probabilistic method, the mean and variance are compared with those obtained by Monte Carlo method based on 10,000 deterministic load flows (section 2.3). The results listed in Table 2.2 show that their differences in the mean (0.022%-0.045%) are very small, and the differences in variance are between 0.324%-1.062%. It can also be observed that the differences in mean and variance of stability margin increase with variance of loads.

Based on the moments, the PDFs obtained by the maximum entropy approach are plotted with black solid line in Fig. 2.6. Stability margins based on 10,000 samples using Monte Carlo method are obtained and the PDFs are also shown in dotted line in Fig. 2.6. Comparing the two curves obtained by different methods, it is observed

that the difference of two probabilistic density curves will increase when the load variances increase.

Alternately, when the load increase direction $\boldsymbol{B}$ is random, i.e. $\boldsymbol{B} = \boldsymbol{S}_0$, the computed probabilistic characteristics of stability margin by the two methods are also listed in Table 2.3, and the probabilistic distribution of stability margin are shown in Fig. 2.7. Similar to Table 2.2, with σ_L increase, the mean value of stability margin slightly decrease, and the variance of stability margin increases, resulting that index I_{SM} also decreases with variance of loads. The difference in mean value computed using the proposed method and Monte Carlo simulation are well within 0.3%. The difference in variance between the proposed method and Monte Carlo simulation was between 2%-7%.

Table 2. 3 Stability margin for 39-bus system with $\boldsymbol{B} = \boldsymbol{S}_0$

	σ_L	Probabilistic Method			Monte Carlo		Difference (%)	
		Mean	Variance (10^{-3})	I_{SM}	Mean	Variance (10^{-3})	Mean	Variance
(a)	0.0389μ	1.3461	2.8993	1.2204	1.3463	2.8445	0.015	1.926
(b)	0.0510μ	1.3420	4.9693	1.1775	1.3428	4.8131	0.060	3.245
(c)	0.0606μ	1.3381	6.9907	1.1429	1.3395	6.6902	0.104	4.492
(d)	0.0694μ	1.3339	9.1486	1.1107	1.3359	8.6495	0.150	5.770
(e)	0.0775μ	1.3295	11.3617	1.0809	1.3323	10.6158	0.210	7.026

Comparing results on the mean value and variance of stability margin in Table 2.2 and Table 2.3, it can be seen that with the same σ_L, while the mean values in Table 2.2 are slightly higher than those in Table 2.3, the margin variances in Table in 2.2 are much smaller than those in Table 2.3. In other words, with the same σ_L, power

system has smaller mean value and larger variance of stability margin if the direction of load increase is random. Taking σ_L=0.0775μ for example, when load increase $\boldsymbol{B}$ is constant, the mean value and variance of stability margin is 1.3476 and 2.0770×10^{-3}, as compared to 1.3295 and 11.3617×10^{-3} obtained when load increase $\boldsymbol{B}$ is random like the initial injection $\boldsymbol{S}_0$.

It is also observed that with the same σ_L, the differences in mean and variance of stability margins in Table 2.2 are smaller than those in Table 2.3. For example, with σ_L=0.0775μ, the differences in mean and variance of stability margin in Table 2.2 are 0.045% and 1.062 %, less than 0.210% and 7.026% in Table 2.3. These may be attributable to two reasons. One reason is that the covariances $\overline{\Delta\lambda\Delta\boldsymbol{S}_{L0}}$ between stability margin λ and initial load $\boldsymbol{S}_{L0}$ in (2.22a) are ignored because it is difficult to determine their values. The other reason is that the linearilized relationship is used to determine the covariance of stability margin and the increment of loads are $(1+\bar{\lambda})\Delta\boldsymbol{S}_{L0}$ in (2.23) larger than $\Delta\boldsymbol{S}_{L0}$ that in (2.16). These factors may lead to a larger error in mean and covariance of stability margin in Table 2.3.

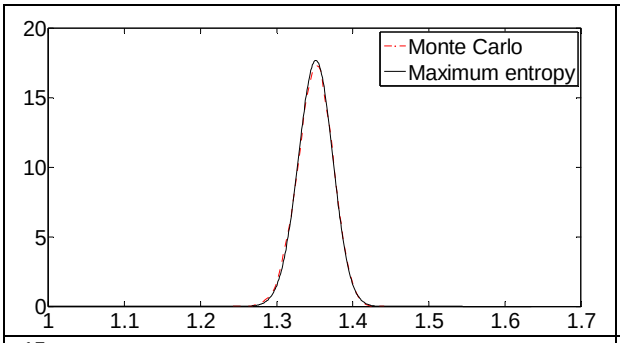	(a) σ=0.0389μ
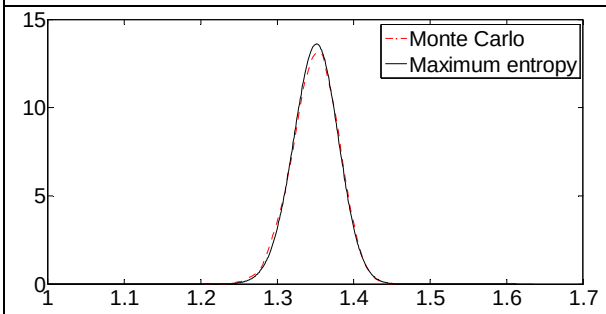	(b) σ=0.0510μ
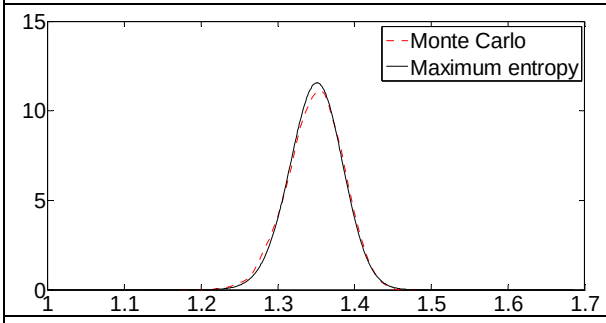	(b) σ=0.0606μ
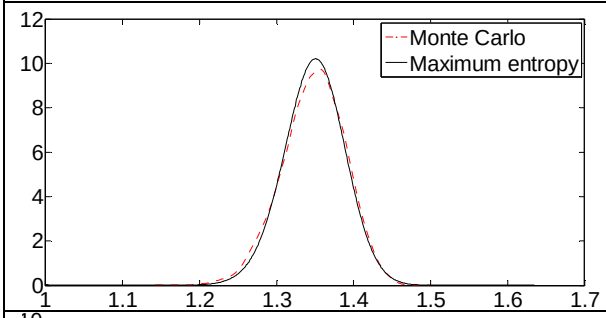	(d) σ=0.0694μ
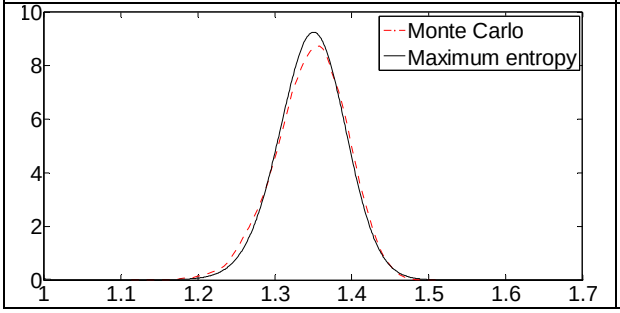	(e) σ=0.0775μ

Fig. 2. 6 Probabilistic distributions of stability margin with different load variance in 39-bus system with $\boldsymbol{B = \overline{S_0}}$

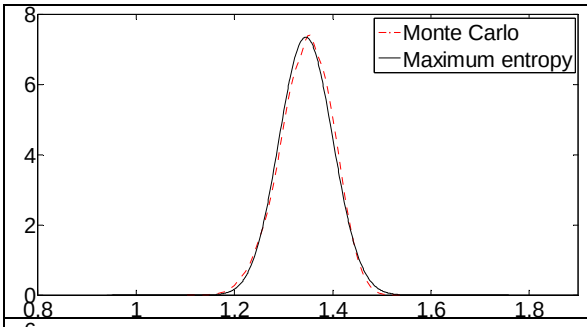	(a) σ=0.0389μ
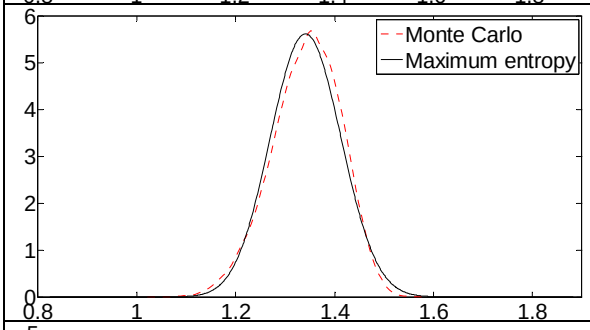	(b) σ=0.0510μ
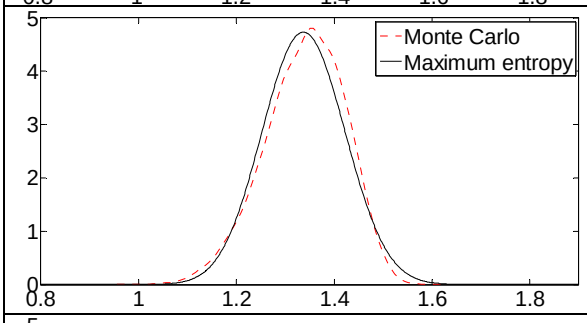	(b) σ=0.0606μ
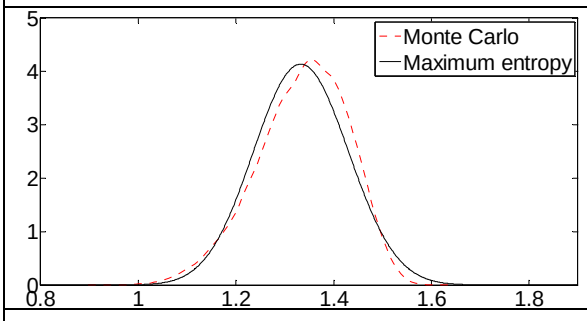	(d) σ=0.0694μ
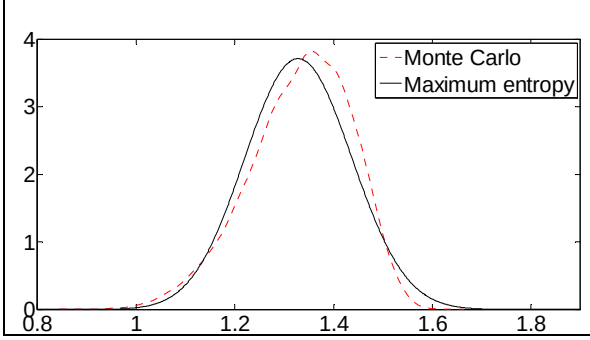	(e) σ=0.0775μ

Fig. 2. 7 Probabilistic distributions of stability margin with different load variance in 39-bus system with $\boldsymbol{B = S_0}$

2.6.2 Case study on 57-bus system

The 57-bus system includes four generating units and three synchronous condensers. Same as the 39-bus system, two cases of load increase directions $\boldsymbol{B} = \overline{\boldsymbol{S}_0}$ and $\boldsymbol{B} = \boldsymbol{S}_0$ are considered. The means and variances of stability margin with different load variances are listed in Table 2.4 and Table 2.5. The probabilistic distributions of stability margin are shown in Fig. 2.8 and 2.9. From Table 2.4 and 2.5, the mean value decreases very little and the covariance increases with load uncertainty. The so-called stability margin index I_{SM} reduces when σ_L increases (i.e. when system uncertainty increases). The mean value and variance of stability margins are also compared with those obtained by Monte Carlo simulation and the differences between two methods are quite small.

Similar to the 39-bus system, while the means of stability margin in Table 2.4 are slightly larger than those in Table 2.5, the variances of stability margin in Table 2.4 are smaller than those in Table 2.5. Nevertheless, the validity of the present probabilistic method is further confirmed, since the differences from the Monte Carlo deterministic method are much reduced in a larger size system of 57 buses.

Table 2. 4 Stability margin for 57-bus system with $\boldsymbol{B} = \overline{\boldsymbol{S}_0}$

	σ_L	Probabilistic Method			Monte Carlo		Difference (%)	
		Mean	Variance (10^{-4})	I_{SM}	Mean	Variance (10^{-4})	Mean	Variance
(a)	0.0389μ	0.80149	0.9553	0.7788	0.80152	0.9552	0.00	0.00
(b)	0.0510μ	0.80139	1.6425	0.7719	0.80143	1.6423	0.00	0.01
(c)	0.0606μ	0.80130	2.3176	0.7663	0.80134	2.3173	0.00	0.01
(d)	0.0694μ	0.80120	3.0429	0.7611	0.80125	3.0423	0.01	0.02
(e)	0.0775μ	0.80110	3.7916	0.7563	0.80115	3.7908	0.01	0.02

Table 2. 5 Stability margin for 57-bus system with $B = S_0$

	σ_L	Probabilistic Method			Monte Carlo		Difference (%)	
		Mean	Variance(10^{-4})	I_{SM}	Mean	Variance (10^{-4})	Mean	Variance
(a)	0.0389μ	0.80119	3.0077	0.7614	0.80129	3.0066	0.01	0.04
(b)	0.0510μ	0.80088	5.1693	0.7489	0.80108	5.1657	0.02	0.07
(c)	0.0606μ	0.80057	7.2915	0.7393	0.80088	7.2840	0.04	0.10
(d)	0.0694μ	0.80024	9.5691	0.7282	0.80066	9.5560	0.05	0.14
(e)	0.0775μ	0.79991	11.9197	0.7195	0.80044	11.8981	0.07	0.18

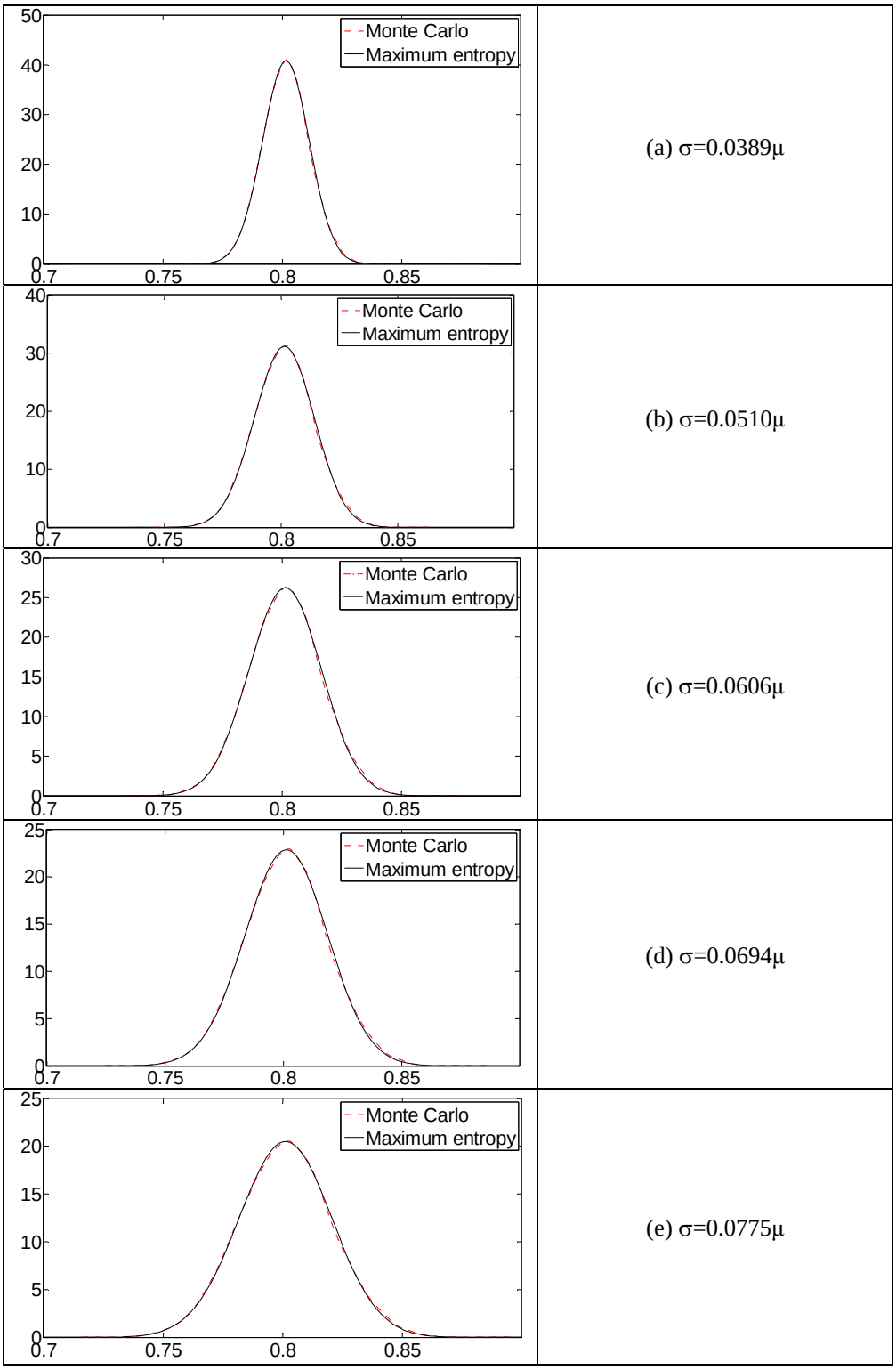

Fig. 2. 8 Probabilistic distributions of stability margin with different load variance in 57-bus system with $\boldsymbol{B} = \overline{\boldsymbol{S_0}}$

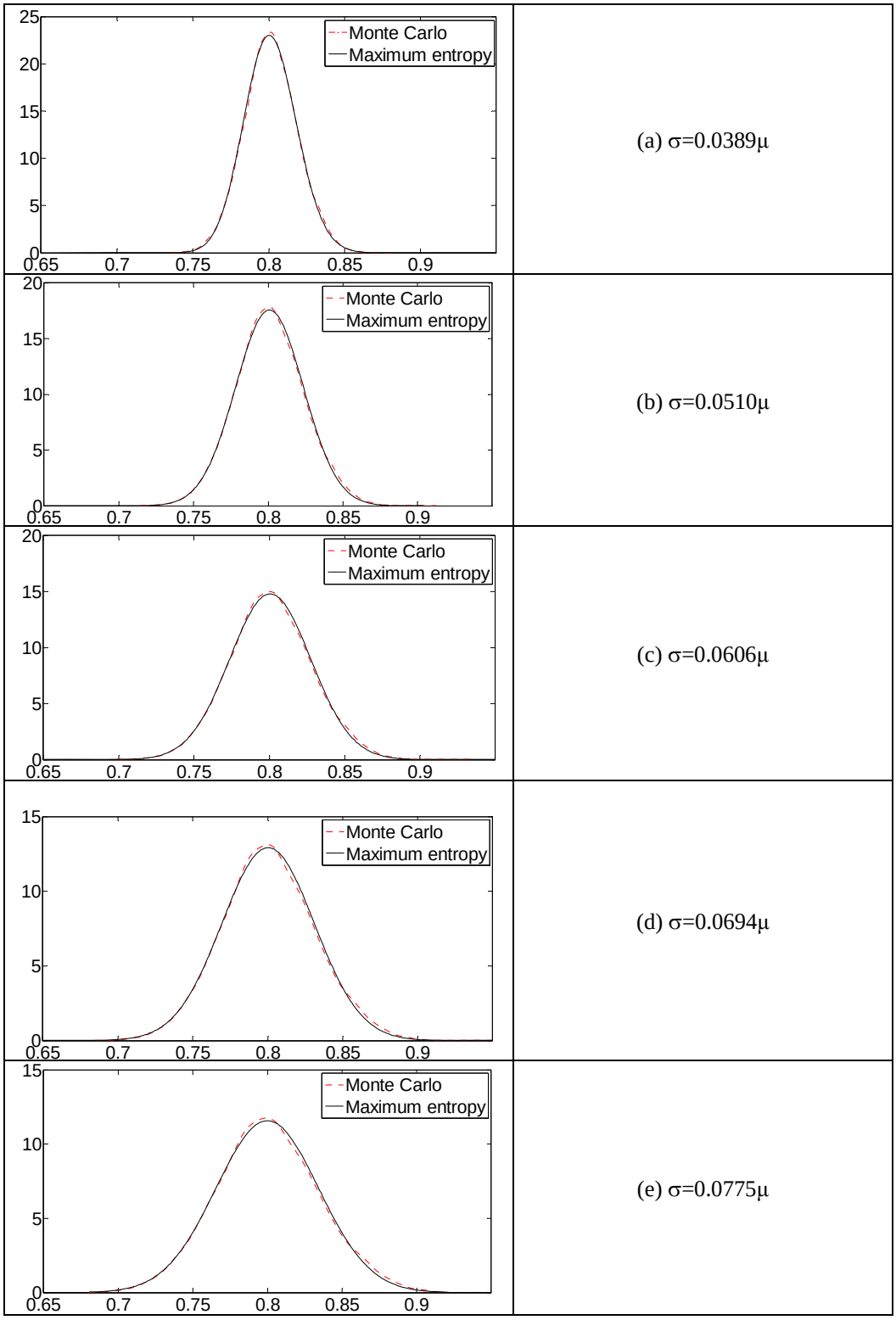

Fig. 2. 9 Probabilistic distributions of stability margin with different load variance in 57-bus system with $\boldsymbol{B = S_0}$

2.7 Summary

This chapter proposes a new probabilistic approach to evaluate the important margin index by taking into account the uncertainty of system loads. Two cases for load increase are considered. One is that load increase direction is constant, i.e. $\boldsymbol{B} = \overline{\boldsymbol{S}_0}$, and the other is that load increase direction is random, i.e. $\boldsymbol{B} = \boldsymbol{S}_0$. With the assumption that all loads are independent Gauss distributions, the prevailed point of collapse method for evaluating stability margin is modified so that the moments of stability margin and critical nodal voltage can be obtained. Maximum entropy technique is then applied to determine the distribution of the stability margin. As expected, the stability margin will be reduced with higher load uncertainty, implying that the stability margins obtained based on traditional deterministic load flows are too 'optimistic'. In addition, when the load increase is random, the variance of stability margin increases. The proposed approach is tested on two test systems. To validate the proposed probabilistic algorithm, the distributions of the stability margin by the proposed method are compared with those by Monte Carlo technique (by 10,000 computation simulation using deterministic method), and the comparison results show they are quite close. As a conclusion, the proposed probabilistic approach (based on single computer run) is very effective and pragmatic to compute the voltage stability margin when there are system uncertainties.

Chapter 3 Determination of probabilistic stability margin considering the uncertainty of loads

3.1 Introduction

Probabilistic voltage stability analysis based on power flow considering the load random variations has been described in chapter 2. However, the voltage instability is a dynamic problem. To consider dynamic elements of power system, dynamic small signal analysis method (Byongjun & Ajjarapu, 1995; Pai, Sauer, Lesieutre, & Adapa, 1995; Rajagopalan, Lesieutre, Sauer, & Pai, 1992) has been presented for voltage stability analysis. Different methods (Wen & Ajjarapu, 2006; Zhou & Ajjarapu, 2005) have been proposed to identify the stability margin. However, these research works are based on deterministic power system condition. In this chapter, load uncertainties will be considered in voltage stability analysis by using probabilistic eigenvalue method to determine the probabilistic stability margin.

Probabilistic eigenvalue algorithm was successfully developed to analyze system small disturbances stability (Wang, Chung, Tse, & Tsang, 2000; Wang, Tse, & Tsang, 1998) and to design and optimize parameters of power system stabilizers (Chung, Wang, Tse, Bian, & David, 2003; Chung, Wang, Tse, & Niu, 2002; Tse, Wang, Chung, & Tsang, 2000, 2001). Different methods (Anders, 1990; Wang, Tse,

& Tsang, 1998; Wang, Chung, Tse, & Tsang, 1998; Wang et al., 2000) for calculation of expectation and covariances of eigenvalues have been presented. This chapter will use the simplest method to determine the expectations and covariances of eigenvalues to obtain the probabilistic stability margin. Deterministic methods based on 10,000 Monte Carlo simulations will be conducted as a reference to validate the proposed method.

3.2 Probabilistic power flow calculation

Probabilistic power flow provides the initial operating state of generators and probabilistic attributes of nodal voltages for probability eigenvalue analysis. This chapter will determine the probabilistic stability margin and probabilistic power flow calculations at different load levels are required. The detail for probabilistic power flow calculation at a load level is as follows.

Power flow equation at load level (1+k) is represented as following equation,

$$\boldsymbol{f}(\boldsymbol{V}) - \boldsymbol{S}_G - \boldsymbol{S}_L = 0 \tag{3.1}$$

where $\boldsymbol{V}$ is vector of nodal voltages. $\boldsymbol{S}_{\mathrm{G}}$ and $\boldsymbol{S}_{\mathrm{L}}$ are generator powers and load powers. System loading is expressed as follows:

$$\boldsymbol{S}_L = (1+k)\boldsymbol{S}_{L0} \tag{3.2}$$

where

$\boldsymbol{S}_{L0}$ stands for original active and reactive load vector;

k is load increase factor.

The load increment is shared by the generator as follows:

$$\boldsymbol{S}_G = \boldsymbol{S}_{G0} + k \cdot \boldsymbol{K}g \tag{3.3}$$

$\boldsymbol{S}_{G0}$ is generation active vector in the base case;

$\boldsymbol{K}_g$ is the rate of change in generation as k varies.

If the nodal voltage is expressed in form of rectangular coordinates, equation (3.1) is represented as,

$$\boldsymbol{f}(V_1V_1,\cdots,V_1V_n,\cdots,V_nV_1,\cdots,V_nV_n) - (\boldsymbol{S}_{G0} + k \cdot \boldsymbol{K}g) - (1+k)\boldsymbol{S}_{L0} = 0 \tag{3.4}$$

The power equation can be expanded at voltage expectation $\overline{\boldsymbol{V}}$ using Taylor series,

$$\begin{aligned}
&\boldsymbol{f}(\overline{V}_1\overline{V}_1,\cdots,\overline{V}_1\overline{V}_n,\cdots,\overline{V}_n\overline{V}_1,\cdots,\overline{V}_n\overline{V}_n)\\
&+\boldsymbol{f}(\Delta V_1\overline{V}_1,\cdots,\Delta V_1\overline{V}_n,\cdots,\Delta V_n\overline{V}_1,\cdots,\Delta V_n\overline{V}_n)\\
&+\boldsymbol{f}(\overline{V}_1\Delta V_1,\cdots,\overline{V}_n\Delta V_1,\cdots,\overline{V}_1\Delta V_n,\cdots,\overline{V}_n\Delta V_n)\\
&+\boldsymbol{f}(\Delta V_1\Delta V_1,\cdots,\Delta V_1\Delta V_n,\cdots,\Delta V_n\Delta V_1,\cdots,\Delta V_n\Delta V_n)\\
&-(\boldsymbol{S}_{G0} + k \cdot \boldsymbol{K}g) - (1+k)\boldsymbol{S}_{L0} = 0
\end{aligned} \tag{3.5}$$

Considering $\overline{\Delta V_i \Delta V_j} = C_{V_{i,j}}$ and $\overline{\Delta \boldsymbol{V}} = \overline{\boldsymbol{V} - \overline{\boldsymbol{V}}} = \overline{\boldsymbol{V}} - \overline{\boldsymbol{V}} = \boldsymbol{0}$ (Bartoszyński, 1996), and only the loads are assumed to be random variables. With $\overline{\boldsymbol{S}}_{G0} = \boldsymbol{S}_{G0}$ and $\overline{\boldsymbol{K}}g = \boldsymbol{K}g$, the expectation of nodal injection is obtained from equation (3.5) as follows,

$$\begin{aligned}
&\boldsymbol{f}(\overline{V}_1\overline{V}_1,\cdots,\overline{V}_1\overline{V}_n,\cdots,\overline{V}_n\overline{V}_1,\cdots,\overline{V}_n\overline{V}_n)\\
&+\boldsymbol{f}(C_{V_{1,1}},\cdots,C_{V_{i,j}},\cdots,C_{V_{n,n}})\\
&-(\boldsymbol{S}_{G0} + k \cdot \boldsymbol{K}g) - (1+k)\overline{\boldsymbol{S}}_{L0} = 0
\end{aligned} \tag{3.6}$$

The expectation of nodal voltage can be obtained by solving equation (3.6) with Newton-Raphson method.

According to the linearized relationship between loads and nodal voltages,

$$\boldsymbol{J}_{\overline{V}}\Delta \boldsymbol{V} = (1+k)(\boldsymbol{S}_{L0} - \overline{\boldsymbol{S}}_{L0}) = (1+k)\Delta \boldsymbol{S}_{L0} \tag{3.7}$$

where,

$\boldsymbol{J}_{\bar{V}} = \left.\dfrac{\partial \boldsymbol{f}}{\partial \boldsymbol{V}}\right|_{V=\bar{V}}$, $\bar{\boldsymbol{S}}_{L0}$ is the given expectation vector of loads.

The covariance of nodal voltages can be obtained in terms of the following equation

$$\boldsymbol{C}_V = (1+k)^2 \boldsymbol{J}_{\bar{V}}^{-1} \boldsymbol{C}_{S_{L0}} (\boldsymbol{J}_{\bar{V}}^{-1})^T \tag{3.8}$$

From equation(3.6), covariances $\boldsymbol{C}_V$ have been taken into account in the calculation of expectations. The effect of $\bar{V}$ on covariance is also considered via $\boldsymbol{J}_{\bar{V}}$ in (3.8).

In probabilistic power flow calculation, according to the different effects of voltage expectations and covariances on the nodal injections, solving expectation of nodal voltages from (3.6) establishes the inner circulation and calculation of covariance of nodal voltage from $\boldsymbol{C}_{S_{L0}}$ is the outer circulation. After probabilistic power flow calculation, the expectation $\bar{V}$ and covariances $\boldsymbol{C}_V$ of nodal voltage are acquired.

Since this work is based on probabilistic eigenvalue analysis, the method adopted for formation of system state matrix in this study, Plug-in Modeling Technique, and eigenvalue sensitivities will be introduced.

3.3 Plug-in modeling technique

Eigenvalue analysis based on the state variables has been widely used for power system dynamic studies. To form the state space equation, many methods (Kundur, 1994; Palmer & Ledwich, 1996; Sauer; & Pai, 1998; Tse & Tso, 1988; Yu, 1983) have been developed for multimachine systems, in which power networks, machines and associated control equipment, such as the excitation system (EXC), governor

system (GOV) and power system stabilizer (PSS), are all included. In most of these methods, transfer functions of linearized machine models and associated controls system are transferred to corresponding differential and algebraic equations. Together with the power network equations, a characteristic coefficient matrix is directly constructed and the state space equation of entire system is obtained by eliminating the non-state variables. This type of technique provides a better insight in the construction of the characteristic coefficient matrix, and the block-matrix techniques can also be efficiently employed.

In this thesis, a highly versatile technique of generalized multimachine representation (GMR) (Tse & Tso, 1988) is adopted to form power system state matrix. In this technique, the differential equations and algebraic equations of networks, machines and associated control equipments are transferred into blocks. This technique was subsequently improved by plug-in modeling technique (PMT) (Chung, Wang, Cheung, Tse, & David, 1998) to model any newly developed power equipment. Comparing with other modeling techniques for multimachine system representation, the outstanding feature of GMR/PMT is that eigenvalue sensitivity with respect to arbitrary parameters can be obtained easily, which is the foundation of probabilistic eigenvalue analysis.

3.3.1 Multimachine system representation technique

In GMR/PMT, the entire system only consists of two types of elementary transfer blocks with 5 types of parameters as shown in Fig. 3.1. All machines and associated

control systems can be derived from these two types of blocks and can be described to any desired degree complexity.

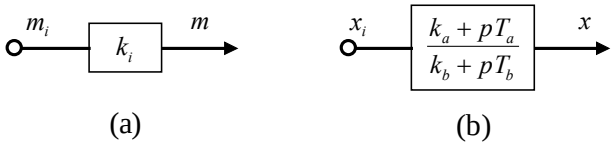

Fig. 3. 1 Two types of elementary transfer blocks

For a system of *m* generators, the multimachine system representation is shown in Fig. 3.2. The control equipments, such as excitation system (EXC), governor (GOV) and PSS, can be amalgamated easily to the machine. Other control devices, such as a static var compensator (SVC) and thyristor controllable series compensator (TCSC), can be easily plugged into the network as shown in Fig 3.2.

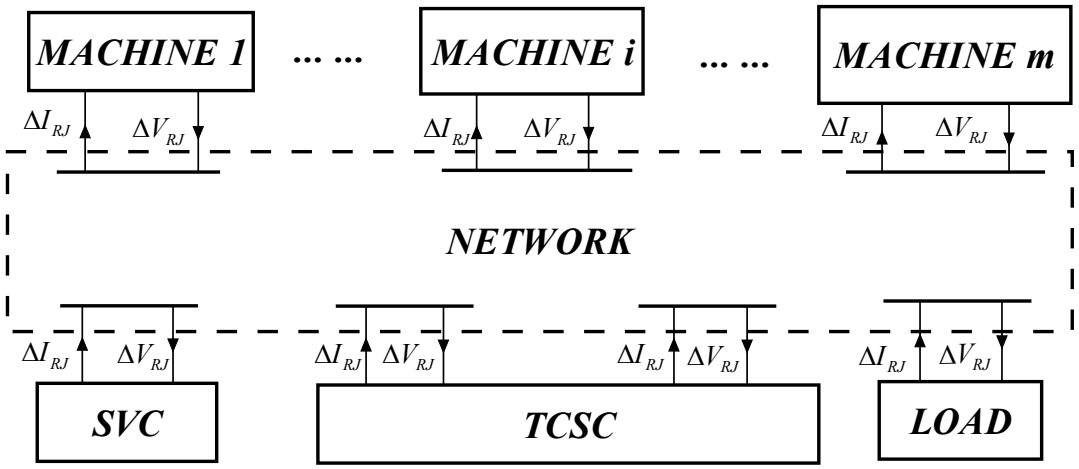

Fig. 3. 2 Overall view of PMT connection

The nodal admittance matrix ***Y*** is usually used to describe the network configuration and parameters of a power system. System loads represented by equivalent admittances are directly merged in the nodal admittance matrix ***Y*** of entire power network (Bian, 2006; Wang, 2000). In order to plug different load models

conveniently in the system, the voltage dependent loads, for example, are also transferred into blocks (see Appendix 2).

3.3.2 State space equation

When all machines and associated control systems are represented only by two types of elementary blocks shown in Fig. 3.1 and connected to power system as shown in Fig. 3.2, a transfer frame for entire system is obtained. To describe the transfer relationship among blocks, a connecting matrix $\boldsymbol{L}$ composed of nine submatrices is constructed as (3.9)

$$\begin{bmatrix} \boldsymbol{X}_i \\ \boldsymbol{Y}_o \\ \boldsymbol{M}_i \end{bmatrix} = \begin{bmatrix} \boldsymbol{L}_1 & \boldsymbol{L}_2 & \boldsymbol{L}_3 \\ \boldsymbol{L}_4 & \boldsymbol{L}_5 & \boldsymbol{L}_6 \\ \boldsymbol{L}_7' & \boldsymbol{L}_8' & \boldsymbol{L}_9' \end{bmatrix} \begin{bmatrix} \boldsymbol{X} \\ \boldsymbol{R} \\ \boldsymbol{M} \end{bmatrix} \tag{3.9}$$

where $\boldsymbol{X}_i$ and $\boldsymbol{X}$ are input/output vectors for first order blocks in Fig.3.1 (b); $\boldsymbol{M}_i$ and $\boldsymbol{M}$ are input/output vectors for zero order blocks in Fig. 3.1 (a); $\boldsymbol{Y}_o$ and $\boldsymbol{R}$ are input/output vectors .

Suppose that $\boldsymbol{K}$ is a diagonal matrix collecting all parameters in zero order blocks such that

$$\boldsymbol{M} = \boldsymbol{K}\boldsymbol{M}_i \tag{3.10}$$

Substituting the last row of equation (3.9) in (3.10) gives

$$\boldsymbol{M} = \boldsymbol{K}\boldsymbol{L}_7'\boldsymbol{X} + \boldsymbol{K}\boldsymbol{L}_8'\boldsymbol{R} + \boldsymbol{K}\boldsymbol{L}_9'\boldsymbol{M} \tag{3.11}$$

Therefore equation (3.9) can be rewritten as

$$\begin{bmatrix} \boldsymbol{X}_i \\ \boldsymbol{Y}_o \\ \boldsymbol{0} \end{bmatrix} = \begin{bmatrix} \boldsymbol{L}_1 & \boldsymbol{L}_2 & \boldsymbol{L}_3 \\ \boldsymbol{L}_4 & \boldsymbol{L}_5 & \boldsymbol{L}_6 \\ \boldsymbol{L}_7 & \boldsymbol{L}_8 & \boldsymbol{L}_9 \end{bmatrix} \begin{bmatrix} \boldsymbol{X} \\ \boldsymbol{R} \\ \boldsymbol{M} \end{bmatrix} \tag{3.12}$$

where $\boldsymbol{L}_7 = \boldsymbol{K}\boldsymbol{L}_7^{'}$, $\boldsymbol{L}_8 = \boldsymbol{K}\boldsymbol{L}_8^{'}$, $\boldsymbol{L}_9 = \boldsymbol{K}\boldsymbol{L}_9^{'} - \boldsymbol{I}$. $\boldsymbol{I}$ stands for identity matrix.

In(3.12), submatrices $\boldsymbol{L}_1$ to $\boldsymbol{L}_3$ are composed of zeros and ones, whilst $\boldsymbol{L}_7$ and $\boldsymbol{L}_9$ describe the algebraic relationship from which the eigenvalue sensitivity expression is developed.

The first order transfer block in Fig. 3.1(b) can be represented as

$$(\boldsymbol{K}_b + p)\boldsymbol{X} = (\boldsymbol{K}_a + p\boldsymbol{K}_t)\mathbf{X}_i \tag{3.13}$$

where, $\boldsymbol{K}_a$, $\boldsymbol{K}_b$ and $\boldsymbol{K}_t$ are diagonal matrices collecting parameters k_a/T_b, k_b/T_b and T_a/T_b in Fig.2(b) respectively. The state space equation (3.14) is obtained by eliminating the non-state vector $\boldsymbol{M}$, $\boldsymbol{M}_i$ and $\boldsymbol{X}_i$ from (3.12) and (3.13),

$$\begin{cases} \dot{\boldsymbol{X}} = \boldsymbol{A}\boldsymbol{X} + \boldsymbol{B}\boldsymbol{R} + \boldsymbol{E}\dot{\boldsymbol{R}} \\ \boldsymbol{Y}_o = \boldsymbol{C}\boldsymbol{X} + \boldsymbol{D}\boldsymbol{R} \end{cases} \tag{3.14}$$

where

$$\boldsymbol{A} = \boldsymbol{S}(\boldsymbol{K}_a\boldsymbol{F} - \boldsymbol{K}_b) \tag{3.15}$$

$$\boldsymbol{B} = \boldsymbol{S}\boldsymbol{K}_a(\boldsymbol{L}_2 + \boldsymbol{L}_3\boldsymbol{H}\boldsymbol{L}_7) \tag{3.16}$$

$$\boldsymbol{E} = \boldsymbol{S}\boldsymbol{K}_t(\boldsymbol{L}_2 + \boldsymbol{L}_3\boldsymbol{H}\boldsymbol{L}_8) \tag{3.17}$$

$$\boldsymbol{C} = \boldsymbol{L}_4 + \boldsymbol{L}_6\boldsymbol{H}\boldsymbol{L}_7 \tag{3.18}$$

$$\boldsymbol{D} = \boldsymbol{L}_5 + \boldsymbol{L}_6\boldsymbol{H}\boldsymbol{L}_8 \tag{3.19}$$

with

$$\boldsymbol{S} = (\boldsymbol{I} - \boldsymbol{K}_t\boldsymbol{F})^{-1} \tag{3.20}$$

$$\boldsymbol{F} = \boldsymbol{L}_1 + \boldsymbol{L}_3\boldsymbol{H}\boldsymbol{L}_7 \tag{3.21}$$

$$\boldsymbol{H} = -\boldsymbol{L}_9^{-1} \tag{3.22}$$

Eigenvalues and eigenvectors will be solved from $\boldsymbol{A}$.

3.4 Eigenvalue sensitivities

3.4.1 General formulas of eigenvalue sensitivities

With the left and right eigenvectors $\boldsymbol{W}_k$ and $\boldsymbol{U}_k$ satisfying $\boldsymbol{W}_k^T\boldsymbol{U}_k = 1$, κ_i and κ_j standing for parameter variables, the general representations for the first and second order eigenvalue sensitivities are ,

$$\frac{\partial \lambda_k}{\partial \kappa_i} = \boldsymbol{W}_k^T \frac{\partial \boldsymbol{A}}{\partial \kappa_i}\boldsymbol{U}_k \tag{3.23}$$

$$\frac{\partial^2 \lambda_k}{\partial \kappa_i \partial \kappa_j} = \boldsymbol{W}_k^T \frac{\partial^2 \boldsymbol{A}}{\partial \kappa_i \partial \kappa_j}\boldsymbol{U}_k + \frac{\partial \boldsymbol{W}_k^T}{\partial \kappa_i}\frac{\partial \boldsymbol{A}}{\partial \kappa_j}\boldsymbol{U}_k + \frac{\partial \boldsymbol{W}_k^T}{\partial \kappa_j}\frac{\partial \boldsymbol{A}}{\partial \kappa_i}\boldsymbol{U}_k \tag{3.24}$$

For a system of n eigenvalues, the derivative of left eigenvector $\boldsymbol{W}_k^T$ is a linear combination of all eigenvectors

$$\frac{\partial \boldsymbol{W}_k^T}{\partial \kappa_i} = \sum_{\substack{m=1 \\ m\neq k}}^{n}\left(\frac{1}{\lambda_k - \lambda_m}\boldsymbol{W}_k^T \frac{\partial \lambda}{\partial \kappa_i}\boldsymbol{U}_m\boldsymbol{W}_m^T \right) \tag{3.25}$$

From the equation (3.23) and (3.24), derivative of matrix $\boldsymbol{A}$ are required and will be determined from equation (3.15), (3.20), (3.21) and (3.22). Because the first order block parameters in multimachine representation are collected by diagonal matrices $\boldsymbol{K_a}$, $\boldsymbol{K_b}$, and $\boldsymbol{K_t}$ in (3.13), while the zero order block parameters appear in $\boldsymbol{L}_7$ and $\boldsymbol{L}_9$, the determination of derivatives of matrix $\boldsymbol{A}$ will be divided into two types.

3.4.2 Derivatives of matrix *A* with regard to zero order block parameters

Derivatives of matrix $\boldsymbol{A}$ are required and will be determined from equation (3.15), (3.20), (3.21) and (3.22) as

$$\frac{\partial \boldsymbol{A}}{\partial \kappa_i} = \boldsymbol{S}\boldsymbol{K}_t \frac{\partial \boldsymbol{F}}{\partial \kappa_i}\boldsymbol{A} + \boldsymbol{S}\boldsymbol{K}_a \frac{\partial \boldsymbol{F}}{\partial \kappa_i} \tag{3.26}$$

$$\frac{\partial^2 \boldsymbol{A}}{\partial \kappa_i \partial \kappa_j} = \boldsymbol{S}\boldsymbol{K}_t \left(\frac{\partial \boldsymbol{F}}{\partial \kappa_i}\frac{\partial \boldsymbol{A}}{\partial \kappa_j} + \frac{\partial \boldsymbol{F}}{\partial \kappa_j}\frac{\partial \boldsymbol{A}}{\partial \kappa_i} \right) + \boldsymbol{S}\left(\boldsymbol{K}_t \frac{\partial^2 \boldsymbol{F}}{\partial \kappa_i \partial \kappa_j}\boldsymbol{A} + \boldsymbol{K}_a \frac{\partial^2 \boldsymbol{F}}{\partial \kappa_i \partial \kappa_j} \right) \tag{3.27}$$

where

$$\frac{\partial \boldsymbol{F}}{\partial \kappa_i} = \boldsymbol{L}_3 \boldsymbol{H} \boldsymbol{L}_7 \left(\frac{\partial \boldsymbol{L}_9}{\partial \kappa_i}\boldsymbol{H}\boldsymbol{L}_7 + \frac{\partial \boldsymbol{L}_7}{\partial \kappa_i} \right) \tag{3.28}$$

$$\begin{aligned} \frac{\partial^2 \boldsymbol{F}}{\partial \kappa_i \partial \kappa_j} = \boldsymbol{L}_3 \boldsymbol{H} \Bigg[& \left(\frac{\partial^2 \boldsymbol{L}_9}{\partial \kappa_i \partial \kappa_j}\boldsymbol{H}\boldsymbol{L}_7 + \frac{\partial^2 \boldsymbol{L}_7}{\partial \kappa_i \partial \kappa_j} \right) \\ & + \frac{\partial \boldsymbol{L}_9}{\partial \kappa_i}\boldsymbol{H}\left(\frac{\partial \boldsymbol{L}_9}{\partial \kappa_j}\boldsymbol{H}\boldsymbol{L}_7 + \frac{\partial \boldsymbol{L}_7}{\partial \kappa_j} \right) + \frac{\partial \boldsymbol{L}_9}{\partial \kappa_j}\boldsymbol{H}\left(\frac{\partial \boldsymbol{L}_9}{\partial \kappa_i}\boldsymbol{H}\boldsymbol{L}_7 + \frac{\partial \boldsymbol{L}_7}{\partial \kappa_i} \right) \Bigg] \end{aligned} \tag{3.29}$$

The derivatives of submatrices $\boldsymbol{L}_7$ and $\boldsymbol{L}_9$ are complex to determine and are described in detail (Wang, 2000).

3.4.3 Derivatives of matrix *A* with regard to first order block parameters

The first order block parameters may be k_a, k_b, T_a or T_b in the first order block of Fig. 3.1(b). Because k_a/T_b, k_b/T_b and T_a/T_b have been collected in diagonal marices $\boldsymbol{K}_a$, $\boldsymbol{K}_a$ and $\boldsymbol{K}_t$ respectively in equation (3.13), derivatives of system matrix $\boldsymbol{A}$ with regard to k_a, k_b, T_a and T_b are derived from equation (3.15), (3.20), (3.21) and (3.22) as

$$\frac{\partial \boldsymbol{A}}{\partial k_{ai}} = -\boldsymbol{S}\frac{\partial \boldsymbol{K}_a}{\partial k_{ai}}\boldsymbol{F} \tag{3.30}$$

$$\frac{\partial \boldsymbol{A}}{\partial k_{bi}} = -\boldsymbol{S}\frac{\partial \boldsymbol{K}_b}{\partial k_{bi}} \tag{3.31}$$

$$\frac{\partial \boldsymbol{A}}{\partial T_{ai}} = \boldsymbol{S}\frac{\partial \boldsymbol{K}_t}{\partial T_{ai}}\boldsymbol{F}\boldsymbol{A} \tag{3.32}$$

$$\frac{\partial \boldsymbol{A}}{\partial T_{bi}} = -\frac{\partial \boldsymbol{A}}{\partial k_{ai}}\frac{\partial k_{ai}}{\partial T_{bi}} - \frac{\partial \boldsymbol{A}}{\partial k_{bi}}\frac{\partial k_{bi}}{\partial T_{bi}} - \frac{\partial \boldsymbol{A}}{\partial T_{ai}}\frac{\partial T_{ai}}{\partial T_{bi}} \tag{3.33}$$

where, the subscript '*i*' denotes the *i*-th first order block, matrices $\boldsymbol{S}$ and $\boldsymbol{F}$ were defined in (3.20) and (3.21). Because a first order block parameter appears in $\boldsymbol{K}_a$, $\boldsymbol{K}_b$, $\boldsymbol{T}_a$ and $\boldsymbol{T}_b$ only once, each of $\partial \boldsymbol{K}_a / \partial k_{ai}$, $\partial \boldsymbol{K}_b / \partial k_{bi}$ and $\partial \boldsymbol{T}_a / \partial T_{ai}$ in (3.30)-(3.33) has only one non-zero element $1/T_{bi}$ on the *i*-th diagonal (*i*, *i*).

3.5 Probabilistic stability analyses

3.5.1 Probabilistic characteristics of eigenvalue

Because nodal voltages and loads are random variables, eigenvalues are random variables. For determination of eigenvalue expectation and covariance, different methods have been used.

Method I

A particular complex eigenvalue λ_k can also be analytically expressed as a nonlinear function of the nodal voltage vector $\boldsymbol{V}$ as

$$\lambda_k = G_k(\boldsymbol{V}) \tag{3.34}$$

in which nodal voltage are defined in rectangular form and the voltage vector $\boldsymbol{V}$ contains 2N real components as $\boldsymbol{V} = [V_1, V_2, \cdots, V_{2N}]^T$ in a power system of N nodes. The general nonlinear function can be linearized using a first-order Taylor series expansion at $\overline{\boldsymbol{V}}$,

$$\lambda_k \approx G_k(\overline{\boldsymbol{V}}) + \sum_{i=1}^{2N} \left(\frac{\partial \lambda_k}{\partial V_i}\bigg|_{\boldsymbol{V}=\overline{\boldsymbol{V}}} \Delta V_i \right) \tag{3.35}$$

Taking expectation in both sides of (3.35), considering $\overline{\Delta V_i} = 0$ (for i=1,2, ..., 2N), the eigenvalue mean can be approximately obtained by:

$$\overline{\lambda}_k \approx G_k(\overline{\boldsymbol{V}}) \tag{3.36}$$

According to the linearised relationship between the eigenvalue vector $\boldsymbol{\lambda}$ and the nodal voltage vector $\boldsymbol{V}$, the covariance matrix $\boldsymbol{C}_\lambda$ of $\boldsymbol{\lambda}$ is obtained from the covariance matrix $\boldsymbol{C}_V$ of nodal voltage $\boldsymbol{V}$ as (Anders, 1990; Burchett & Heydt, 1978; Wang, Tse et al., 1998)

$$\boldsymbol{C}_\lambda = \boldsymbol{J}_{\lambda,V} \boldsymbol{C}_V \boldsymbol{J}_{\lambda,V}^T \tag{3.37}$$

where, $\boldsymbol{J}_{\lambda,V}$ is the first order eigenvalue sensitivity matrix with respect to nodal voltage $\boldsymbol{V}$.

Method II (Wang et al., 2000)

If (3.34) is expanded in Taylor series with second order terms retained as,

$$\lambda_k \approx G_k(\overline{\boldsymbol{V}}) + \sum_{i=1}^{2N} \left(\frac{\partial \lambda_k}{\partial V_i}\bigg|_{\boldsymbol{V}=\overline{\boldsymbol{V}}} \Delta V_i \right) + \frac{1}{2} \sum_{i=1}^{2N} \sum_{j=1}^{2N} \left(\frac{\partial^2 \lambda_k}{\partial V_i \partial V_j}\bigg|_{\boldsymbol{V}=\overline{\boldsymbol{V}}} \Delta V_i \Delta V_j \right) \tag{3.38}$$

where $G_k(\overline{\boldsymbol{V}})$ is solved from state matrix $\boldsymbol{A}$ with nodal voltages set at their expectations. Considering $\overline{\Delta V_i} = 0$ (for i=1,2, ..., 2N) and the nodal voltage

covariance $\overline{\Delta V_i \Delta V_j} = C_{V_{i,j}}$ between V_i and V_j, the expectation of eigenvalue λ_k is expressed as,

$$\bar{\lambda}_k \approx G_k(\bar{\boldsymbol{V}}) + \frac{1}{2}\sum_{i=1}^{2N}\sum_{j=1}^{2N}\left(\frac{\partial^2 \lambda_k}{\partial V_i \partial V_j}\bigg|_{\boldsymbol{V}=\bar{\boldsymbol{V}}} C_{V_{i,j}}\right) \tag{3.39}$$

From (3.39), the effect of covariance has been considered in the calculation of eigenvalue expectation. The eigenvalue covariance between eigeavalues λ_m and λ_n is calculated from the following equation

$$C_{\lambda_{m,n}} = E[(\lambda_m - \bar{\lambda}_m)(\lambda_n - \bar{\lambda}_n)] \tag{3.40}$$

Substituting (3.35) and (3.39) into (3.40) gives,

$$C_{\lambda_{mn}} = \sum_{i=1}^{2N}\sum_{j=1}^{2N}(J_{\lambda_{m,i}} J_{\lambda_{n,j}} C_{V_{ij}}) + H_m H_n \tag{3.41}$$

where $H_m = \frac{1}{2}\sum_{i=1}^{2N}\sum_{j=1}^{2N}\left(\frac{\partial^2 \lambda_m}{\partial V_i \partial V_j}\bigg|_{\boldsymbol{V}=\bar{\boldsymbol{V}}} C_{V_{i,j}}\right)$ and $H_n = \frac{1}{2}\sum_{i=1}^{2N}\sum_{j=1}^{2N}\left(\frac{\partial^2 \lambda_n}{\partial V_i \partial V_j}\bigg|_{\boldsymbol{V}=\bar{\boldsymbol{V}}} C_{V_{i,j}}\right)$.

Method III (Wang, Tse et al., 1998)

From GMR/PMT technique, state coefficient matrix $\boldsymbol{A}$ can be regarded as a nonlinear function of nodal voltage as

$$\boldsymbol{A} = \boldsymbol{G}_A(\boldsymbol{V}) \tag{3.42}$$

The expectation of state matrix can be corrected by voltage covariances as

$$\bar{\boldsymbol{A}} \approx \bar{\boldsymbol{A}}_0 + \frac{1}{2}\sum_{i=1}^{2N}\sum_{j=1}^{2N}\left(\frac{\partial^2 \boldsymbol{A}}{\partial V_i \partial V_j}\bigg|_{\boldsymbol{V}=\bar{\boldsymbol{V}}} C_{V_{i,j}}\right) \tag{3.43}$$

$\bar{\boldsymbol{A}}_0$ is determined from the expectation of nodal voltages. Eigenvalue expectation vector $\bar{\lambda}$ is then calculated from $\bar{\boldsymbol{A}}$.

The covariance matrix $\boldsymbol{C}_{\lambda}$ of eigenvalue is obtained from the covariance matrix $\boldsymbol{C}_{V}$ of nodal voltage $\boldsymbol{V}$ as (3.37).

Although different methods have been developed to determine the expectation and covariance of eigenvalue, only method I will be adopted in this chapter. Due to calculation of the second order sensitivity of matrix $\boldsymbol{A}$ or eigenvalue with regard to nodal voltages, method II and method III need much more calculation effort. Taking calculation requirement into account, method I is employed to determine the expectation and covariance of eigenvalue.

3.5.2 Assessment criterion of stability probability

According to (3.36) and (3.37), the means and covariances of eigenvalues of system state matrix can be obtained. If loads are normally distributed, then eigenvalues are approximately normal distribution from the linear relationship (Anders, 1990). In this study, eigenvalues are assumed normal distribution. The stability probability of power system can be determined from the most critical eigenvlaues λ_k, according to (3.44) (Wang, Tse et al., 1998)

$$P\{\alpha_k < 0\} = \int_{-\infty}^{0} f(a_k)da_k \tag{3.44}$$

where α_k is the real part of the λ_k, and $f(a_k)$ is the probabilistic density function of λ_k. In angular stability, to ensure system stability being adequate in wide range of operation, a high reliable index of $4\sigma_{\alpha_k}$ has been employed (Chung et al., 2003; Chung et al., 2002; Tse et al., 2000) such that the stability probability under the

distribution range $\{-\infty, \bar{\alpha}_k + 4\sigma_{\alpha_k}\}$ is $P\{\alpha_k<0\}=0.99997$. i.e. if $\bar{\alpha}_k + 4\sigma_{\alpha_k} \leq 0$, 99.997% of operation scenarios will not experience system instability. For voltage instability, however, an alternate probabilistic assessment criterion for voltage stability is employed.

3.5.3 Load margin for probabilistic voltage stability

Load margin is a reasonable measure to the bifurcation-related instability, defined as the amount of additional load on a specified pattern of load increase that would cause system instability (Zhou & Ajjarapu, 2005). If the initial operating point and load increase are specific, the stability margin is specific and can be obtained easily. However, if the loads at current point are random variables, the stability margin is also random. For illustration, consider a system which is very stable. If the load level is increased to load level (1+k)=1.8443, the distribution of the critical eigenvalue in Fig. 3.3a shows that 99% of scenarios are stable. In other words, 99% scenarios have stability margin higher than 0.8443. If the load is further increased to (1+k)=1.8714 (Fig. 3.3b), 50% of scenarios are stable. In other words, 50% scenarios have stability margin higher than 0.8714. Likewise, the 'load margin' can be obtained for any specified percentage scenario (cumulative), as shown in Table 3.1, from which the distribution of the load margin can be derived in Fig. 3.4. Note that, whilst the eigenvalue in Fig. 3.3 is assumed normal distribution (for normal distributed load); the distribution of the load margin of Fig.3.4 is not symmetric.

Table 3. 1 Probabilistic stability margin with different probability requirement

Cumulative Density	Probabilistic stability margin
99%	0.8443
90%	0.8556
80%	0.8606
70%	0.8646
60%	0.8681
50%	0.8714
40%	0.8748
30%	0.8787
20%	0.8833
10%	0.8902
1%	0.9093

For normal distribution of critical eigenvalue, the degree of voltage stability at a certain operating point can be fully depicted by the mean and standard deviation: $\bar{\alpha}$ and σ_α. However to assess the stability margin, the entire distribution (such at Fig. 3.4 or Table 3.1) may be necessary since the distribution is asymmetric. For simplicity, the margin distribution will be reflected by the two most key indices: I_{SM} and k_c, corresponding to 99% and 50% stable scenarios of Fig. 3.3a and Fig. 3.3b (each with different $\bar{\alpha}$ and σ_α). These two indices will be employed to assess the voltage stability in the present thesis.

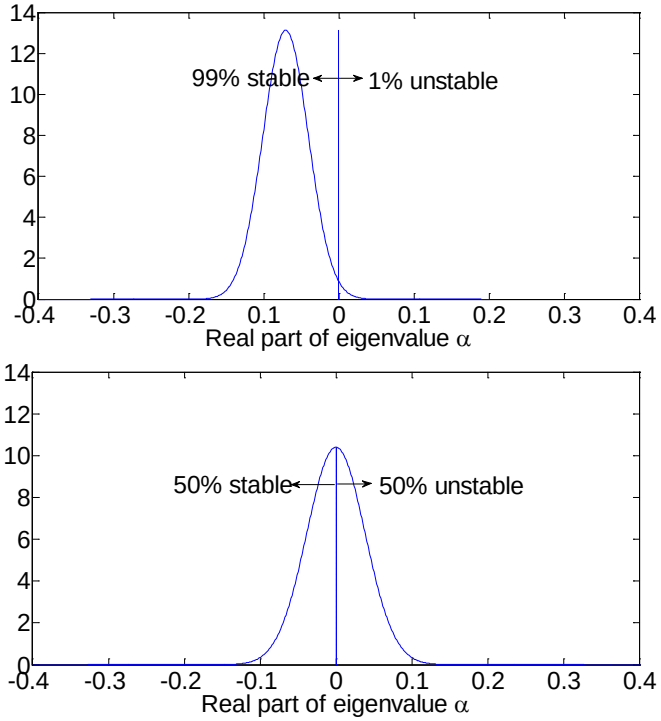

(a) $\bar{\alpha}$ **=-0.0707 and**

σ_α **= 0.0303 at**

load level (1+k)=1.8443

(b) $\bar{\alpha}$ **=0.0 and**

σ_α **= 0.0383**

at load level(1+k)=1.8714

Fig. 3. 3 Probabilistic density function of a critical eigenvalue for σ_L=0.0389μ

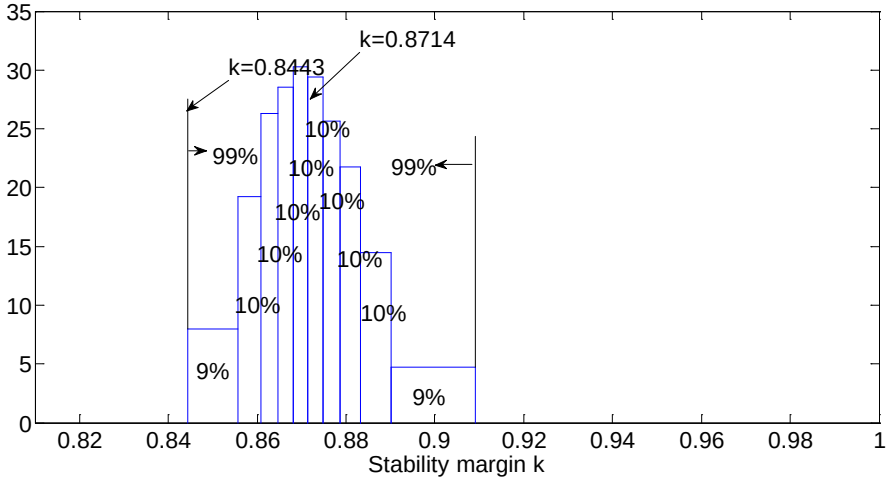

Fig. 3. 4 Distribution of stability margin of 9-bus system for σ_L=0.0389μ (without reactive limit of generator)

3.5.4 Probabilistic load characteristics

Loads having normal distribution characteristic are commonly adopted for probabilistic stability analysis (Aboreshaid, Billinton, & Fotuhi-Firuzabad, 1996; Schellenberg, Rosehart, & Aguado, 2006), and the distribution can be adequately

described in terms of two parameters: mean and standard deviation. In probabilistic stability analysis (Aboreshaid, Billinton, & Fotuhi-Firuzabad, 1996; Schellenberg, Rosehart, & Aguado, 2006), the normal bus loading is often regarded as mean value μ for the random load. To describe the load uncertainty, 4% standard deviation σ (Aboreshaid et al., 1996) and 99% 'confidence' (Schellenberg et al., 2006) have been used. 99% 'confidence' implies that 99% of loads are within ±10% deviation from μ, corresponding $\sigma=0.0389\mu$, slightly less than $\sigma=4\%$. (Note: this 99% confidence is not the 99% scenario of I_{SM} described in Section 3.5.3.) In this chapter, 'confidences' of 99%, 95%, 90%, 85% and 80% (for load deviation within ±10% from μ) will be used, corresponding standard deviations σ_L of 0.0389μ, 0.0510μ, 0.0606μ, 0.0694μ and 0.0775μ respectively. The lower the confidence (say 80%), the larger is σ_L and the smaller is the 'density' within ±10%, implying the higher is the load uncertainty.

3.6 Case studies

The proposed method to determine the probabilistic stability margin is to be validated on two systems: a 9-bus system and a 39-bus system.

3.6.1 Test system I

The 9-bus system (Fig. 3.5) consists of three generator buses (7, 8, 9), three load buses (4, 5, 6) and three connecting buses (1, 2, 3). In the analysis, the fourth order generator model and IEEE type I excitation system are adopted. Network parameters, nodal data and controller parameters are listed in Appendix 3. Constant power load model is adopted for all loads.

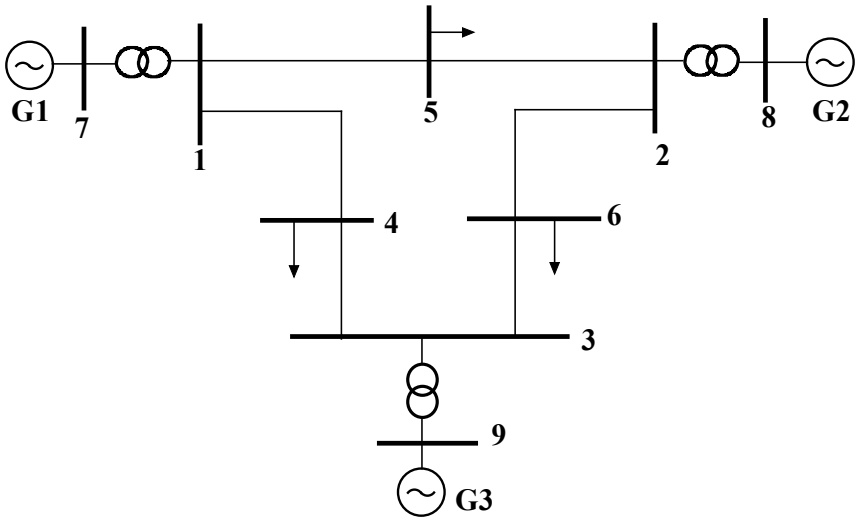

Fig. 3. 5 9-bus system

The present study is first started with σ_L=0.0389μ. Using probabilistic power flow calculation, the probabilistic characteristics of nodal voltages are obtained, and the expectation and the convariances of eigenvalues are evaluated according to (3.36) and (3.37). The real part $\bar{\alpha}$ of a complex eigenvalue increases and becomes positive at load level (1+k) =1.8714 (Fig. 3.3b) and Hopf bifurcation occurs. (This complex eigenvalue is associated with E'_{q3} and E_{fd3} and Hopf bifurcation point is regarded as the critical point in the present work). In other words, if a stability margin k is evaluated using expectation of eigenvalue, it only guarantees 50% scenario being stable at that load level (1+k). To be more pragmatic, the present study will introduce a scenario of 99% (Fig. 3.3a), and this k value is termed as stability margin index I_{SM} in order to distinguish from other k. Likewise, 50% scenario is termed as k_c in the present study. Taking scenario of 99% as example, the process to determine the probabilistic stability margin I_{SM} is described as follows.

After probabilistic power flow calculation of the expectation and covariance of nodal voltages at a load level, according to sections 3.5.1 and 3.5.2, the stability probability of power system can be determined at load level 1+k. If the stability probability is larger than 99%, then increase load factor k; otherwise, decrease load factor k, until the stability probability at load level 1+k is 99%, and I_{SM} equals to this k value.

To validate the proposed probabilistic approach, deterministic method of Monte Carlo is employed to obtain the stability margin by counting the number of stable cases based on 10,000 deterministic samples. By adjusting the load factor k, once the number of unstable cases reaches 100 (1% of 10,000) at a load level 1+k, the probabilistic stability margin I_{SM} determined by Monte Carlo method is k. Likewise, the unstable count for k_c is 5,000 (50% of 10,000).

Table 3.2 gives the probabilistic stability margins without consideration of reactive power limit of generators. For load standard deviation σ_L=0.0389μ, k_c=0.8714 and I_{SM}=0.8443. The corresponding values computed by Monte Carlo method are 0.8714 and 0.8505. The differences in probabilistic stability margins between the probabilistic method and Monte Carlo are 0.00% and 0.73% respectively. The difference in k_c is less than that in I_{SM}. This conclusion also applies to other σ_L. Nevertheless, the maximum difference is 0.03% for k_c and 0.79% for I_{SM}, and the present probabilistic approach should be validated.

Table 3. 2 Probabilistic stability margin with different load variance σ_L of 9-bus system (without reactive power limit of generator)

	σ_L	Density within ±10%	Probabilistic Method		Mont Carlo		Difference	
			k_c	I_{SM}	k_c	I_{SM}	k_c	I_{SM}
(a)	**0.0389μ**	99%	**0.8714**	**0.8443**	**0.8714**	**0.8505**	0.00%	0.73%
(b)	0.0510μ	95%	0.8710	0.8368	0.8711	0.8435	0.01%	**0.79%**
(c)	0.0606μ	90%	0.8706	0.8311	0.8708	0.8376	0.02%	0.78%
(d)	0.0694μ	85%	0.8703	0.8261	0.8705	0.8324	0.02%	0.76%
(e)	0.0775μ	80%	0.8699	0.8216	0.8702	0.8273	**0.03%**	0.69%

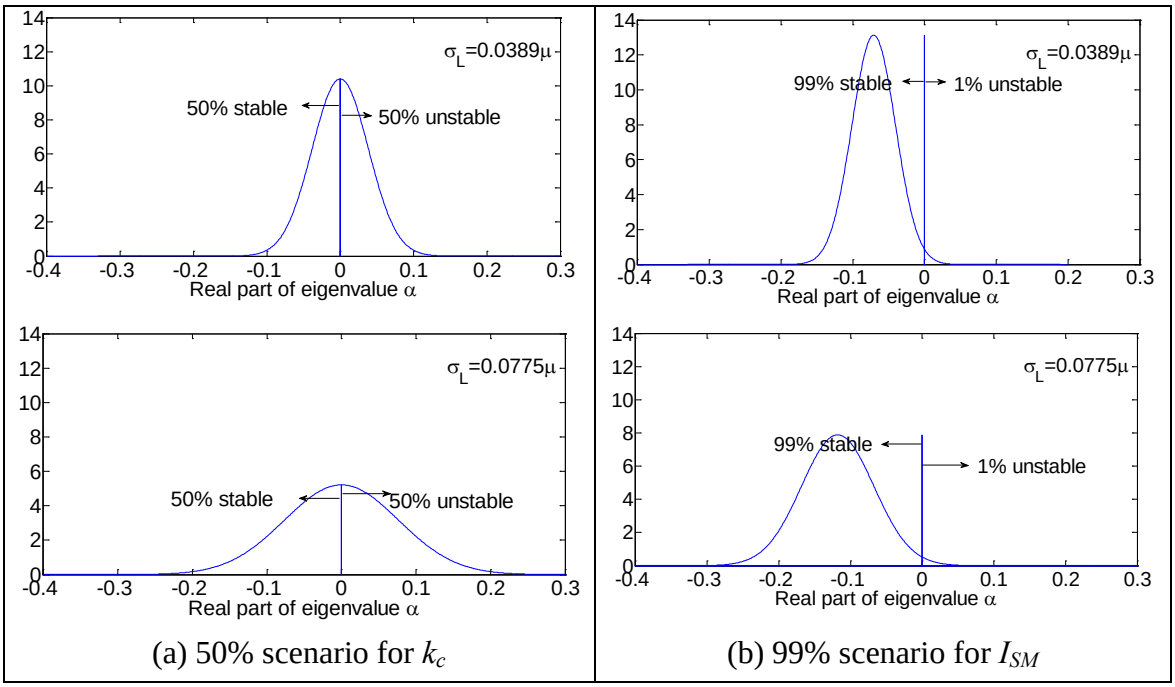

(a) 50% scenario for k_c (b) 99% scenario for I_{SM}

Fig. 3. 6 Distribution of critical α with load variance σ_L

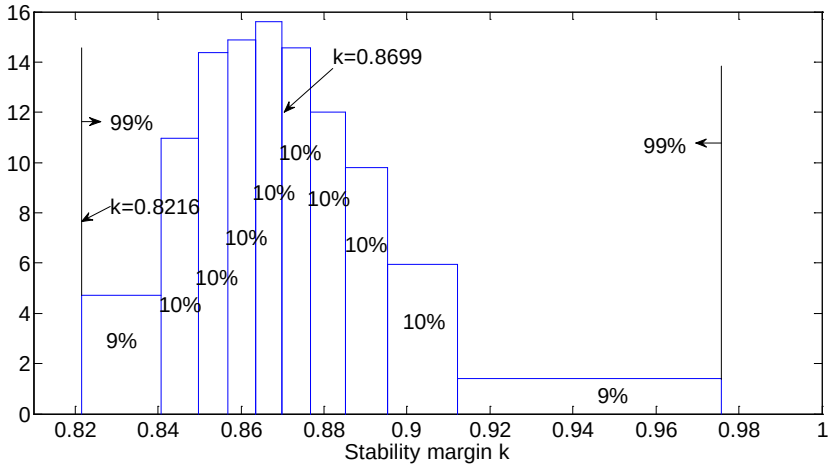

Fig. 3. 7 Distribution of stability margin of 9-bus system for σ_L=0.0775μ (without reactive limit of generator)

For closer examination to Table 3.2, with the increase of load uncertainty (i.e. with increase of σ_L), k_c decreases very slightly, and I_{SM} gradually decreases from 0.8443 to 0.8216. It is because if σ_L is increased from 0.0389μ to 0.0775μ, σ_α will increase from 0.0303 to 0.0506 and the α distribution becomes wider and is shifted to the left, resulting in decrease of I_{SM} as shown in Fig. 3.6b. However, as for k_c, the change is negligible in Fig. 3.6a.

The rough distribution of stability margin of 9-bus system for σ_L=0.0389μ and σ_L=0.0775μ are shown in Fig. 3.4 and Fig. 3.7. With increase of σ_L, the distribution range of stability margin becomes wider, which may echo that I_{SM} will decrease with increase of load uncertainty, described by σ_L.

The study is then repeated with more realistic assumption by considering reactive power limits exhibited in generators. Table 3.3 once more shows that, with increase in load uncertainty, k_c has only very slight change and I_{SM} drops more. As compared to Table 3.2, the stability limits without reactive power constraints are always larger than those with 'constraints' in Table 3.3.

Table 3.3 Probabilistic stability margin with different load variance σ_L of 9-bus system (with reactive power limit of generator of Q_{max}=1)

	σ_L	Density within ±10%	Probabilistic Method		Mont Carlo		Difference	
			k_c	I_{SM}	k_c	I_{SM}	k_c	I_{SM}
(a)	0.0389μ	99%	0.8319	0.8061	0.8320	0.8045	0.01%	0.20%
(b)	0.0510μ	95%	0.8314	0.7994	0.8315	0.7955	0.01%	0.49%
(c)	0.0606μ	90%	0.8308	0.7944	0.8312	0.7884	0.05%	0.76%
(d)	0.0694μ	85%	0.8302	0.7937	0.8308	0.7818	0.07%	1.52%
(e)	0.0775μ	80%	0.8296	0.7932	0.8303	0.7757	0.08%	2.25%

3.6.2 Test system II

The second test system of 39-bus in Fig. 3.8 has ten generators. The third and fourth order models are adopted for synchronous machines. The loads are regarded as constant power load model. All excitations are IEEE Type 1 rotating excitation system model. The system data, generator data and associated controller data are listed in Appendix 3.

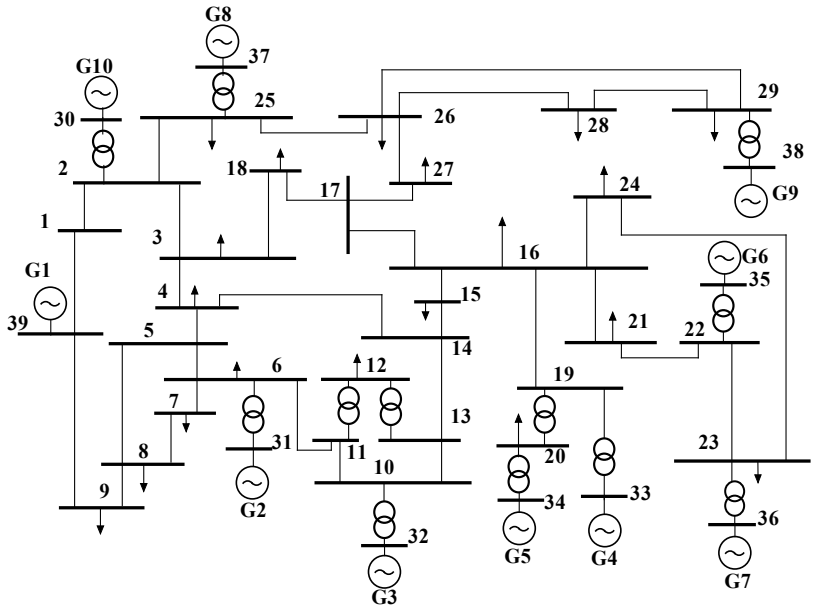

Fig. 3. 8 39-bus system

Again, the k_c and I_{SM} for without and with considering the reactive power limit of generators for 39-bus system are computed as shown in Tables 3.4 and 3.5 respectively. Comparing with the 9-bus system, the trends of margin reduction with load uncertainty are basically the same. As comparing with Monte Carlo results, the maximum differences are 0.54% for k_c and 2.19% for I_{SM}. As a conclusion, the validity of the present proposed probabilistic method is more confirmed.

Table 3.4 Probabilistic stability margin with different load variance σ_L of 39-bus system (without reactive power limit of generator)

	σ_L	Density within ±10%	Probabilistic Method		Mont Carlo		Difference	
			k_c	I_{SM}	k_c	I_{SM}	k_c	I_{SM}
(a)	0.0389μ	99%	0.2416	0.2276	0.2420	0.2277	0.16%	0.04%
(b)	0.0510μ	95%	0.2411	0.2232	0.2416	0.2224	0.21%	0.35%
(c)	0.0606μ	90%	0.2406	0.2199	0.2413	0.2180	0.29%	0.87%
(d)	0.0694μ	85%	0.2400	0.2168	0.2410	0.2138	0.41%	1.40%
(e)	0.0775μ	80%	0.2394	0.2141	0.2407	0.2095	**0.54%**	**2.19%**

Table 3.5 Probabilistic stability margin k with different load variance σ_L of 39-bus system (with reactive power limit of generator of Q_{max}=3)

	σ_L	Density within ±10%	Probabilistic Method		Mont Carlo		Difference	
			k_c	I_{SM}	k_c	I_{SM}	k_c	I_{SM}
(a)	0.0389μ	99%	0.2408	0.2270	0.2411	0.2271	0.12%	0.04%
(b)	0.0510μ	95%	0.2403	0.2227	0.2408	0.2219	0.21%	0.36%
(c)	0.0606μ	90%	0.2398	0.2194	0.2405	0.2175	0.29%	0.87%
(d)	0.0694μ	85%	0.2392	0.2164	0.2402	0.2133	0.41%	1.45%
(e)	0.0775μ	80%	0.2386	0.2137	0.2398	0.2091	0.50%	2.19%

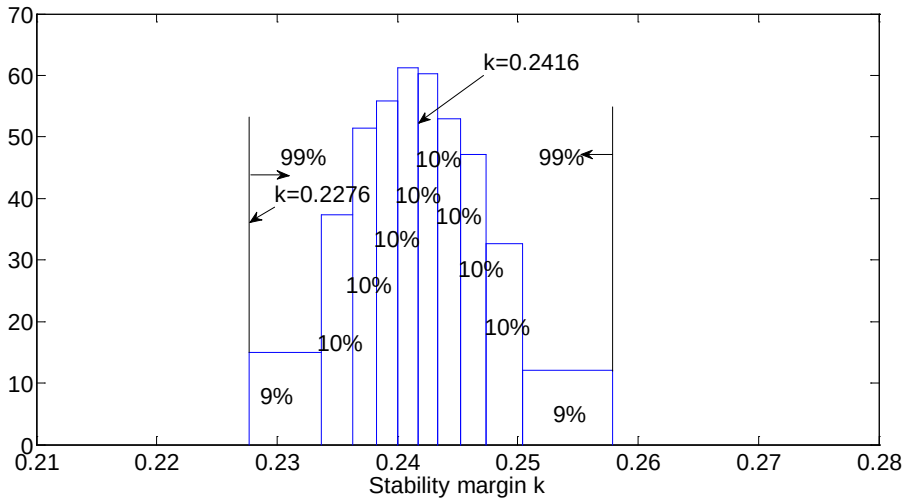

Fig. 3. 9 Distribution of stability margin of 39-bus system for σ_L=0.0389μ (without reactive limit of generator)

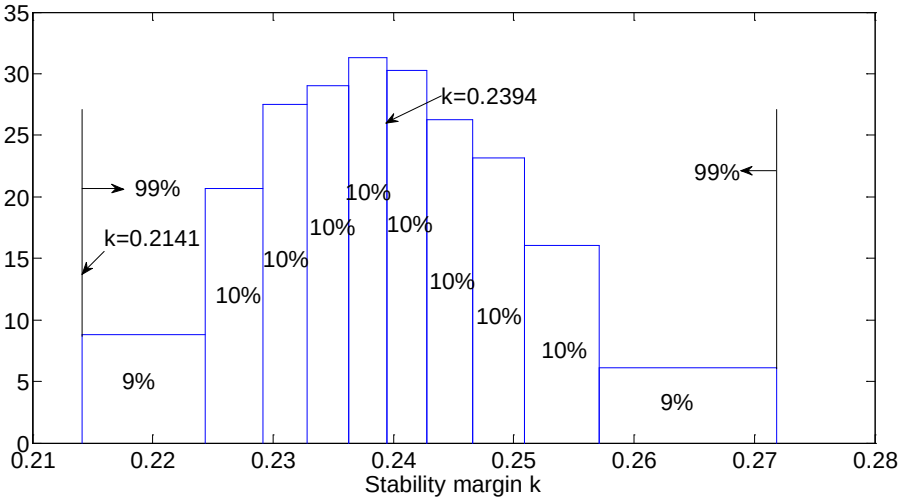

Fig. 3. 10 Distribution of stability margin of 39-bus system for σ_L=0.0775μ (without reactive limit of generator)

From the rough distribution of stability margins of Fig. 3.9 and Fig. 3.10, it once more demonstrates that the distribution range of stability margin becomes wider with increase of σ_L.

3.7 Conclusion

Many uncertainties exist in power system operation and one of them is the load variation which will affect the assessment of voltage stability margin. This chapter has exploited the in-house versatile technique to develop a systematic probabilistic technique to evaluate stability margin under the uncertainty of loads. With the assumptions that these loads are normal distributions, two stability margin indices (k_c for 50% scenario and I_{SM} for 99% scenario) are introduced. The results show that, with the increase of load uncertainty, the k_c only decreases very slightly, and I_{SM} gradually decreases.

The accuracy of the proposed probabilistic method is compared with Monte Carlo

results based on multi 10,000 deterministic samples for each load variance. The comparison shows the proposed probabilistic method has small difference from Monte Carlo method for the determination of k_c and I_{SM}. Consequently, the proposed method can effectively compute stability margin under the uncertainty of loads.

Chapter 4 Voltage stability analysis considering the uncertainties of dynamic load parameters

4.1 Introduction

Probabilistic stability margin has been used to assess voltage stability under load uncertainties. This chapter will extend the probabilistic eigenvalue method to study voltage stability considering effects of dynamic load parameters.

With the development of voltage stability study, researchers have gradually realized the important effect of dynamic load on voltage stability. After exponential recovery load model (Karlsson & Hill, 1994) and adaptive load model (Xu & Mansour, 1994) were proposed according to the results from the measurement of actual power system load, dynamic load model have been introduced to voltage stability analysis. Byongjun & Ajjarapu (1995) adopted generic load model for a piecewise global small-disturbance voltage stability analysis. Exponential recovery load model and adaptive load model (Zeng, Berizzi, & Marannino, 1997) have been adopted for voltage analysis where excitation and governor systems are in quasi steady-state.

Load parameters also affect the result of voltage stability studies. Different ranges of parameters for the same load model have been reported (Byongjun & Ajjarapu,

1995; Makarov, Maslennikov, & Hill, 1996; Zeng et al., 1997). Furthermore, there is always some uncertainty associated with load parameters due to the load variation. The influence of dynamic load parameters on small disturbance stability (Makarov et al., 1996) has been revealed via quasi-optimization procedure with the cost function which reflects shifts of selected eigenvalues along the real axis when all load parameters vary within their constraints. However the related research above is based on deterministic operations and load parameters.

To consider uncertainties of load parameters, the probabilistic eigenvalue algorithm is extended to handle the uncertainties of dynamic load parameters under the assumption that the load parameter variations follow normal distribution with a mean value and a standard deviation. Based on this proposed method, the probabilistic critical load level can be obtained.

4.2 Exponential recovery load model

The exponential recovery load model can be represented by following equations (Zeng et al., 1997)

$$T_p \dot{x}_p = P_s(V) - P_d \tag{4.1}$$

$$T_q \dot{x}_q = Q_s(V) - Q_d \tag{4.2}$$

$$P_d = x_p + P_t(V) \tag{4.3}$$

$$Q_d = x_q + Q_t(V) \tag{4.4}$$

$$P_s(V) = P_0(V/V_0)^{\alpha_s} \tag{4.5}$$

$$Q_s(V) = Q_0(V/V_0)^{\beta_s} \tag{4.6}$$

$$P_t(V) = P_0(V/V_0)^{\alpha_t} \tag{4.7}$$

$$Q_t(V) = Q_0(V/V_0)^{\beta_t} \tag{4.8}$$

where

T_P, T_q active and reactive load recovery time constant;

P_d, Q_d active power and reactive power consumption;

$P_s(V), Q_s(V)$ steady-state part of active power and reactive power consumption;

$P_t(V), Q_t(V)$ transient part of active power and reactive power consumption;

α_s, β_s steady-state active and reactive load-voltage dependent exponents;

α_t, β_t transient active and reactive load-voltage dependent exponents;

P_0, Q_0 active power and reactive power consumption at nominal voltage;

V supply voltage

V_0 nominal voltage.

Since the present work focuses on small disturbance stability analysis, the linearized representation of dynamic load (4.9)-(4.12) can be obtained from (4.1)-(4.8). In order to employ Plug-in Modeling Technique (PMT) (Tse & Tso, 1988), the linearized exponential recovery load model is transferred into diagram representation as shown in Fig. 4.1.

$$T_p \Delta \dot{x}_p = P'_s(V) \Delta V - \Delta P_d \tag{4.9}$$

$$T_q \Delta \dot{x}_q = Q'_s(V) \Delta V - \Delta Q_d \tag{4.10}$$

$$\Delta P_d = \Delta x_p + P'_t(V) \Delta V \tag{4.11}$$

$$\Delta Q_d = \Delta x_q + Q'_t(V)\Delta V \tag{4.12}$$

$P'_s(V), Q'_s(V)$ derivatives of $P_s(V), Q_s(V)$ with respect to voltage V;

$P'_t(V), Q'_t(V)$ derivatives of $P_t(V), Q_t(V)$ with respect to voltage V.

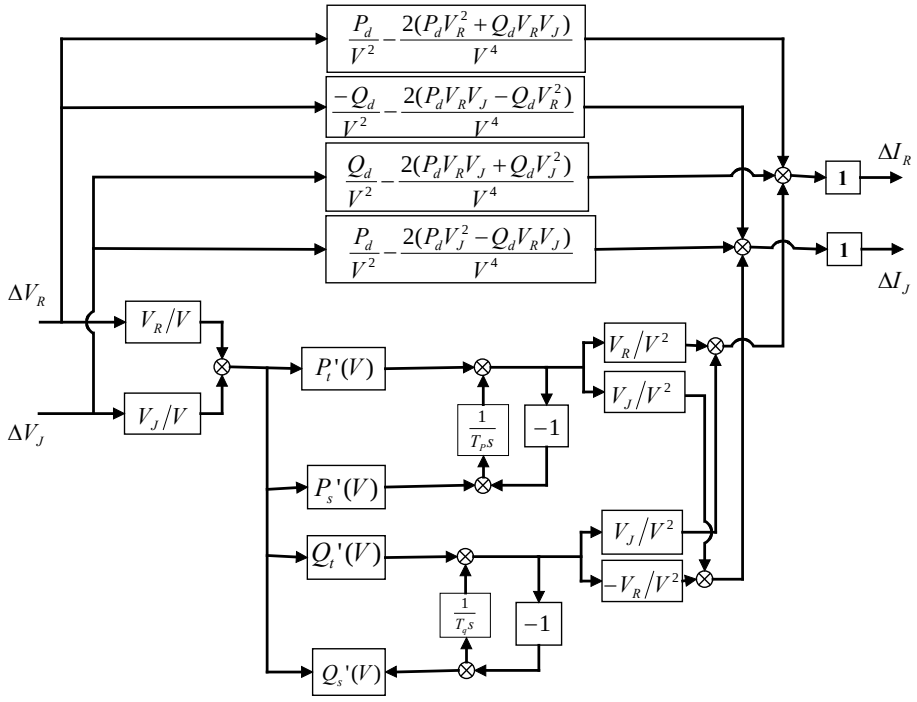

Fig. 4.1 Exponential recovery load representation

4.3 Probabilistic eigenvalue

System matrix is an explicit function of dynamic load parameters and operating parameters described as (Wang, Tse, & Tsang, 1998)

$$\boldsymbol{A} = G(\boldsymbol{K}) \tag{4.13}$$

When equation (4.13) is expanded at expectation $\overline{\boldsymbol{K}}$ of load parameters, the Taylor series retaining the second order term can be expressed as equation (4.14) (Wang et al., 1998)

$$\boldsymbol{A} \approx \boldsymbol{A}_{\overline{\boldsymbol{K}}} + \left.\frac{\partial \boldsymbol{A}}{\partial \boldsymbol{K}}\right|_{\boldsymbol{K}=\overline{\boldsymbol{K}}} \Delta \boldsymbol{K} + \frac{1}{2}\sum_{\substack{i=1 \\ j=1}}^{n,n} \left(\left.\frac{\partial^2 \boldsymbol{A}}{\partial K_i \partial K_j}\right|_{\boldsymbol{K}=\overline{\boldsymbol{K}}} \Delta K_i \Delta K_j\right) \tag{4.14}$$

The expectation of state matrix can be expressed as follows

$$\overline{\boldsymbol{A}} \approx \boldsymbol{A}_{\overline{\boldsymbol{K}}} + \frac{1}{2}\sum_{\substack{i=1 \\ j=1}}^{n,n} \left(\left.\frac{\partial^2 \boldsymbol{A}}{\partial K_i \partial K_j}\right|_{K=\overline{K}} C_{K_{i,j}}\right) \tag{4.15}$$

where, $C_{K_{i,j}}$ is the covariance between load parameters K_i and K_j.

As a result, the expectation of eigenvalues $\overline{\lambda}$ can be solved from the system state matrix expectation $\overline{\boldsymbol{A}}$.

Eigenvalue λ is regarded as a nonlinear function of load parameter $\boldsymbol{K}$ with a linearized expression as

$$\Delta\boldsymbol{\lambda} = \boldsymbol{J}_{\boldsymbol{K}} \Delta \boldsymbol{K} \tag{4.16}$$

where $\boldsymbol{J}_K$ is the first order derivative matrix of eigenvalue with respect to load parameters. The eigenvalue covariance matrix $\boldsymbol{C}_\lambda$ is obtained as

$$\boldsymbol{C}_{\lambda \boldsymbol{K}} = \boldsymbol{J}_{\boldsymbol{K}} \boldsymbol{C}_{\boldsymbol{K}} \boldsymbol{J}^{T} \tag{4.17}$$

Diagonal elements of matrix $\boldsymbol{C}_\lambda$ are the variances of eigenvalues, and the off-diagonal elements are covariances between two eigenvalues.

According to equation (4.15) and(4.17), the means and variance of eigenvalues can be calculated.

4.4 Determination of probabilistic critical load level

Eigenvalues are functions of load parameters and load parameters are random variables. Therefore, eigenvalues are random variables. A random complex eigenvalue $\lambda=\alpha+j\beta$ will distribute over a certain range in the complex plane. The stability degree of mode i can be assessed by the probability of

$$P\{\alpha_i < 0\} = \int_{-\infty}^{0} f(\alpha_i) d\alpha_i \tag{4.18}$$

where $f(.)$ denotes the probabilistic density function. In case of $f(.)$ approximating to normal distribution, the distribution pattern can be depicted by the expectation $\overline{\alpha}$ and the standard deviation σ. The stability probability of power system is determined by the critical eigenvalue. Again, two indexes will be used to assess stability margin: k_c for 50% scenario and I_{SM} for 99% scenario. The flowchart for the solution of probabilistic critical load level considering uncertainties of load parameters is illustrated in Fig. 4.2. k_0 in the flowchart is the probabilistic stability margin.

4.5 Case studies

In this chapter, probabilistic eigenvalue method is used to determine the stability margin considering probabilistic characteristic of load parameters. The method is applied to three systems: a 9-bus system, a 14-bus system and a 39-bus system.

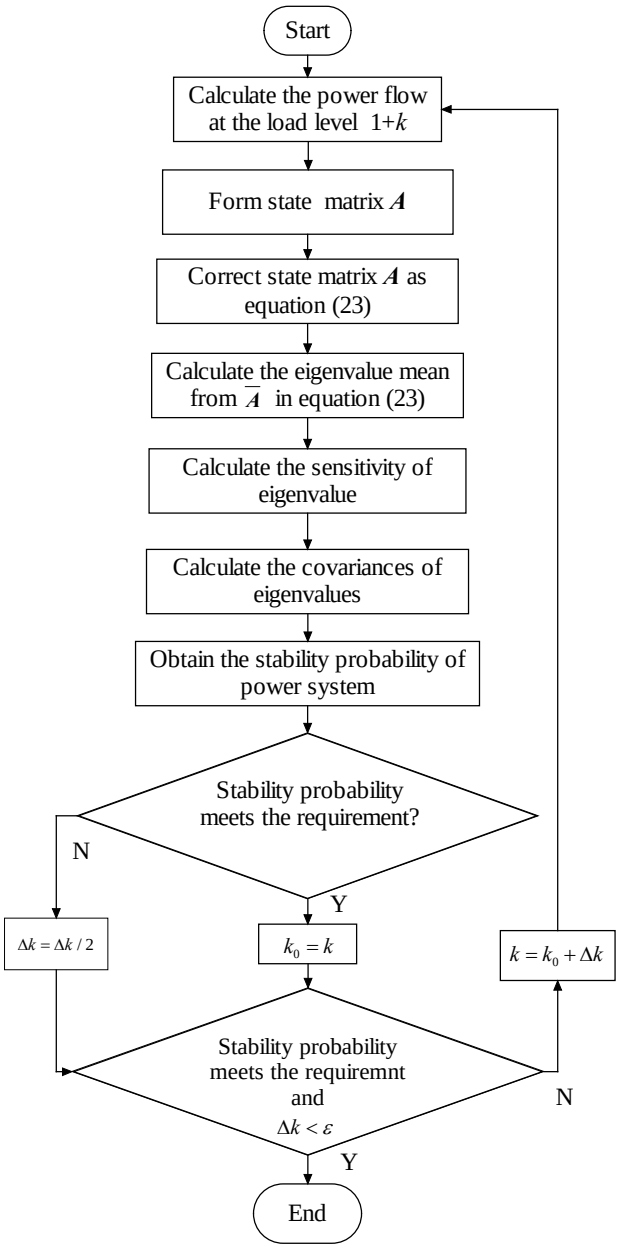

Fig. 4. 2 Flowchart to obtain critical load level

4.5.1 Test system I

The 9-bus system (Fig. 3.5) consists of three generator buses (7, 8, 9), three load buses (4, 5, 6) and three connecting buses (1, 2, 3). In the analysis, the fourth order generator model and IEEE type I excitation system are adopted. The data of 9-bus

system are listed in detail in appendix 3.

With load increase in the same proportion and keeping constant power factor, the load can be expressed as

$$P_{Li} = P_{Li0}(1+k), Q_{Li} = Q_{Li0}(1+k) \tag{4.19}$$

where, P_{Li0} and Q_{Li0} are load of bus i at the initial operating point; (1+k) is regarded as load level.

All loads are exponential recovery model shown in Fig. 4.1. The model has six load parameters α_s, β_s, α_t, β_t, T_p and T_q, which have different values in literatures (Byongjun & Ajjarapu, 1995; Makarov et al., 1996; Zeng et al., 1997). The ranges of voltage dependent exponentials are (Makarov et al., 1996):

$$0 \le \alpha_s \le 3; 0 \le \beta_s \le 7; 1.5 \le \alpha_t \le 2.5; 4 \le \beta_t \le 7 \tag{4.20}$$

The recovery time constants have different values in literatures: T_p=T_q=25s (Byongjun & Ajjarapu, 1995), T_p=T_q=30s (Zeng et al., 1997), but T_p<1s and T_q<1s (Makarov et al., 1996).

Normal distribution is one of the most common distributions in nature. Load parameters following normal distributions have been adopted to take uncertainty of load parameters into voltage stability analysis of series-compensation of EHV transmission lines (Indulkar & Viswanathan, 1983). In this chapter, with the assumption of normal distribution, these parameters are assumed to have expected

values of α_s=1.5, β_s=3.5, α_t=2.0, β_t=5.5, T_p=T_q=25s, denoted by μ, but the standard deviation σ_P of these parameter are not yet determined.

The present study is first started with σ_P=0.0389μ and the expectation and the convariances of eigenvalues are evaluated according to (4.15) and(4.17). The expectation of critical eigenvalues at different load levels are computed as listed in Table 4.1.

Table 4.1 Critical eigenvalues at different load levels with σ_P=0.0389μ

Load level 1+ k	Critical eigenvalue $\bar{\alpha}$	Associated state variables
2.346	-0.1848+j2.5234	E'_{q3}, E_{fd3}
2.347	-0.0655+j2.5913	E'_{q3}, E_{fd3}
2.348	0.0640+j2.6191	E'_{q3}, E_{fd3}
2.351	0.3929+j2.5871	E'_{q3}, E_{fd3}, ω_1,ω_3
2.352	0.4867+j2.5608 0.0005	E'_{q3}, E_{fd3}, ω_1,ω_3 x_{p1},x_{q2}
2.360	1.1438+j2.2093 0.0006	E'_{q3}, E_{fd3}, ω_1,ω_3 x_{p1},x_{q2}
2.370	2.087+j0.7931 0.0235	E'_{q3}, E_{fd3},ω_3, ω_1 x_{p1},x_{q2}
2.3707	2.1823+j0.2898 0.0261	E'_{q3}, E_{fd3} ω_3, ω_1 x_{p1},x_{q2}
2.3708	2.2179,2.2176 0.0265	E'_{q3}, E_{fd3}, ω_3, ω_1 x_{p1},x_{q2}
2.373	4.2463,0.9835 0.0417	E'_{q3}, E_{fd3}, ω_3, ω_1 x_{p1},x_{q2}

Table 4.1 shows the expectation of critical eigenvalues at different load levels. When load increases, the real part of the critical eigenvalue increases. When the load level increases from 2.347 to 2.348, the real part of the critical eigenvalue becomes positive (point **A** in Fig. 4.3), i.e. Hopf bifurcation (Byongjun & Ajjarapu, 1995) occurs. By participation factor analysis, this mode is associated with the excitation

system of generator 3. If load level increases to 2.352, another real eigenvalue passes the origin and turns positive, and saddle node bifurcation (Byongjun & Ajjarapu, 1995) occurs (point **C** in Fig. 4.3). At load level of 2.3708, the complex eigenvalue turns into two real eigenvalues, and node focus (Byongjun & Ajjarapu, 1995) occurs (point **B** in Fig. 4.3). With further load increase, one of the real eigenvalues decreases and the other two increase until power flow divergences.

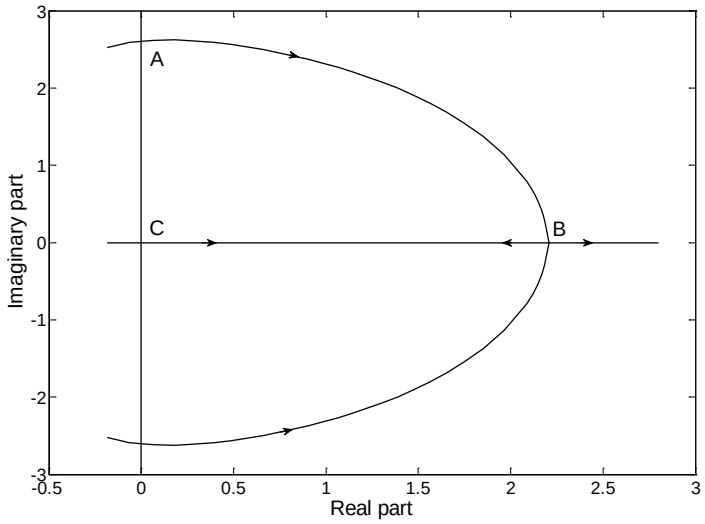

Fig. 4. 3 Loci of the critical eigenvalues

In this chapter, the point A is regarded as the critical operating point and k_c=1.347 is stability margin with loads at expected values. Note that Table 4.1 depicts the expectation of critical eigenvalue variations at different load levels. In other words, under the uncertainty of load parameters, about 50% of scenarios may experience voltage instability when k_c=1.347 for σ_P=0.0389μ as Tabled 4.2(a). If σ_P is increased to 0.0775μ, 50% of scenarios will experience voltage instability at a lower k_c=1.344 as Table 4.2 (e). (According to section 3.5.4, σ_P =0.0775μ in normal distribution implies that 80% of the density distribution is within ±10% of their expected values). Again, the pragmatic stability margin index I_{SM} for 99% scenario

is used in Table 4.2. For example, I_{SM}=1.342 in Table 4.2(a) implies that if the system load is increased by 134.2%, 99% of the scenarios will not experience voltage instability. The probabilistic technique is repeated for different parameter variances, and the results in Table 4.2 show that whilst k_c has negligible change, I_{SM} will be reduced with increase of parameter uncertainty.

The stability margin distributions (asymmetric) for σ_P= 0.0389μ and σ_P= 0.0606μ of Table 4.2(a) and 4.2(e) are plotted in Fig. 4.4 and Fig. 4.5 respectively, which may help to explain why k_c in the middle has slight change and I_{SM} at the rear end has a larger change with σ_P.

Table 4.2 Stability margin with different variances σ_P of load parameter for 9-bus system

	σ_P	Density within ±10%	Probabilistic Method		Monte Carlo Method		Difference	
			k_c	I_{SM}	k_c	I_{SM}	k_c	I_{SM}
(a)	**0.0389**μ	99%	**1.347**	1.342	1.348	1.329	0.07%	0.97%
(b)	0.0510μ	95%	1.346	1.340	1.348	1.321	0.15%	1.42%
(c)	0.0606μ	90%	1.346	1.338	1.347	1.315	0.07%	1.72%
(d)	0.0694μ	85%	1.345	1.337	1.347	1.308	0.15%	2.17%
(e)	**0.0775**μ	80%	**1.344**	1.336	1.346	1.301	0.15%	2.62%

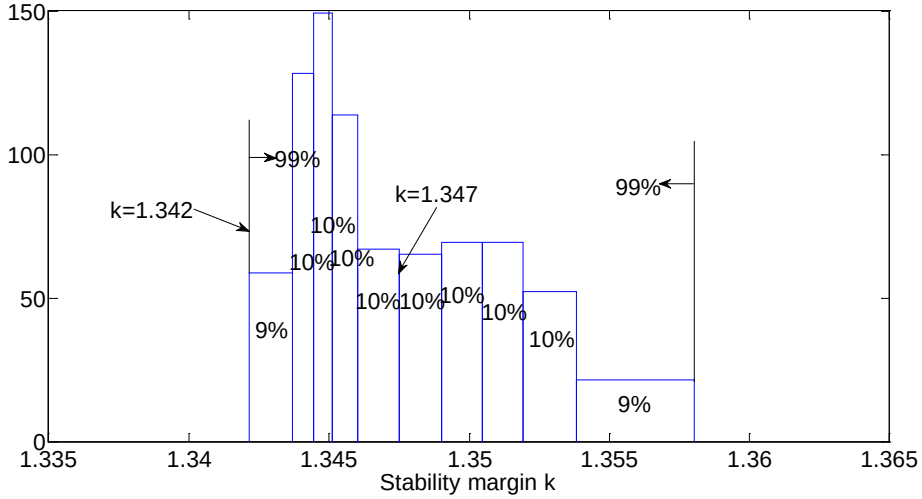

Fig. 4. 4 Distribution of stability margin of 9-bus system for σ_P=0.0389μ

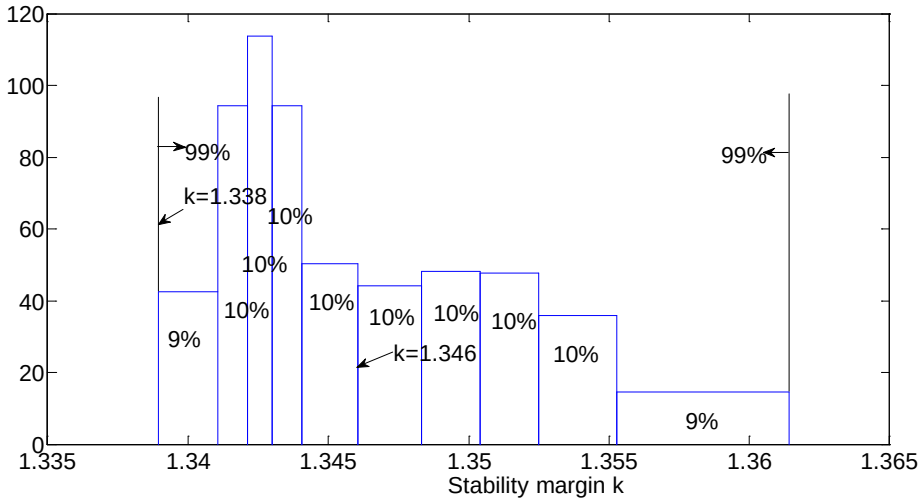

Fig. 4. 5 Distribution of stability margin of 9-bus system for σ_P=0.0606μ

To validate the probabilistic approach, Monte Carlo method is employed to count the number of stable cases based on 10,000 deterministic samples for each σ and load level (1+k). With deceasing k, k_c is obtained for stability count equal to 5,000 (i.e. 50%) and I_{SM} for count equal to 9,900 (i.e. 99%). Comparing the results in Table 4.2, the differences of stability margins obtained by the two methods are quite small.

4.5.2 Test system II

The second test system of 14-bus in Fig. 4.6 has two generators and three synchronous compensators. The fifth order model is adopted for slack generator, and the sixth order model for the other synchronous machines. The data of this test system are listed in appendix 3. The loads are all exponential recovery load model and the load parameters are same as those of the 9-bus system.

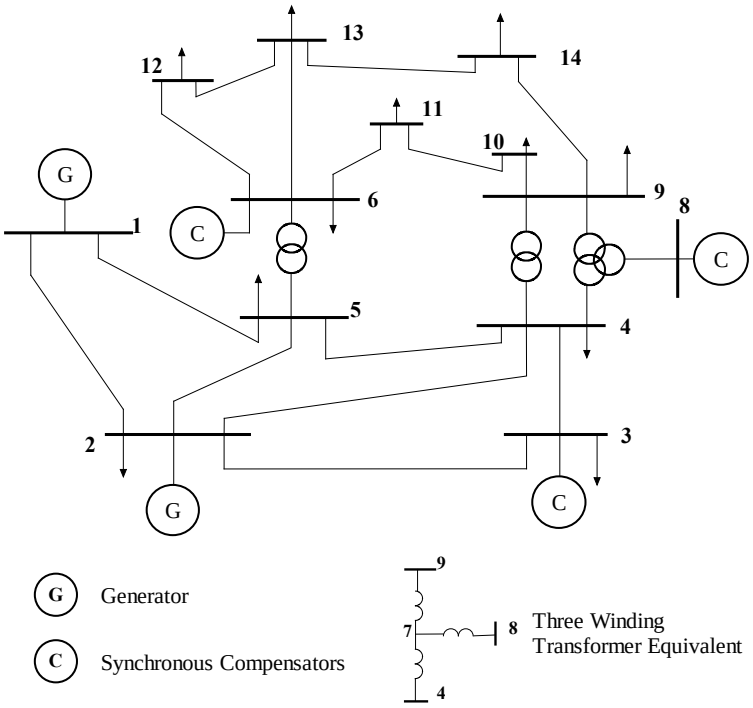

Fig. 4. 6 14-bus system

Computation results for different σ_P are listed in Table 4.3 with the stability margin distributions shown in Fig. 4.7 and Fig. 4.8. Again, whilst k_c has negligible change, I_{SM} of 99% will be reduced with increase of parameter uncertainty. The distribution range of stability margin becomes wider with increase of σ_P. The probabilistic results are then compared with Monte Carlo deterministic method, and the two sets of computation results are very close.

Table 4. 3 Stability margin with different variances σ_P of load parameter for 14-bus system

	σ_P	Density within ±10%	Probabilistic Method		Monte Carlo Method		Difference	
			k_c	I_{SM}	k_c	I_{SM}	k_c	I_{SM}
(a)	0.0389μ	99%	1.304	1.246	1.304	1.252	0.0%	0.48%
(b)	0.0510μ	95%	1.304	1.226	1.304	1.236	0.0%	0.81%
(c)	0.0606μ	90%	1.303	1.212	1.304	1.224	0.8%	0.99%
(d)	0.0694μ	85%	1.303	1.204	1.303	1.212	0.0%	0.66%
(e)	0.0775μ	80%	1.303	1.198	1.303	1.202	0.0%	0.33%

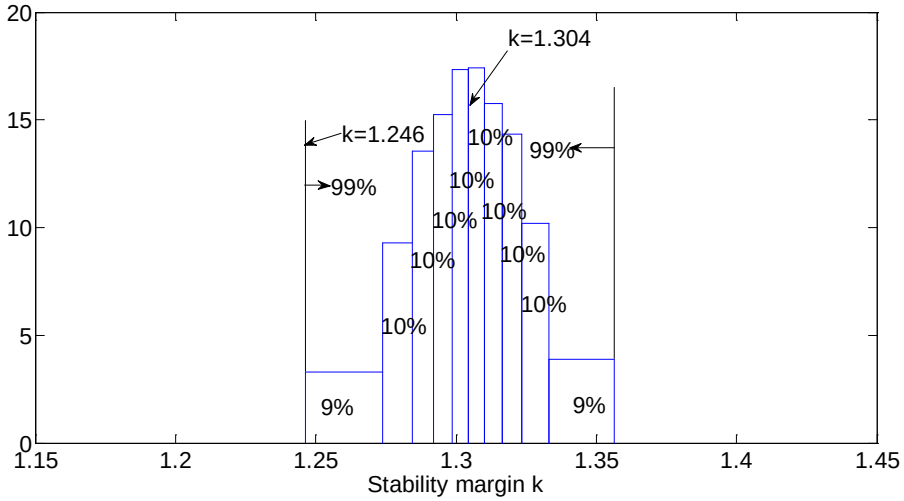

Fig. 4. 7 Distribution of stability margin of 14-bus system for σ_P=0.0389μ

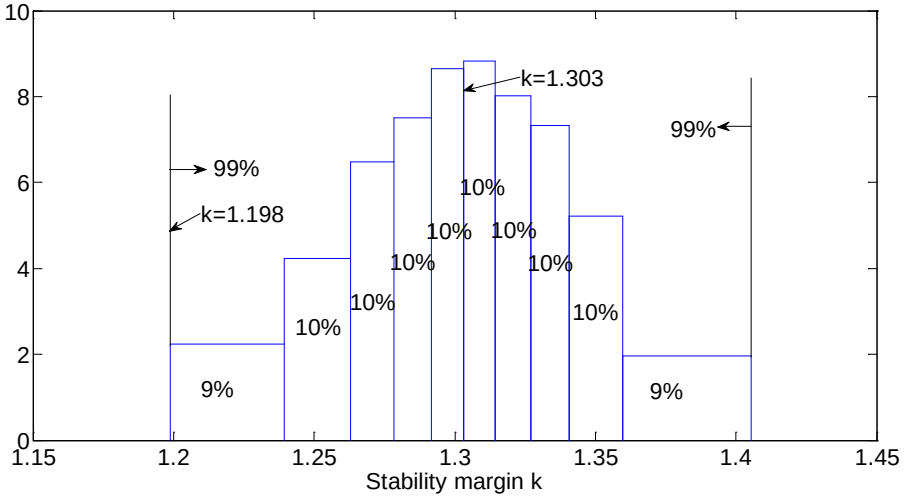

Fig. 4. 8 Distribution of stability margin of 14-bus system for σ_P=0.0775μ

4.5.3 Test system III

The third test system of 39-bus system shown in Fig. 2.5 has ten generators. The fourth order and third order generator model and IEEE type-1 rotating excitation system model are adopted for this test system. Exponential recovery load model is adopted for all loads and load parameters have the same characteristics as those of the 9-bus system. The computed stability index k_c and I_{SM} are shown in Table 4.4 and the stability margin distribution in Fig. 4.9 and Fig. 4.10. The stability margin of this 39-bus system is relatively low, e.g. k_c=0.364 and I_{SM}=0.346 for σ_P=0.0389μ

(Table 4.4), as compared to those in Table 4.2 or Table 4.3. It is also observed I_{SM} decreases with σ_P. From Fig. 4.9 and Fig. 4.10, it can be seen that distribution range of stability margin becomes wider with increase of σ_P. The proposed method is validated because the difference from the Monte Carlo method is quite small.

Table 4. 4 Stability margin with different variances σ_P of load parameter for 39-bus system

	σ_P	Density within ±10%	Probabilistic Method		Monte Carlo Method		Difference	
			k_c	I_{SM}	k_c	I_{SM}	k_c	I_{SM}
(a)	0.0389μ	99%	**0.364**	**0.346**	0.364	0.347	0.00%	0.29%
(b)	0.0510μ	95%	0.364	0.341	0.364	0.341	0.00%	0.00%
(c)	0.0606μ	90%	0.364	0.337	0.364	0.337	0.00%	0.00%
(d)	0.0694μ	85%	0.364	0.334	0.364	0.333	0.00%	0.30%
(e)	0.0775μ	80%	0.364	0.331	0.364	0.329	0.00%	0.60%

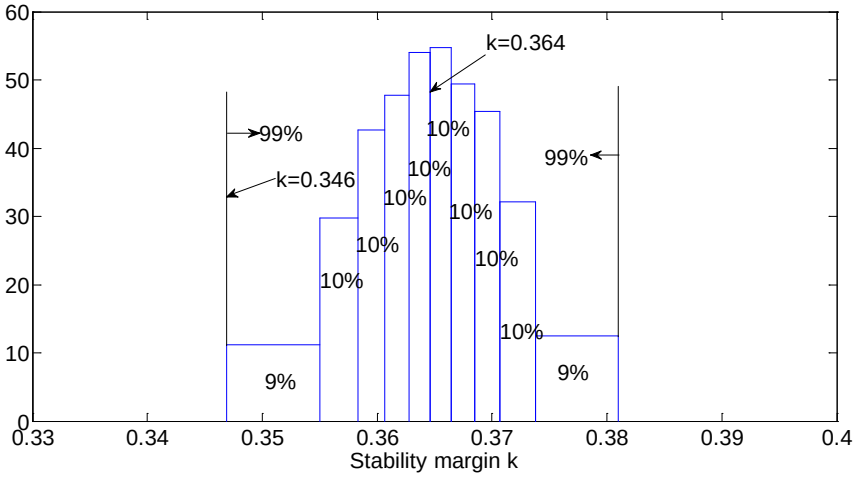

Fig. 4. 9 Distribution of stability margin of 39-bus system for σ_P=0.0389μ

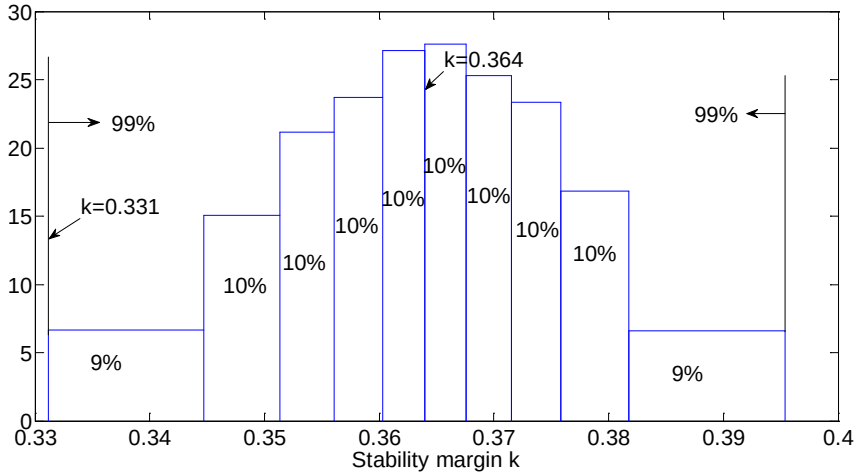

Fig. 4. 10 Distribution of stability margin of 39-bus system for σ_P=0.0775μ

4.5.4 Observation of results

Stability margins have been computed for 3 systems for same variance of system dynamic load parameters. Results show that difference between the probabilistic method and Monte Carlo method are quite small: less than 0.15% for k_c and less than 2.62% for I_{SM}, which may validate the present algorithm. It is also observed, when σ_P increases from 0.0389μ to 0.0775μ, whilst k_c remains fairly constant, I_{SM} decreases e.g. I_{SM} decreases by 0.4%, 4% and 4.5% for test system I, II and III respectively. In the present probabilistic method, the analysis is not affected by the system size. Instead, the major concern is the computer time, which increases rapidly with the system size, e.g. from 1.2s for the small 9-bus system to 135.3s for the 39-bus system (Table 4.5). From Table 4.5, it is also observed that most of the computation effort is spent on the calculation of the second order sensitivities of state matrix $\boldsymbol{A}$ in (4.14) and (4.15). It is desirable to have an effective method to improve the computation technique of the second order sensitivities of state matrix $\boldsymbol{A}$.

Table 4. 5 The computational time for I_{SM} of different test systems

System	9-bus	14-bus	39-bus
Total computation time	1.165s	23.994s	135.313s
Time for 2nd order sensitivity of Matrix $\boldsymbol{A}$	0.408s	18.611s	114.638s

4.6 Conclusion

Many uncertainties exist in power system operation and one of them is the load dynamic parameter variation which will affect the assessment of voltage stability

margin. If the parameter variation follows normal distribution, k_c obtained by existing deterministic methods can only provide a margin index that ensures about 50% of scenarios having a margin higher than k_c. This chapter has exploited the in-house versatile eigenvalue technique to develop a systematic probabilistic technique to evaluate stability margin under the uncertainty of load parameters. With the assumptions that these parameters are normal distributions, the indices k_c for 50% and I_{SM} for 99% scenario are once more used to assess the stability margin. Computations show that whilst k_c has negligible change, I_{SM} will be reduced with increase of parameter uncertainty. The observation becomes obvious by the stability margin distribution plotting.

The probabilistic results are then validated with Monte Carlo approach based on multi 10,000 samples for each parameter variance. Because the two sets of computation results are close, the effectiveness and accuracy of the proposed probabilistic method (based on single computation) are confirmed.

The present computation study assumes that the expected values of the load parameters are given but their variances are undetermined. In practice, both the expected values and the variances may be obtained by site measurements. Moreover, the proposed technique of I_{SM} evaluation can be applied to any percentage, to be assigned by the system planning engineers.

Chapter 5 Probabilistic power system voltage stabilizer design considering uncertainties of loads

5.1 Introduction

Probabilistic voltage stability analysis by probabilistic eigenvalue considering uncertainties of loads and load parameters has been introduced in chapter 3 and chapter 4. This chapter will present a method to design controller to improve voltage stability of power system under probabilistic environment.

Voltage collapse has become a challenge to power engineers and scientists in the last decades. Hence, a great deal of efforts has been devoted to voltage stability enhancement. One of factors causing voltage instability is that there is a lack of sufficient reactive power support. In order to improve the voltage stability margin, reactive power compensation devices are installed to provide reactive power support. It is impractical to install reactive power compensation devices on each bus. The selection of efficient reactive power compensation location is vital. Based on power flow equations, singular vector of minimum singular value (Chen, Chang, & Liu, 1995), Voltage-collapse proximity indicator method (Chen, 1996; Chen et al., 1995), relative voltage change method (Obadina & Berg, 1990), sensitivity method (Begovic & Phadke, 1992; Obadina & Berg, 1990) and participation factor of bus to mode (Gao et al., 1992) are used to determine the weak buses or weak areas for the

location of reactive power compensation. Considering dynamic elements of power system, small disturbance analysis method adopted voltage instability mode coefficient (Liu, Cheng, & Cheng, 1999) to determine the weak nodes of power system.

Another measure is to optimize reactive power outputs of generators and condensers and other system components to improve voltage stability (Menezes, da Silva, Affonso, & da Costa, 2004; Thukaram, Jenkins, & Visakha, 2006). Modal participation factors are used to identify the most adequate reactive-power injection for each generator or synchronous condenser to maximize voltage stability margins (Menezes et al., 2004). The reactive power was optimized by adjusting reactive power control variables for voltage stability improvement in AC/DC system (Thukaram et al., 2006).

Similar to power system stabilizers (PSS) used for angular stability, power system voltage stabilizer (PSVS) has been presented for dynamic voltage stability enhancement of power systems or prevention of fast voltage instability (Radman et al., 2007). Probabilistic method had been used to design robust PSS for rotor angular stability (Tse et al., 2000). This chapter extends the application of the probabilistic method to design PSVS considering the random variations of loads. The selection of PSVS location and input signal, and the design PSVS parameters by optimization method will be presented.

5.2 Probability of stability

Loads are assumed normal distribution in this study. The eigenvalues are assumed normal distribution according to the linearized relationship. For a special eigenvalue with the mean values $\overline{\alpha}_i$ and standard deviation σ_{α_i}, the distribution of a typical eigenvalue is shown in Fig. 5.1. The stability probability of critical eigenvlaues is determined according to equation (Wang, et al., 1998).

$$P\{\alpha_i < 0\} = \int_{-\infty}^{0} f(a_i)da_i \tag{5.1}$$

where α_i is the real part of the *i*th eigenvalue, and $f(a_i)$ is the probabilistic density function of the eigenvalue. The stability probability of power system is determined by the stability probability of critical eigenvalues. A high reliable index of $4\sigma_{\alpha_i}$ has been employed to ensure system stability being adequate in wide range of operation (Chung et al., 2003; Chung et al., 2002; Tse et al., 2000). In case of normal distribution, the probability of α_i distributed within $\left\{-\infty, \overline{\alpha}_i + 4\sigma_{\alpha_i}\right\}$ is 0.99997, where $\overline{\alpha}_i$ and σ_{α_i} are the mean value and standard deviation of real part of eigenvalue respectively. If $\alpha'_i = \overline{\alpha}_i + 4\sigma_i \le 0$ (i.e. $\alpha_i^* = -\overline{\alpha}_i / \sigma_{\alpha_i} \ge 4$), the system stability is regarded as adequate.

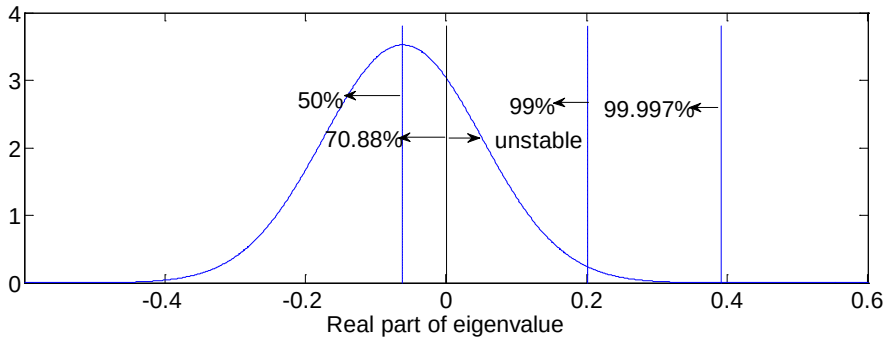

Fig. 5. 1 Distribution of eigenvalue with $\bar{\alpha} = -0.0618$ and $\sigma_\alpha = 0.1131$

Thus, a system having an eigenvalue distribution of Fig. 5.1 and α_i^*=0.0618/0.1131 =0.5457 is highly inadequate since only about 70.88% of scenario is stable, far from the 99.997%. In terms of stability margin, Fig. 5.1 is equivalent to 70.88% of operation scenarios having positive load margin, i.e. k>0. (In Chapters 3 and 4, the degree of voltage stability is assessed by k_c and I_{sm} values at 50% and 99% of scenarios.)

5.3 Power system voltage stabilizers

In order to improve the voltage stability, the concept of power system voltage stabilizer has been introduced (Radman et al., 2007). It works similar to the well known power system stabilizer (PSS). A PSS operates on the excitation system of a generator and provides additional damping torque to angular stability of a power system. The PSVS also operates on the excitation system of a generator/condenser in order to save the system from fast voltage collapse. The symbolic representation of power system voltage stabilizer (Radman et al., 2007) is shown in Fig. 5.2. The selected input of the PSVS should appropriately reflect the voltage deficiency of the system (Radman et al., 2007). In this chapter, the input is the weak bus voltage

deviation. The output of a PSVS is injected to the summing junction of the excitation system block as shown in Fig. 5.2. Different models for PSVS can be designed. One may design sophisticated PSVS controller. In this chapter a simple lead-lag block with a gain of *K* is used (Fig. 5.2).

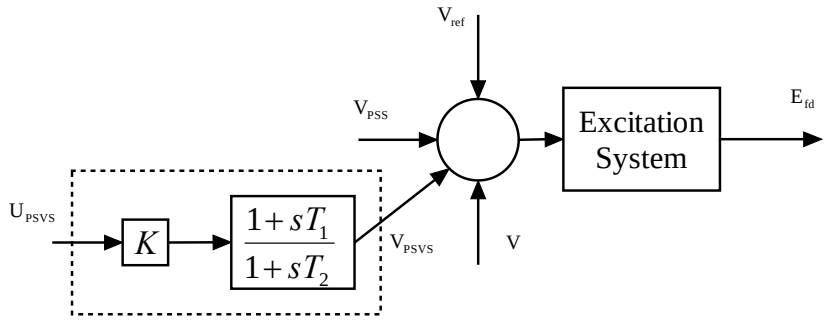

Fig. 5. 2 Symbolic representation of the excitation system of a generator including PSVS

5.4 Design of PSVS

5.4.1 Location of PSVS

PSVS operates on excitation system of a generator/condenser. It may be impractical to install PSVS to all generators. To efficiently enhance the voltage stability, location of PSVS is first considered.

In this study, the mode participation factor will be used to determine the location of PSVS. For small disturbance stability analyses, participation factors will determine which excitation system of generators is the most associated with the critical eigenvalue.

5.4.2 Selection of PSVS input signal

A. Modal analysis method

In this research work, the nodal voltage is concerned; therefore, the output vector is the nodal voltage magnitude represented as

$$\boldsymbol{Y} = \Delta \boldsymbol{V} = \begin{bmatrix} \frac{\boldsymbol{V}_R}{\boldsymbol{V}} & \frac{\boldsymbol{V}_J}{\boldsymbol{V}} \end{bmatrix} \begin{bmatrix} \Delta \boldsymbol{V}_R \\ \Delta \boldsymbol{V}_J \end{bmatrix} \tag{5.2}$$

Algebraic variable $\boldsymbol{M}$ consists of $[\Delta \boldsymbol{I}_R, \Delta \boldsymbol{I}_J, \Delta \boldsymbol{V}_R, \boldsymbol{V}_{J\ other}]^T$. $\Delta \boldsymbol{V}_R$ and $\Delta \boldsymbol{V}_J$ are deviations of node voltage; $\Delta \boldsymbol{I}_R$ and $\Delta \boldsymbol{I}_J$ are deviations of generator injection current; $\boldsymbol{V}_{other}$ are outputs of other zero order blocks. Therefore, the output vector $\boldsymbol{Y}$ can be rewritten as

$$\boldsymbol{Y} = \boldsymbol{C}_1 \Delta \boldsymbol{M} \tag{5.3}$$

In terms of the relationship between algebraic and state variables

$$\Delta \boldsymbol{M} = -\boldsymbol{L}_9^{-1} \boldsymbol{L}_7 \Delta \boldsymbol{X} \tag{5.4}$$

Substituting (5.4) into (5.3) gives

$$\boldsymbol{Y} = \boldsymbol{C} \Delta \boldsymbol{X} \tag{5.5}$$

where $\boldsymbol{C} = \boldsymbol{C}_1(-\boldsymbol{L}_9^{-1} \boldsymbol{L}_7)$

The diagonal matrix $\boldsymbol{\Lambda} = diag(\lambda_1, \lambda_2, \cdots, \lambda_n)$ consists of eigenvalue of state equation $\Delta \dot{\boldsymbol{X}} = \boldsymbol{A} \Delta \boldsymbol{X}$. $\boldsymbol{U}$ is right eigenvector matrix, according to,

$$\boldsymbol{A}\boldsymbol{U} = \boldsymbol{U}\boldsymbol{\Lambda} \tag{5.6}$$

the system is linearly transformed by using right eigenvector matrix. A new set of state variables are expressed as

$$\Delta \boldsymbol{X} = \boldsymbol{U}\Delta \boldsymbol{Z} \tag{5.7}$$

The new state equation is represented as follows

$$\Delta \dot{\boldsymbol{Z}} = \boldsymbol{U}^{-1}\boldsymbol{A}\boldsymbol{U}\Delta \boldsymbol{Z} = \boldsymbol{\Lambda}\Delta \boldsymbol{Z} \tag{5.8}$$

Since $\boldsymbol{\Lambda}$ is diagonal matrix, the system can be decoupled in the new state space. One of equations is expressed as follows

$$\Delta Z_i = \lambda_i \Delta Z_i \tag{5.9}$$

One of the time domain solutions is

$$\Delta Z_i = z_{i0} e^{\lambda_i t} \ (i = 1,2,\cdots,n) \tag{5.10}$$

where z_{i0} is the initial value of ΔZ_i.

Substituting equation (5.8) into equation(5.7), power system state variables is represented as

$$\Delta X = \boldsymbol{U}\Delta \boldsymbol{Z} = U_1 \Delta Z_1 + U_2 \Delta Z_2 +,\cdots, U_n \Delta Z_n = z_{10} U_1 e^{\lambda_1 t} + z_{20} U_2 e^{\lambda_2 t} +,\cdots, + z_{n0} U_n e^{\lambda_n t} \tag{5.11}$$

Substituting equation (5.11) into equation(5.5), the deviation of node voltage magnitude can be expressed as equation (5.12)

$$\boldsymbol{Y} = \Delta \boldsymbol{V} = \boldsymbol{C}\boldsymbol{U}\Delta \boldsymbol{Z} = \boldsymbol{W}\Delta \boldsymbol{Z} = z_{10} w_1 e^{\lambda_1 t} + z_{20} w_2 e^{\lambda_2 t} +,\cdots, + z_{n0} w_n e^{\lambda_n t} \tag{5.12}$$

For a instable mode $e^{\lambda_i t}$, w_{ji} indicates the effect of instable mode on nodal voltage magnitude. If some w_{ji} are large, the corresponding node voltage is affected heavily by instable mode and is prone to collapse. w_{ji} is called instable mode coefficient (Liu et al., 1999). The node which is most associated with the largest w_{ji} is the weak node, and the voltage magnitude deviation of this node is an appropriate input signal of PSVS. The input signal of PSVS may not be local signal. The remote signals for

controllers (Aboul-Ela, Sallam, McCalley, & Fouad, 1996; Chaudhuri & Pal, 2004; Farsangi, Nezamabadi-pour, Song, & Lee, 2007) have been used.

B. Probabilistic sensitivity index

Residue method and different sensitivity coefficients have been proposed and successfully used for selecting PSS sites. The relationship between residue and eigenvalue sensitivity (Wang, 2000) has been discussed. The residue of an open-loop system can also be obtained by the eigenvalue sensitivity from its closed-loop system when the gain of feedback is zero. The residue index is successfully extended to probabilistic environment (Wang, 2000) for design of power system stabilizer considering a wide operating condition, called probabilistic sensitivity index.

Under the assumption of normal distribution, the statistic nature of a random can be determined by its expectation and variance. In order to ensure the system robust stable as mentioned in section 5.2, the upper limit should be negative, i.e.

$$\alpha'_k = \bar{\alpha}_k + 4\sigma_k \le 0 \tag{5.13}$$

The probabilistic sensitivity index (PSI) adopted to determine the input signal in this chapter can be expressed as the following equation,

$$PSI_{\alpha'_{k,m}} = S_{\alpha'_{k,m}} = \left.\frac{\partial \alpha'_k}{\partial K_m}\right|_{K_m=0} = \left.\frac{\partial \bar{\alpha}_k}{\partial K_m}\right|_{K_m=0} + 4\left.\frac{\partial \sigma_k}{\partial K_m}\right|_{K_m=0} \tag{5.14}$$

5.4.3 PSVS parameter optimization

To ensure that the system is robust stable, the inequality of (5.15) for the *k*-th complex eigenvalue $\lambda_k = \alpha_k + j\beta_k$ should be achieved.

$$\alpha_k^* = -\overline{\alpha}_k / \sigma_{\alpha_k} \geq 4 \tag{5.15}$$

where α_k^* is the standardized expectation, as well as a direct measure of the stable probability of $P\{\alpha_k < 0\}$ under the normal distribution.

Optimization method is used to determine appropriate PSVS parameters to improve voltage stability of power system. A nonlinear objective function can be established as equation (5.16) with $\boldsymbol{K}$ standing for the PSVS parameter vector,

$$\text{Minimize} F(\boldsymbol{K}) = \sum_{\alpha_k^* < 4} (\alpha_k^* - 4)^2 \tag{5.16}$$

Problem (5.16) can be solved by the steepest descent approach. To steed up the convergence, the quasi-Newton method with correcting equation (5.17) can be applied.

$$\boldsymbol{K}^{(i+1)} = \boldsymbol{K}^{(i)} - \mu_2^{(i)} \boldsymbol{H}^{(i)} \nabla F(\boldsymbol{K}^{(i)}) \tag{5.17}$$

The optimal step length $\mu_2^{(i)}$ is also obtained by the one-dimensional search. $\boldsymbol{H}^{(i)}$ is the approximation to the inverse of the second order derivative matrix of $F(\boldsymbol{K})$ at point $\boldsymbol{K}^{(i)}$ and will be improved in each iteration. The iterative procedure of the method can be stated as follows,

(a) Start with an initial point $\boldsymbol{K}^{(1)}$, and $\boldsymbol{H}^{(1)} = [\boldsymbol{I}]$. Set iteration number $i = 1$.

(b) Compute the objective function $F(\boldsymbol{K}^{(i)})$, if $\left|F(\boldsymbol{K}^{(i)})\right| < \varsigma$, stop; otherwise, go to (c);

(c) Compute the gradient $\nabla F(\boldsymbol{K}^{(i)})$, and set

$$\boldsymbol{S}^{(i)} = -\boldsymbol{H}^{(i)} \nabla F(\boldsymbol{K}^{(i)}) \tag{5.18}$$

(d) Check the convergence. If $\left|\boldsymbol{S}^{(i)}\right| < \varepsilon$, stop.

(e) Find the optimal step length $\mu_2^{(i)}$ in the direction $\boldsymbol{S}^{(i)}$ and set

$$\boldsymbol{K}^{(i+1)} = \boldsymbol{K}^{(i)} + \mu_2^{(i)} \boldsymbol{S}^{(i)} \tag{5.19}$$

(f) Calculate the objective function $F(\boldsymbol{K}^{(i+1)})$. If $\left|F(\boldsymbol{K}^{(i)})\right| < \varsigma$, terminate the iterative process; otherwise, go to (g).

(g) Compute $\nabla F(\boldsymbol{K}^{(i+1)})$ at the point $\boldsymbol{K}^{(i+1)}$, and set

$$\Delta \boldsymbol{G}^{(i)} = \nabla F(\boldsymbol{K}^{(i+1)}) - \nabla F(\boldsymbol{K}^{(i)}) \tag{5.20}$$

(h) Update the $\boldsymbol{H}$ matrix as

$$\boldsymbol{H}^{(i+1)} = \boldsymbol{H}^{(i)} + \frac{\Delta \boldsymbol{K}^{(i)} \Delta \boldsymbol{K}^{(i)^T}}{\Delta \boldsymbol{K}^{(i)^T} \Delta \boldsymbol{G}^{(i)}} - \frac{(\boldsymbol{H}^{(i)} \Delta \boldsymbol{G}^{(i)})(\boldsymbol{H}^{(i)} \Delta \boldsymbol{G}^{(i)})^T}{\Delta \boldsymbol{G}^{(i)^T} \boldsymbol{H}^{(i)} \Delta \boldsymbol{G}^{(i)}} \tag{5.21}$$

(i) Set the iteration number $i = i + 1$, and go to (c).

However, along with the parameter optimization, some modes are improved by parameter adjustment, but some of other modes may be jeopardized and become unstable. Eigenvalues considered in $F(\boldsymbol{K}^{(i+1)})$ may be different from those in $F(\boldsymbol{K}^{(i)})$. In this case, the gradient difference $\Delta \boldsymbol{G}^{(i)}$ may provide an ineffective or

wrong correction for $\boldsymbol{H}^{(i+1)}$. At this case, $\boldsymbol{H}^{(i+1)}$ has to be restarted from the identity matrix $\boldsymbol{H}^{(i+1)} = [\boldsymbol{I}]$.

5.5 Case studies

The effect of PSVS to improve power system voltage stability is investigated on two test systems: 9-bus system of Fig. 3.5, and the 39-bus system of Fig. 3.8. All loads in the two systems are independent random variables with mean values at the nominal bus loading value from the original system, and the variance of each load is chosen such that the 90% confidence interval is ±10% of the nominal loading value. Constant power load model is adopted for all loads. All load increase at the same proportion is assumed.

5.5.1 9-bus system

There are three generators and three loads in the system shown in Fig. 3.5. The fourth order model is adopted for all generators. The exciter is assumed to be identical for all the machines and is the IEEE-Type I shown in appendix 3.

Based on probabilistic analysis, the stability is assessed and the critical eigenvalue $\bar{\lambda}$ =-0.0618±j1.6368 is associated with the exciter of generator G3 (Table 5.1). With an eigenvalue distribution of Fig. 5.1, voltage stability with only about 70.88% stable operation scenarios is inadequate, as reflected in α^*=0.5457 less than 4. In terms of stability margin index, k_c=0.0069 for 50% is rather small and I_{SM}=-0.0164 for 99% is even negative. The probabilistic stability margins for other ‘cumulative

densities' are computed in Table 5.2 such that the rough distribution of stability margin under the load uncertainty can be derived as Fig 5.3.

Table 5. 1 The critical eigenvalue at a critical load level without PSVS

Critical eigenvalue	Associated state variables	$\alpha^* = -\overline{\alpha}/\sigma_\alpha$	Stability probability
-0.0618±j1.6368	E'_{q3}, E_{fd3}	0.5457	70.88%

Table 5. 2 Probabilistic stability margin of 9-bus system without PSVS

Cumulative density	Probabilistic stability margin
99%	-0.0164
90%	-0.0076
80%	-0.0032
70%	0.0002
60%	0.0035
50%	0.0069
40%	0.0107
30%	0.0155
20%	0.0221
10%	0.0353
4%	0.0560

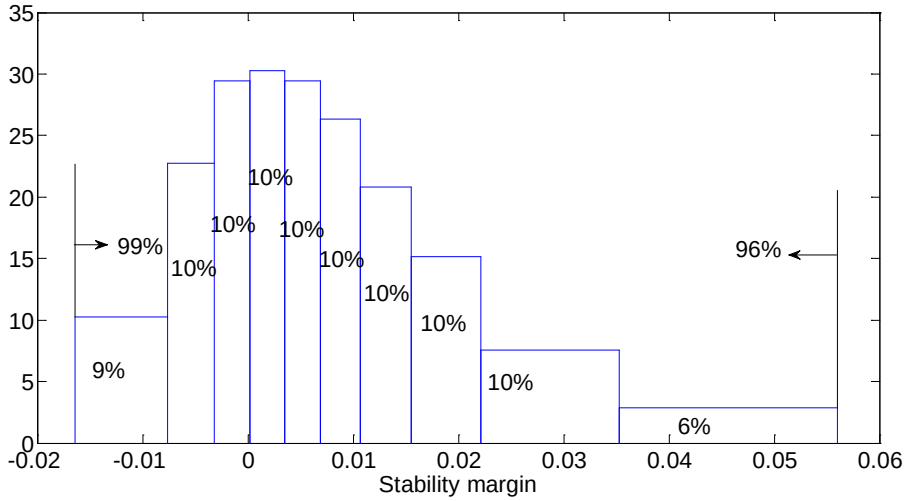

Fig. 5. 3 Distribution of probabilistic stability margin of 9-bus system without PSVS

In order to improve the probabilistic voltage stability of this weak system, PSVS is introduced. As the critical mode is associated with the exciter of generator G3, the

suitable location of the PSVS should be the G3 exciter. For the signal selection, two indexes of modal coefficient and probabilistic sensitivity index are used. Fig. 5.4 and Fig. 5.5 for the two indices reach the similar conclusion: the voltage magnitude deviation of bus 1 and 5 can be the input signal of PSVS. Here, the voltage magnitude deviation of bus 5 is selected as the input signal.

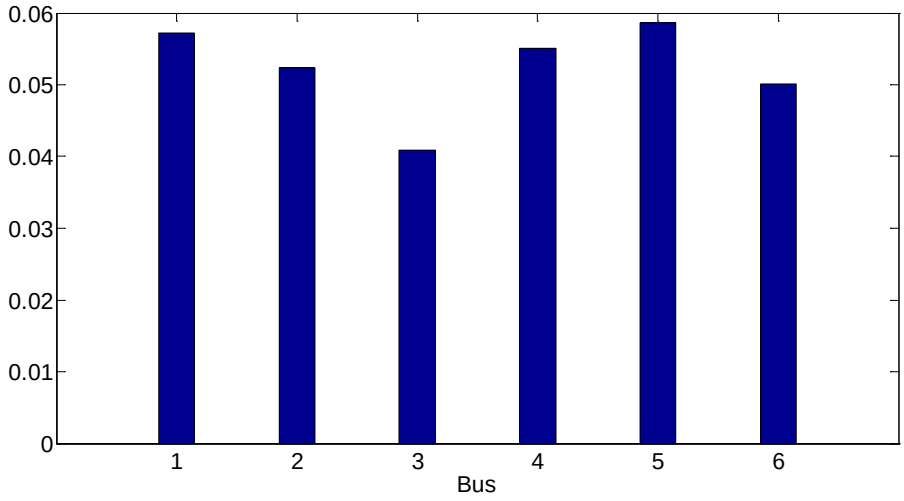

Fig. 5. 4 Voltage instability mode coefficient in 9-bus system

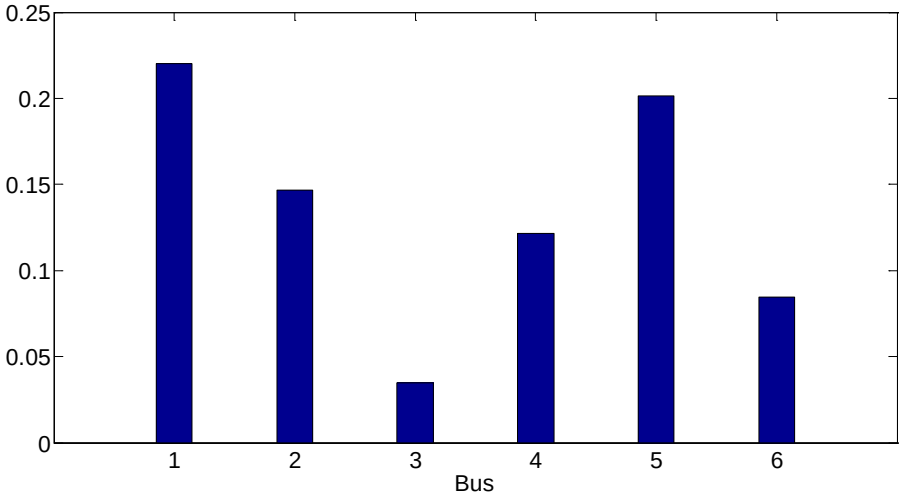

Fig. 5. 5 PSI corresponding to residue with input signals of nodal voltage of 9-bus system

After the selection of location and signals, the initial parameters of PSVS are chosen as $K = 1.0,\ T_a = 0.2,\ T_b = 0.1$: system stability is improved but α^*=1.3530 is still less

than 4 in Table 5.3. After the PSVS parameters optimized with the quasi-Newton method, α^* is increased to 7.7163 and the system stability becomes adequate and more than 99.997% of scenarios has positive load margin.

Table 5. 3 Voltage stability without and with PSVS

	K	T_a	T_b	$\alpha^* = -\overline{\alpha}/\sigma_\alpha$	k_c	I_{SM}
Without PSVS	0	-	-	0.5457	0.0069	-0.0164
PSVS with Initial settings	1.0	0.2	0.1	1.3530	0.0137	-0.0071
PSVS with optimized setting	1.6054	0.3111	0.0994	7.7163	0.0304	0.0142

Load margin changes are also examined. With the initial parameters, the stability margins are: k_c=0.0137 for 50% and I_{SM}=-0.0071 for 99%. After the parameter optimization, the stability margin margins are increased to k_c=0.0304 and I_{SM} =0.0142. Finally more probabilistic stability margins are computed in Table 5.4 and the derived distribution of stability margin is as shown in Fig. 5.6. Comparing Fig. 5.3 and Fig. 5.6, the distribution of the stability margin has been shifted to the right by the PSVS and the stability of power system is much improved.

Table 5. 4 Probabilistic stability margins with PSVS

Cumulative density	Probabilistic stability margin
99%	0.0142
90%	0.0192
80%	0.0221
70%	0.0245
60%	0.0273
50%	0.0304
40%	0.0341
30%	0.0383
20%	0.0428
10%	0.0492
4%	0.0566

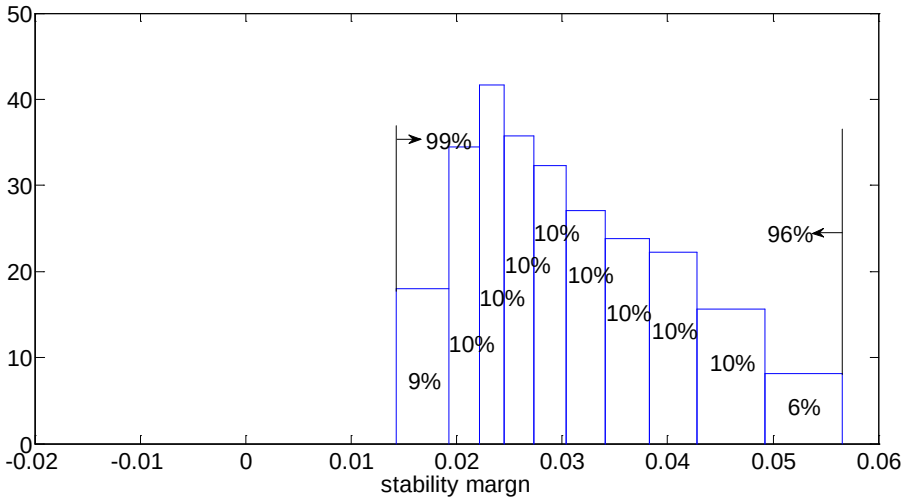

Fig. 5. 6 Distribution of probabilistic stability margin of 9-bus system with optimized PSVS

5.5.2 39-bus system

This system includes ten generators and nineteen loads shown in Fig. 3.8. The fourth and third order model is adopted for generators. The critical eigenvalue and the associated state variables are listed in Table 5.5. Since α^* =0.2531<4, the power system stability is inadequate. The computed stability margins are listed in Table 5.6, and the rough distribution of stability margin under load uncertainty is derived as shown in Fig.5.7.

Table 5. 5 Critical eigenvalues at critical load level without PSVS

Critical eigenvalue	Associated state variables	$\alpha^* = -\overline{\alpha}/\sigma_\alpha$	Stability probability
-0.0123±j 2.8090	$E_{q9}^{'}, E_{fd9}$	0.2531	59.87%

Table 5. 6 Probabilistic stability margins of 39-bus system without PSVS

Cumulative density	Probabilistic stability margin
99%	-0.0152
90%	-0.0079
80%	-0.0046
70%	-0.0022
60%	0.0000
50%	0.0021
40%	0.0041
30%	0.0065
20%	0.0092
10%	0.0131
4%	0.0172

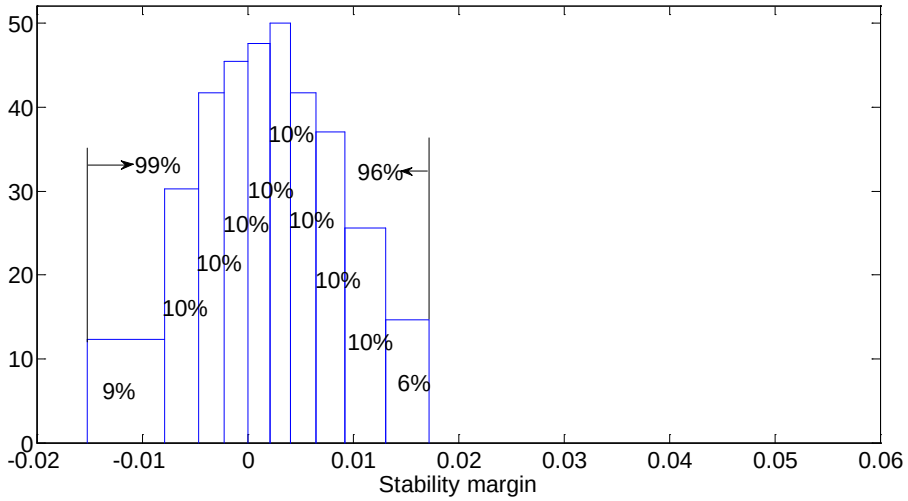

Fig. 5. 7 Distribution of probabilistic stability margin of 39-bus system without PSVS

Since the critical eigenvalue is associated with the exciter of generator G9, PSVS should be installed to the exciter of generator G9 in Fig. 3.8. The two indices (modal coefficients and the PSIs of residue index) are computed as illustrated in Fig. 5.8 and 5.9. The decision is that the best input signal of PSVS is the deviation of bus-29.

With initial PSVS parameters $K = -0.1, T_a = 0.2, T_b = 0.2$, the improved α^*=1.5410 is less than 4. To enhance the stability, the PSVS parameters are then tuned by the nonlinear optimization technique. After optimization of PSVS parameters, the final α^*= 6.7130 is larger than 4 (Table 5.7), and system stability is adequate. Once more, the stability is reassessed with voltage margins k_c and I_{SM}. Without PSVS, the probabilistic stability margins are poor with k_c =0.0021 and I_{SM}=-0.0152. With PSVS having initial parameters, the probabilistic stability margin k_c=0.0118 and I_{SM}=-0.0054. With optimized PSVS, k_c=0.0421 and I_{SM}=0.0250. Finally, the computed probabilistic stability margins are listed in Table 5.8 and the derived distribution of stability margin is shown in Fig. 5.10. Comparing Fig. 5.7 and Fig. 10, the distribution of stability margin is shifted to the right by the optimized PSVS and the stability of power system is enhanced by the optimized PSVS.

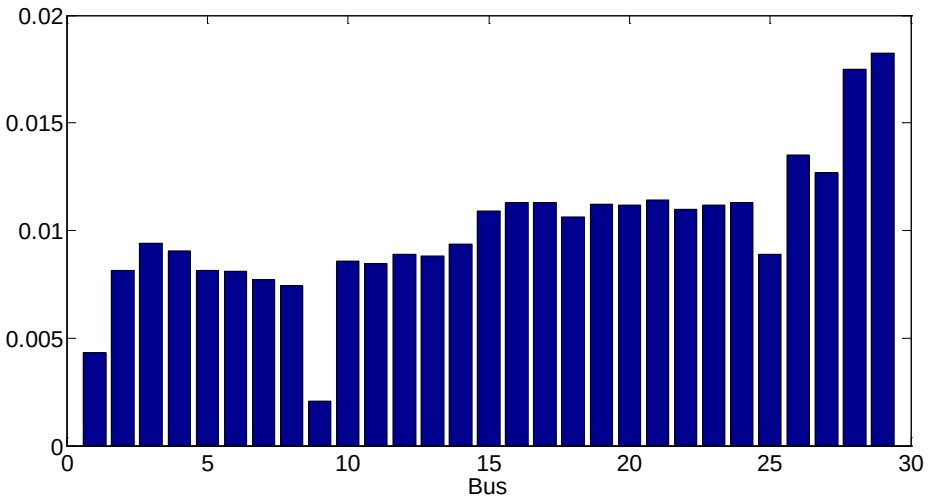

Fig. 5. 8 Voltage instability mode coefficient of 39-bus system

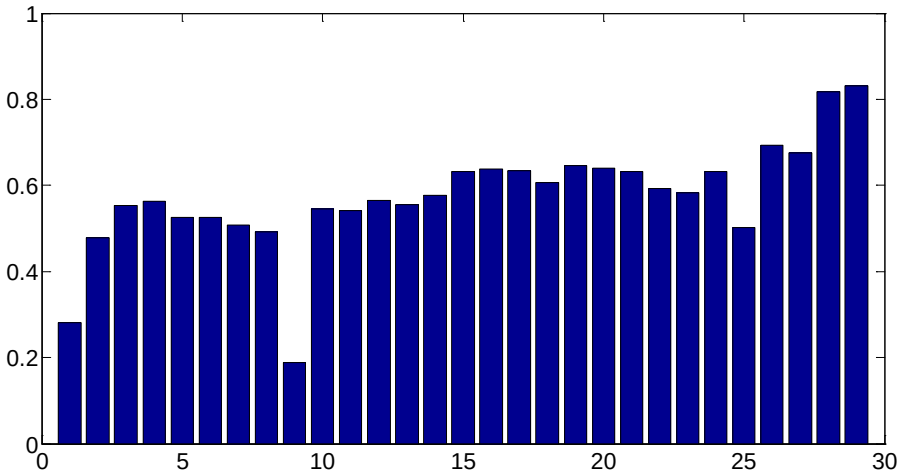

Fig. 5. 9 PSI with input signals of nodal voltage of 39-bus system

Table 5. 7 Voltage stability without and with PSVS

	K	T_a	T_b	$\alpha^* = -\overline{\alpha}/\sigma_\alpha$	k_c	I_{SM}
Without PSVS	0	-	-	0.2531	0.0021	-0.0152
PSVS with Initial settings	-0.1	0.2	0.2	1.5410	0.0118	-0.0054
PSVS with optimized setting	-0.4219	0.1949	0.2004	6.7130	0.0421	0.0250

Table 5. 8 Probabilistic stability margins of 39-bus system with PSVS

Cumulative density	Probabilistic stability margin
99%	0.0250
90%	0.0323
80%	0.0355
70%	0.0379
60%	0.0401
50%	0.0421
40%	0.0441
30%	0.0466
20%	0.0492
10%	0.0531
4%	0.0574

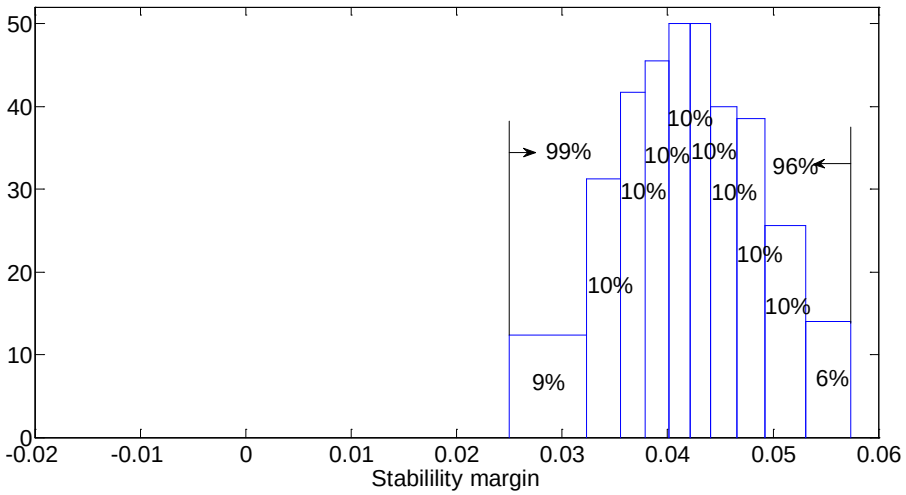

Fig. 5. 10 Distribution of probabilistic stability margin of 39-bus system with optimized PSVS

5.6 Conclusion

In this chapter, PSVS was used to improve the voltage stability of power system considering the load uncertainties. In order to ensure power system being stable under the load uncertainty, a high reliable index $\alpha^{*}>4$ was used to assess the adequacy of stability. The PSVS were installed to two weak systems having $\alpha^{*}<4$. First, the participation factor of the critical eigenvalue was used to locate PSVS. Then modal instable coefficient and PSI were adopted to determine the input signal of PSVS. Finally, the PSVS parameters were optimized by quasi-Newton method. Moreover, probabilistic stability margins indices (k_c of 50% and I_{SM} of 99%) and distributions of stability margin were used to quantify the stability improvements. The results confirm the designed PSVS with appropriate parameters can improve the voltage stability of power system.

Chapter 6 Conclusions and future work

6.1 Conclusions

Power system voltage stability is being paid increasing attention in last decades because several blackouts occurred is likely due to voltage instabilities. A great achievement has been developed in voltage stability study, and many methods have been proposed for assessment and enhancement of voltage stability. Most of the existing voltage stability analysis methods are based on predetermined set of severe but credible situations. However, there exist uncertainties such as measurement errors, forecast inaccuracy and outages of system elements in power systems. Considering these uncertainty factors, a few of probabilistic voltage stability analysis has been used to assess voltage stability, but they did not provide the probabilistic stability margin index which is a useful index to quantify the voltage stability of power system. The main objective of this research was to analyze voltage stability and to improve voltage stability of power system taking into account uncertainties in loads and load parameters.

Probabilistic voltage stability analysis based on power flow had been conducted to get the probabilistic distribution of stability margin in chapter 2. If the current point and load increase are predetermined, the stability margin and voltage collapse point can be easily obtained with point of collapse method. However, in this study, the

loads are random variables; therefore, stability margin and the critical point are also random. To obtain the statistical characteristics, such as expectation, covariance and moments of stability margin and nodal voltage at voltage collapse points, point of collapse method has been incorporated with probabilistic power flow. With these characteristics, maximum entropy has been adopted to determine the density function of stability margin. Furthermore, the effect of load uncertainty on the distribution of probabilistic stability margin had been analyzed. The load uncertainty has a slight effect on the stability margin mean value, but has a significant effect on the covariance of stability margin. In other words, with increase of load uncertainty, the stability margin will distribute in a wider range. In comparison with Monte Carlo simulation results which are obtained by analysis with point of collapse approach on numerous scenarios, the results showed that the proposed probabilistic method can obtain the probabilistic distribution of stability margin accurately and efficiently.

The above analysis in chapter 2 regards voltage stability as static problem and the voltage stability was analyzed based on power flow. The dynamic nature of voltage stability was studied in chapter 3. Under small disturbances, voltage stability margin is a reasonable index to the bifurcation-related instability. Since the loads are random variables, the load margin is also random. In this study, the probabilistic stability margin was obtained by probabilistic eigenvalue method. Firstly, probabilistic power flow at a particular load level was implemented, which provides the initial operating state of generators and probabilistic attributes of nodal voltages. Secondly, sensitivities of eigenvalues were used to determine the expectations and

covariances of eigenvalues. With the assumption that the distribution of eigenvalues is also close to normal, the stability probability of power system is determined by the critical eigenvalue. Finally, the probabilistic stability margin has been obtained by adjusting the load level to obtain the 'maximal' to reach the stability requirement. Two probabilistic stability margins indexes, k_c corresponding to 50% scenario and I_{SM} of 99% scenario, have been obtained by probabilistic eigenvalue method. Furthermore, the effect of load uncertainty on probabilistic stability margin has been examined. With increase in load uncertainty, k_c has only very slight change and I_{SM} drops gradually. The proposed method was validated by Monte Carlo simulation based on multi 10000 samples.

After analyzing voltage stability using the probabilistic eigenvalue by considering the uncertainties of loads, the research work was extended to examine the effect of dynamic load parameter uncertainty on voltage stability in chapter 4. A dynamic load model is established for the voltage stability analysis. Due to the random variation and other uncertain factor, different load parameter values have been used even for the same dynamic load model. The uncertainties of load parameters can affect the result of stability analysis. Voltage stability was analyzed taking into account the uncertainties of load parameters to obtain the probabilistic voltage stability margin, provided that the load parameters are normal random variables. The two probabilistic stability margin indexes, k_c and I_{SM} used in chapter 3, were once more used to determine the system stability and the results obtained were then compared with those obtained by Monte Carlo methods. It is shown that the

proposed probabilistic eigenvalue method can obtain the probabilistic stability margin accurately and efficiently.

Probabilistic voltage stability analysis has conducted considering the uncertainties of loads and dynamic load parameters. Based on the probabilistic analysis, power system voltage stabilizer (PSVS) was then used to improve the stability of very weak power systems in chapter 5. Similar to power system stabilizers (PSS) used for angular stability, PSVS output will be injected to excitation system of a generator. First, mode participation factors have been used to determine the most associated generator. Then, instability modal coefficient and probabilistic sensitivity index have been employed to determine the input signal of PSVS. Here, the index $\alpha^{*}>4$ (employed in angular stability) was used to ensure the system stability being adequate. Based on this α^{*} index, the PSVS parameters are optimized using nonlinear programming technique. The effect of PSVS to voltage stability was then examined by the probabilistic stability margin indexes k_c and I_{SM}. To derive the distribution of the stability margin, more indexes for different scenarios (other than 50% and 99%) are computed. The result comparisons of α^{*} as well as the voltage margin distribution on two test systems manifest that the PSVS with appropriate parameters can effectively improve the stability of power system.

6.2 Recommended future work

The research work presented in this thesis has attempted to develop probabilistic method to study voltage stability taking into account some uncertainties of power

system. With the progress made in this research work, the following issues are expected to be further explored in the future:

1. Effects of the load uncertainty and dynamic load parameter uncertainty were separately analyzed in this thesis. It will be more challenging if their effects can be simultaneously considered.

2. The probabilistic voltage stability analysis in this thesis is based on the system under normal operations. Contingencies such as transmission line or generator outages (which have been considered in other deterministic voltage stability studies) should be included in the future probabilistic study.

3. In this thesis, the uncertainties of loads or load parameters are assumed normal distribution. For probabilistic eigenvalue analysis, the variable can be any distribution. Any distribution uncertainties of loads can be included in voltage stability study.

4. Only PSVS for generator is used to improve voltage stability of power system in this thesis for wide range of system operation. A more effective PSVS design should be coordinated with reactive compensation in the system.

Appendix 1 Machine models

The third-order generator model is used in the thesis for modeling the d-axis and q-axis transient dynamics with the following equations,

$$p\delta / \Omega_0 = \Delta\Omega - \Delta\Omega_{ref} \tag{A1.1}$$

$$p\Omega = [P_m - P_e] / M \tag{A1.2}$$

$$pE_q' = [E_{fd} - (X_d - X_d')I_d - E_q'] / T_{do}' \tag{A1.3}$$

$$V_t^2 = V_d^2 + V_q^2 \tag{A1.4}$$

$$V_d = -R_a I_d + X_q I_q \tag{A1.5}$$

$$V_q = E_q' - X_d' - R_a I_q \tag{A1.6}$$

$$P_e = V_d I_d + V_q I_q + (I_d^2 + I_q^2) \tag{A1.7}$$

The GMT/PMT representation of the model is given in Fig. A1.1.

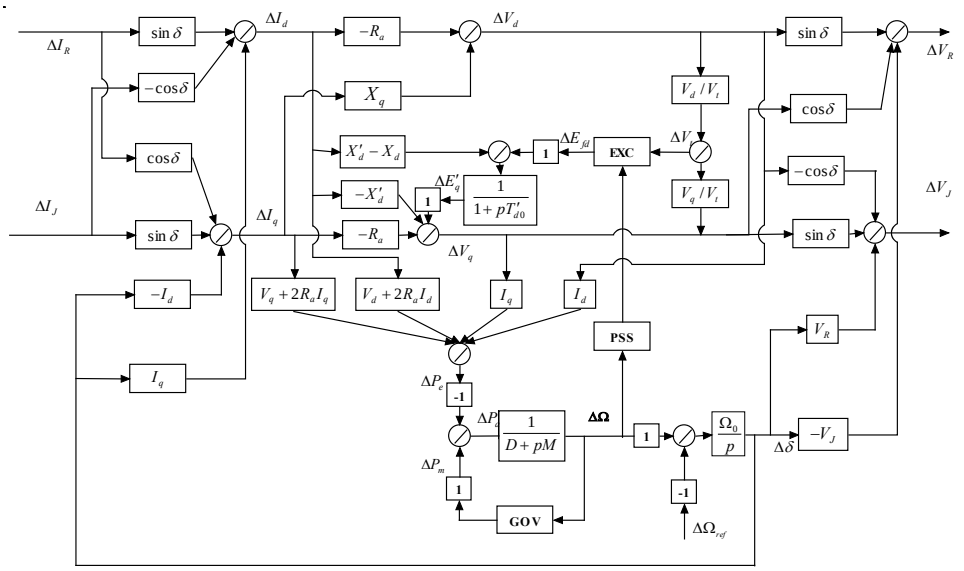

Fig. A1. 1 The GMT/PMT representation of the third-order generator model

The fourth-order generator model is used in the thesis for modeling the d-axis and q-axis transient dynamics with the following equations,

$$p\delta / \Omega_0 = \Delta\Omega - \Delta\Omega_{ref} \tag{A1.8}$$

$$p\Omega = [P_m - P_e] / M \tag{A1.9}$$

$$pE_q' = [E_{fd} - (X_d - X_d')I_d - E_q'] / T_{do}' \tag{A1.10}$$

$$pE_d' = [(X_q - X_q')I_q - E_d'] / T_{qo}' \tag{A1.11}$$

$$V_t^2 = V_d^2 + V_q^2 \tag{A1.12}$$

$$V_d = -R_a I_d + X_q I_q \tag{A1.13}$$

$$V_q = E_q' - X_d' - R_a I_q \tag{A1.14}$$

$$P_e = V_d I_d + V_q I_q + (I_d^2 + I_q^2) \tag{A1.15}$$

The GMT/PMT representation of the model is given in Fig. A1.2.

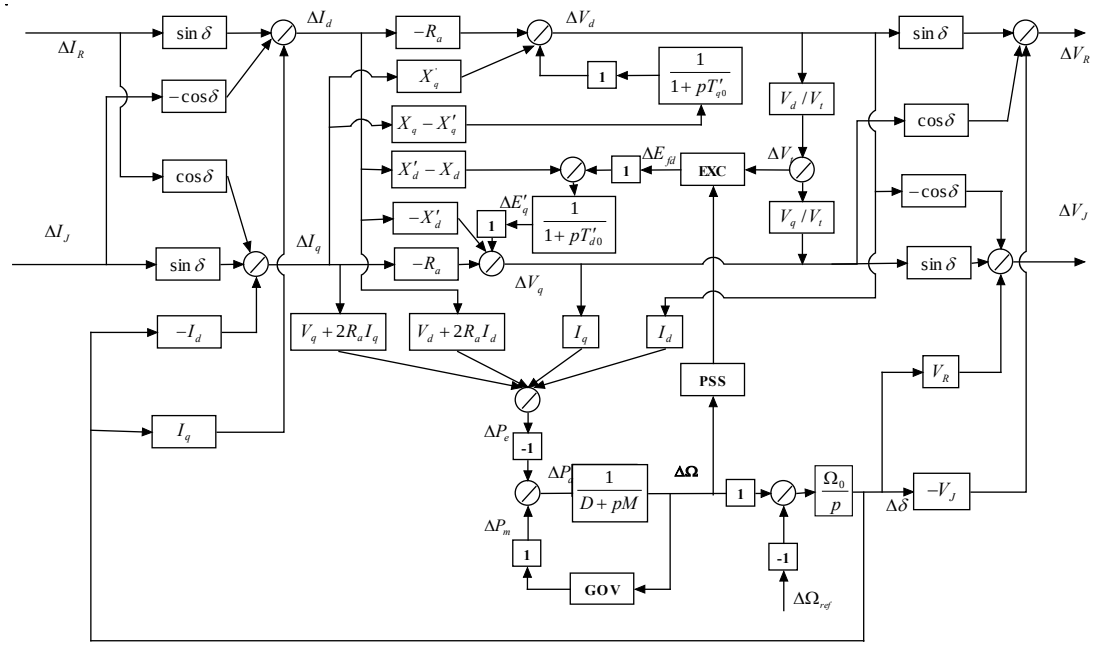

Fig. A1. 2 The GMT/PMT representation of the fourth-order generator model

Appendix 2 Representation of voltage dependent load

The voltage dependency of load characteristic is represented by an exponential function in (A2.1) for the load at node *i*

$$S_{Li} = P_i + jQ_i = P_0 V^a + jQ_0 V^b \tag{A2.1}$$

The load current is represented as

$$I_i = \frac{S_i^*}{V_i^*} = \frac{S_i^* V_i}{V_i^* V_i} = \frac{1}{V_i^2}(P_i - jQ_i)(V_{Ri} + jV_{Ji}) \tag{A2.2}$$

Equating the real and imaginary parts of the load current $I_i = I_{Ri} + jI_{Ji}$,

$$\begin{bmatrix} I_{Ri} \\ I_{Ji} \end{bmatrix} = \frac{1}{V_i^2}\begin{bmatrix} P_i & Q_i \\ -Q_i & P_i \end{bmatrix}\begin{bmatrix} V_{Ri} \\ V_{Ji} \end{bmatrix} \tag{A2.3}$$

Differentiating

$$\begin{bmatrix} \Delta I_{Ri} \\ \Delta I_{Ji} \end{bmatrix} = \frac{1}{V_i^2}\begin{bmatrix} P_i & Q_i \\ -Q_i & P_i \end{bmatrix}\begin{bmatrix} \Delta V_{Ri} \\ \Delta V_{Ji} \end{bmatrix} + \frac{1}{V_i^2}\begin{bmatrix} \Delta P_i & \Delta Q_i \\ -\Delta Q_i & \Delta P_i \end{bmatrix}\begin{bmatrix} V_{Ri} \\ V_{Ji} \end{bmatrix} - \frac{2\Delta V_i}{V_i^3}\begin{bmatrix} P_i & Q_i \\ -Q_i & P_i \end{bmatrix}\begin{bmatrix} V_{Ri} \\ V_{Ji} \end{bmatrix} \tag{A2.4}$$

where

$$\begin{bmatrix} \Delta P_i \\ \Delta Q_i \end{bmatrix} = \begin{bmatrix} aP_{0i} V_i^{a-1} \\ bQ_{0i} V_i^{b-1} \end{bmatrix} \Delta V_i = \begin{bmatrix} aP_i \\ bQ_i \end{bmatrix} \frac{\Delta V_i}{V_i} \tag{A2.5}$$

and

$$\Delta V_i = \frac{V_{Ri}}{V_i}\Delta V_{Ri} + \frac{V_{Ji}}{V_i}\Delta V_{Ji} \tag{A2.6}$$

because

$$V_i^2 = V_{Ri}^2 + V_{Ji}^2 \tag{A2.7}$$

Substitute (A2.5)and (A2.6) in(A2.4), $\Delta \boldsymbol{I}_i$ can be obtained by

$$\begin{bmatrix} \Delta I_{Ri} \\ \Delta I_{Ji} \end{bmatrix} = \frac{1}{V_i^2} \begin{bmatrix} Y_{RRi} & Y_{RJi} \\ Y_{JRi} & Y_{JJi} \end{bmatrix} \begin{bmatrix} \Delta V_{Ri} \\ \Delta V_{Ji} \end{bmatrix} \tag{A2.8}$$

where

$$\begin{aligned} Y_{RR} &= \frac{(a-2)PV_R^2}{V^4} + \frac{(b-2)QV_RV_J}{V^4} + \frac{P}{V^2} \\ Y_{RJ} &= \frac{(a-2)PV_RV_J}{V^4} + \frac{(b-2)QV_J^2}{V^4} + \frac{Q}{V^2} \\ Y_{JR} &= \frac{(a-2)PV_RV_J}{V^4} - \frac{(b-2)QV_R^2}{V^4} - \frac{Q}{V^2} \\ Y_{JJ} &= \frac{(a-2)PV_J^2}{V^4} - \frac{(b-2)QV_RV_J}{V^4} + \frac{Q}{V^2} \end{aligned} \tag{A2.9}$$

(A2.10)

The voltage dependent load module is shown in fig A1.1,

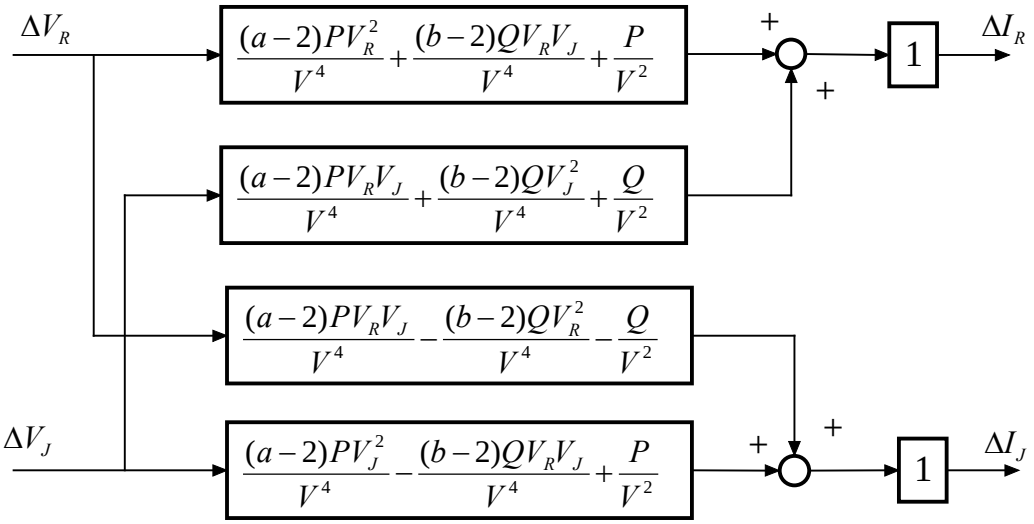

Fig. A2. 1 Voltage dependant load module

For the constant power load adopted in this thesis, a=b=0.

Appendix 3 Test system data

A) 39-bus system dada

Table A3. 1 Bus data of 39-bus system

Bus	Type (0=P-Q) (0=P-V)	Volts	Load MW	Load MVAR	Gen Load	Gen MVAR
1	0	-	0.0	0.0	0.0	0.0
2	0	-	0.0	0.0	0.0	0.0
3	0	-	322.0	2.40	0.0	0.0
4	0	-	500.0	184.0	0.0	0.0
5	0	-	0.0	0.0	0.0	0.0
6	0	-	0.0	0.0	0.0	0.0
*6	0	-	9.2	4.6	0.0	0.0
7	0	-	233.8	84.0	0.0	0.0
8	0	-	522.0	176.0	0.0	0.0
9	0	-	0.0	0.0	0.0	0.0
*9	0		1104.0	250.0	0.0	0.0
10	0	-	0.0	0.0	0.0	0.0
11	0	-	0.0	0.0	0.0	0.0
12	0	-	7.5	88.0	0.0	0.0
13	0	-	0.0	0.0	0.0	0.0
14	0	-	0.0	0.0	0.0	0.0
15	0	-	320.0	153.0	0.0	0.0
16	0	-	329.0	32.3	0.0	0.0
17	0	-	0.0	0.0	0.0	0.0
18	0	-	158.0	30.0	0.0	0.0
19	0	-	0.0	0.0	0.0	0.0
20	0	-	628.0	103.0	0.0	0.0
21	0	-	274.0	115.0	0.0	0.0
22	0	-	0.0	0.0	0.0	0.0
23	0	-	247.5	84.60	0.0	0.0
24	0	-	308.6	-92.20	0.0	0.0
25	0	-	224.0	47.20	0.0	0.0
26	0	-	139.0	17.0	0.0	0.0
27	0	-	281.0	75.5	0.0	0.0
28	0	-	206.0	27.6	0.0	0.0
29	0	-	283.5	26.9	0.0	0.0
30	1	1.0475	0.0	0.0	250.0	-
31	1	0.9820	9.2	4.60	-	-
*31	1	0.9802	0.0	0.0	-	-
32	1	0.9831	0.0	0.0	650.0	-
33	1	0.9972	0.0	0.0	632.0	-
34	1	1.0123	0.0	0.0	508.0	-
35	1	1.0493	0.0	0.0	650.0	-
36	1	1.0635	0.0	0.0	560.0	-
37	1	1.0278	0.0	0.0	540.0	-
38	1	1.0265	0.0	0.0	830.0	-
39	1	1.03	1104.0	250.0	1000.0	-
*39	1	1.03	0.0	0.0	1000.0	-

* Data used in chapter 3 and 5.

Table A3. 2 Line data for 39-bus system

Line Data				Transformer Tap			
No.	Bus	Bus	Resistance R	Reactance X	Susceptance B	Magnitude	Angle
1	1	2	0.0035	0.0411	0.6987	0.000	0.00
2	1	39	0.0010	0.0250	0.7500	0.000	0.00
3	2	3	0.0013	0.0151	0.2572	0.000	0.00
4	2	25	0.0070	0.0086	0.1460	0.000	0.00
5	3	4	0.0013	0.0213	0.2214	0.000	0.00
6	3	18	0.0011	0.0133	0.2138	0.000	0.00
7	4	5	0.0008	0.0128	0.1342	0.000	0.00
8	4	14	0.0008	0.0129	0.1382	0.000	0.00
9	5	6	0.0002	0.0026	0.0434	0.000	0.00
10	5	8	0.0008	0.0112	0.1476	0.000	0.00
11	6	7	0.0006	0.0092	0.1130	0.000	0.00
12	6	11	0.0007	0.0082	0.1389	0.000	0.00
13	7	8	0.0004	0.0046	0.0780	0.000	0.00
14	8	9	0.0023	0.0363	0.3804	0.000	0.00
15	9	39	0.0010	0.0250	1.2000	0.000	0.00
*15	9	39	0.0001	0.0025	1.2000	0.000	0.00
16	10	11	0.0004	0.0043	0.0729	0.000	0.00
17	10	13	0.0004	0.0043	0.0729	0.000	0.00
18	13	14	0.0009	0.0101	0.1723	0.000	0.00
19	14	15	0.0018	0.0217	0.3660	0.000	0.00
20	15	16	0.0009	0.0094	0.1710	0.000	0.00
21	16	17	0.0007	0.0089	0.1342	0.000	0.00
22	16	19	0.0016	0.0195	0.3040	0.000	0.00
23	16	21	0.0008	0.0135	0.2548	0.000	0.00
24	16	24	0.0003	0.0059	0.0680	0.000	0.00
25	17	18	0.0007	0.0082	0.1319	0.000	0.00
26	17	27	0.0013	0.0173	0.3216	0.000	0.00
27	21	22	0.0008	0.0140	0.2565	0.000	0.00
28	22	23	0.0006	0.0096	0.1846	0.000	0.00
29	23	24	0.0022	0.0350	0.3610	0.000	0.00
30	25	26	0.0032	0.0323	0.5130	0.000	0.00
31	26	27	0.0014	0.0147	0.2396	0.000	0.00
32	26	28	0.0043	0.0474	0.7802	0.000	0.00
33	26	29	0.0057	0.0625	1.0290	0.000	0.00
34	28	29	0.0014	0.0151	0.2490	0.000	0.00
35	12	11	0.0016	0.0435	0.0000	1.006	0.00
36	12	13	0.0016	0.0435	0.0000	1.006	0.00
37	6	31	0.0000	0.0250	0.0000	1.070	0.00
*37	6	31	0.0000	0.0125	0.0000	1.070	0.00
38	10	32	0.0000	0.0200	0.0000	1.070	0.00
39	19	33	0.0007	0.0142	0.0000	1.070	0.00
40	20	34	0.0009	0.0180	0.0000	1.009	0.00
41	22	35	0.0000	0.0143	0.0000	1.025	0.00
42	23	36	0.0005	0.0272	0.0000	1.000	0.00
43	25	37	0.0006	0.0232	0.0000	1.025	0.00
44	2	30	0.0000	0.0181	0.0000	1.025	0.00
45	29	38	0.0008	0.0156	0.0000	1.025	0.00
46	19	20	0.0007	0.0138	0.0000	1.060	0.00

* Data used in chapter 3 and chapter 5.

Table A3. 3 Detailed model unit data of 39-bus system

Unit No.	H (sec)	R_a	X_d'	X_q'	X_d	X_q	T_{d0}'	T_{q0}'	X_l
1	500.0	0	0.006	0.08	0.02	0.019	7.0	0.7	0.003
2	30.3	0	0.0697	0.170	0.295	0.282	6.56	1.5	0.035
3	35.8	0	0.0531	0.0876	0.2495	0.237	5.7	1.5	0.0304
4	28.6	0	0.0436	0.166	0.262	0.258	5.69	1.5	0.0295
5	26.0	0	0.132	0.166	0.67	0.62	5.4	0.44	0.054
6	34.8	0	0.05	0.0814	0.254	0.241	7.3	0.4	0.0224
7	26.4	0	0.049	0.186	0.295	0.292	5.66	1.5	0.0322
8	24.3	0	0.057	0.0911	0.290	0.280	6.7	0.41	0.028
9	34.5	0	0.057	0.0587	0.2106	0.205	4.79	1.96	0.0298
10	42.0	0	0.031	0.08	0.1	0.069	10.2	0.0	0.0125

Table A3. 4 Detailed model generator excitation system data of 39-bus system

Unit No.	K_A	T_A	V_{RMIN}	V_{RMAX}	K_E	T_E	K_F	T_F	C_1	C_2
1	0	0	0	1	0	0	0	0	0	0
2	6.2	0.05	-1.0	1.0	-0.633	0.405	0.057	0.5	0.66	0.88
3	5.0	0.06	-1.0	1.0	-0.0198	0.5	0.08	1.0	0.13	0.34
4	5.0	0.06	-1.0	1.0	-0.0525	0.5	0.08	1.0	0.08	0.314
5	40.0	0.02	-10.0	10.0	1.0	0.785	0.03	1.0	0.07	0.91
6	5.0	0.02	-1.0	1.0	-0.0419	0.471	0.0754	1.246	0.064	0.251
7	40.0	0.02	-6.5	6.5	1.0	0.73	0.03	1.0	0.53	0.74
8	5.0	0.02	-1.0	1.0	-0.047	0.528	0.0854	1.26	0.072	0.282
9	40.0	0.02	-10.5	10.5	1.0	1.4	0.03	1.0	0.62	0.85
10	5.0	0.06	-1.0	1.0	-0.0485	0.25	0.04	1	0.08	0.26

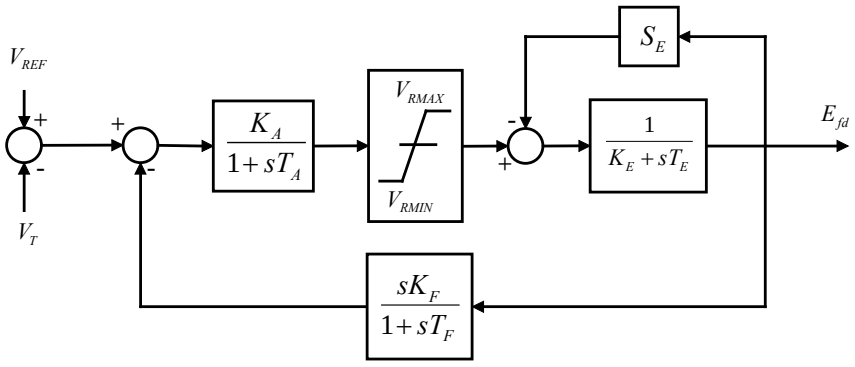

Fig. A3. 1 IEEE Type 1 rotating excitation system model adopted for 39-bus system

Note: A & Bin Fig. A3.1 are computed as follows:

$$EX_2 = \frac{V_{RMAX}}{K_E + C_2},\ EX_1 = 0.75EX_2$$

$$B = \ln(C_2 - C_1)/(EX_2 - EX_1),\ A = C_2 / e^{B \cdot EX_2}$$

$$S_E = Ae^{B \cdot E_{fd}}$$

Generator 1 has constant excitation.

B) 57-bus system

Table A3. 5 Bus data of 57-bus system

Bus No.	Type (1=P-Q) (2=P-V) (3=Slack)	voltage	Load MV	Load MVAR
1	3	1.04	-	-
2	2	1.01	3	88
3	2	0.985	41	21
4	1	-	0.0	0.0
5	1	-	13	4
6	2	0.98	75	2
7	1	-	0	0
8	2	1.005	150	22
9	2	0.98	121	26
10	1	-	5	2
11	1	-	0	0
12	2	1.1015	377	24
13	1	-	18	2.3
14	1	-	10.5	5.3
15	1	-	22	5
16	1	-	43	3
17	1	-	42	8
18	1	-	27.2	9.8
19	1	-	3.3	0.6
20	1	-	2.3	1
21	1	-	0.0	0.0
22	1	-	0.0	0.0
23	1	-	6.3	2.1
24	1	-	0.0	0.0
25	1	-	6.3	3.2
26	1	-	0.0	0.0
27	1	-	9.3	0.5
28	1	-	4.6	2.3
29	1	-	17	2.6
30	1	-	3.6	1.8
31	1	-	5.8	2.9
32	1	-	1.6	0.8
33	1	-	3.8	1.9

34	1	-	0.0	0.0
35	1	-	6	3
36	1	-	0.0	0.0
37	1	-	0.0	0.0
38	1	-	14	7
39	1	-	0.0	0.0
40	1	-	0.0	0.0
41	1	-	6.3	3
42	1	-	7.1	4.4
43	1	-	2	1
44	1	-	12	1.8
45	1	-	0.0	0.0
46	1	-	0.0	0.0
47	1	-	29.7	11.6
48	1	-	0.0	0.0
49	1	-	18	8.5
50	1	-	21	10.5
51	1	-	18	5.3
52	1	-	4.9	2.2
53	1	-	20	10
54	1	-	4.1	1.4
55	1	-	6.8	3.4
56	1	-	7.6	2.2
57	1	-	6.7	2.0

Table A3. 6 Line data of 75-bus system

No.	Bus	Bus	R	X	B	T
1	2	1	0.0083	0.028	0.129	
2	3	2	0.0298	0.085	0.0818	
3	4	3	0.0112	0.0366	0.038	
4	5	4	0.0625	0.132	0.0258	
5	6	4	0.043	0.148	0.0348	
6	7	6	0.02	0.102	0.0276	
7	8	6	0.0339	0.173	0.047	
8	9	8	0.0099	0.0505	0.0548	
9	10	9	0.0369	0.1679	0.044	
10	11	9	0.0258	0.0848	0.0218	
11	12	9	0.0648	0.295	0.0772	
12	13	9	0.0481	0.158	0.0406	
13	14	13	0.0132	0.0434	0.011	
14	15	13	0.0269	0.0869	0.023	
15	15	1	0.0178	0.091	0.0988	
16	16	1	0.0454	0.206	0.0546	
17	17	1	0.0238	0.108	0.0286	
18	15	3	0.0162	0.053	0.0544	
19	4	18	0.0	0.555	0.0	0.97
20	4	18	0.0	0.43	0.0	0.978
21	6	5	0.0302	0.0641	0.0124	
22	8	7	0.0139	0.0712	0.0194	
23	12	10	0.0277	0.1262	0.0328	
24	13	11	0.0223	0.0732	0.0188	
25	13	12	0.0178	0.058	0.0604	
26	16	12	0.018	0.0813	0.0216	
27	17	12	0.0397	0.179	0.0476	

28	15	14	0.0171	0.0547	0.0148	
29	19	18	0.461	0.685	0.0	
30	20	19	0.461	0.685		
31	21	20	0.0	0.7767	0.0	1.043
32	22	21	0.0736	0.117		
33	23	22	0.0099	0.0152		
34	24	23	0.166	0.256	0.0084	
35	24	25	0.0	1.182		
36	24	25	0.0	1.23		
37	24	26	0.0	0.0473		1.043
38	27	26	0.165	0.254		
39	28	27	0.0618	0.0954		
40	29	28	0.0418	0.0587		
41	7	29	0.0	0.0648		0.967
42	30	25	0.135	0.202		
43	31	30	0.326	0.497		
44	32	31	0.507	0.755		
45	33	32	0.0392	0.036		
46	34	32	0.0	0.953		0.975
47	35	34	0.052	0.078	0.032	
48	36	35	0.043	0.0537	0.0016	
49	37	36	0.029	0.0366		
50	38	37	0.0651	0.1009	0.002	
51	39	37	0.0239	0.0379		
52	40	36	0.03	0.0466		
53	38	22	0.0192	0.0295		
54	11	41	0.0	0.749		0.955
55	42	41	0.207	0.352		
56	43	41	0.0	0.412		
57	44	38	0.0289	0.0585	0.002	
58	15	45	0.0	0.1042		0.955
59	14	46	0.0	0.0735		0.9
60	47	46	0.023	0.068	0.0032	
61	48	47	0.0182	0.0233		
62	49	48	0.0834	0.129	0.0048	
63	50	49	0.0801	0.128		
64	51	50	0.1386	0.22		
65	10	51	0.0	0.0712		0.93
66	13	49	0.0	0.191		0.895
67	52	29	0.1442	0.187		
68	53	52	0.0762	0.0984		
69	54	53	0.1878	0.232		
70	55	54	0.1732	0.2265		
71	11	43	0.0	0.153		0.958
72	45	44	0.0624	0.1242	0.004	
73	40	56	0.0	0.1195		0.958
74	41	56	0.553	0.549		
75	42	56	0.2125	0.354		
76	39	27	0.0	1.355		0.98
77	56	57	0.174	0.26		
78	49	38	0.115	0.177	0.003	
79	48	38	0.115	0.177		
80	9	55	0.0	0.1205		0.94

C) 9-bus system

Table A3. 7 Load-flow results of 9-bus system

	Bus type	Voltage (pu)	P_G (pu)	Q_G (pu)	$-P_L$ (pu)	$-Q_L$ (pu)
1	(P-Q)	$1.026\angle 3.7^o$	-	-	-	-
2	(P-Q)	$1.032\angle 2.0^o$	-	-	-	-
3	(P-Q)	$1.026\angle -2.2^o$	-	-	-	-
4	(P-Q)	$0.996\angle -4.0^o$	-	-	1.25	0.5
5	(P-Q)	$1.016\angle 0.7^o$	-	-	1.00	0.35
6	(P-Q)	$1.013\angle -3.7^o$	-	-	0.9	0.3
7	(P-V)	$1.025\angle 9.3^o$	1.63	0.067		
8	(P-V)	$1.025\angle 4.7^o$	0.85	-0.109	-	-
9	(swing)	1.04	-	-	-	-

Table A3. 8 Line data of 9-bus system

No.	From	To	R	X	B	T
1	1	5	0.0085	0.072	0.1490	1.0
2	5	2	0.0119	0.1008	0.2090	1.0
3	1	4	0.0320	0.161	0.3060	1.0
4	4	3	0.01	0.085	0.176	1.0
5	2	6	0.039	0.17	0.358	1.0
6	3	6	0.017	0.092	0.158	1.0
7	7	1	0.0	0.0625	0.0	1.0
8	8	2	0.0	0.0586	0.0	1.0
9	9	3	0.0	0.0576	0.0	1.0

Table A3. 9 Generator data of 9-bus system

Generator No.	H	X_d	X_d'	X_q	X_q'	T_{d0}'	T_{q0}'
1	6.4	0.8958	0.1198	0.8645	0.1969	6.0	0.535
2	3.01	1.3125	0.1813	1.2578	0.25	5.89	0.6
3	23.64	0.146	0.0608	0.0969	0.0969	8.96	0.31

Table A3. 10 Exciter data of 9-bus system

No.	K_A	T_A (sec)	K_E	T_E (sec)	K_F	T_F (sec)
1	20	0.2	1.0	0.314	0.063	0.35
2	20	0.2	1.0	0.314	0.063	0.35
3	20	0.2	1.0	0.314	0.063	0.35

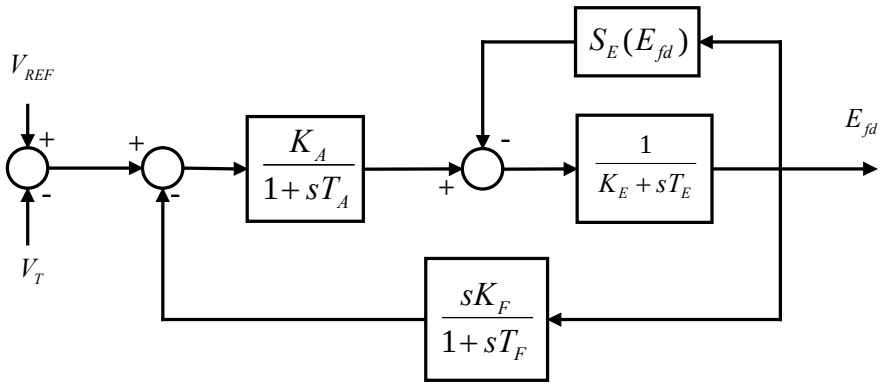

Fig. A3. 2 Exciter model adopted for 9-bus system

Note: $S_{Ei}(E_{fdi}) = 0.0039e^{1.555E_{fdi}} \quad i = 1,2,3$

D) 14-bus system

Table A3. 11 Bus data of 14-bus system

Bus No.	Type (1=P-Q) (2=P-V) (3=Slack)	voltage	Load MV	Load MVAR	Gen MV	Gen MVAR
1	3	1.06	-	-	-	-
2	2	1.045	-0.217	0.127-	0.4	-
3	2	1.01	0.942	0.19	0.0	-
4	1		0.478	0.04		
5	1		0.076	0.016		
6	2	1.07	0.112	0.075	0.0	-
7	1		0.0	0.0	-	-
8	2	1.09	0.0	0.0	0.0	-
9	1		0.295	0.166	-	-
10	1		0.09	0.058	-	-
11	1		0.035	0.018	-	-
12	1		0.061	0.016	-	-
13	1		0.135	0.058	-	-
14	1		0.149	0.05	-	-

Table A3. 12 Line data of 14-bus system

Line Data						Transformer Tap	
No.	Bus	Bus	Resistance R	Reactance X	Susceptance B	Magnitude	Angle
1	2	5	0.05695	0.17388	0.034		
2	6	12	0.12291	0.25581	0.0		
3	12	13	0.22092	0.19988	0.0		
4	6	13	0.06615	0.13027	0.0		
5	6	11	0.09498	0.1989	0.0		
6	11	10	0.08205	0.19207	0.0		
7	9	10	0.03181	0.0845	0.0		
8	9	14	0.12711	0.27038	0.0		
9	14	13	0.17093	0.34802	0.0		
10	7	9	0.0	0.11001	0.0		
11	1	2	0.01938	0.05917	0.0528		
12	3	2	0.04699	0.19797	0.0438		
13	3	4	0.06701	0.17103	0.0346		
14	1	5	0.05403	0.22304	0.0492		
15	5	4	0.01335	0.04211	0.0128		
16	2	4	0.05811	0.17632	0.0374		
17	5	6	0.0	0.25202	0.0	0.932	
18	4	9	0.0	0.55618	0.0	0.969	
19	4	7	0.0	0.20912	0.0	0.978	
20	8	7	0.0	0.17615	0.0		

Table A3. 13 Generator data of 14-bus system

	G1	G2	G3	G4	G5
X_l	0.0	0.0	0.0	0.0	0.0
R_a	0.0	0.0031	0.0031	0.0014	0.0014
X_d	0.8979	1.05	1.05	1.25	1.25
$X_d^{'}$	0.6	0.185	0.185	0.232	0.232
$X_d^{''}$	0.23	0.13	0.13	0.12	0.12
$T_{d0}^{'}$	7.4	6.1	6.1	4.75	4.75
$T_{d0}^{''}$	0.03	0.04	0.04	0.06	0.06
X_q	0.646	0.98	0.98	1.22	1.22
$X_q^{'}$	0.646	0.36	0.36	0.715	0.715
$X_q^{''}$	0.4	0.13	0.13	0.12	0.12
$T_{q0}^{'}$	2	0.3	0.3	1.5	1.5
$T_q^{''}$	0.033	0.099	0.099	0.21	0.21
M	10.296	13.08	13.08	10.12	10.12
D	2	2	2	2	2

Table A3. 14 Exciter data of 14-bus system

	EXC1	EXC2	EXC3	EXC4	EXC5
V_{rmax}	7.32	4.38	4.38	6.81	6.81
V_{rmin}	0	0	0	1.395	1.395
K_a	20	20	20	20	20
T_a	0.02	0.02	0.02	0.02	0.02
K_f	0.002	0.001	0.001	0.001	0.001
T_f	1.0	1.0	1.0	1.0	1.0
T_e	0.01	0.01	0.01	0.01	0.01
T_r	0.2	1.98	1.98	0.7	0.7
A_e	0.001	0.001	0.001	0.001	0.001
B_e	0.0006	0.0006	0.0006	0.0006	0.0006

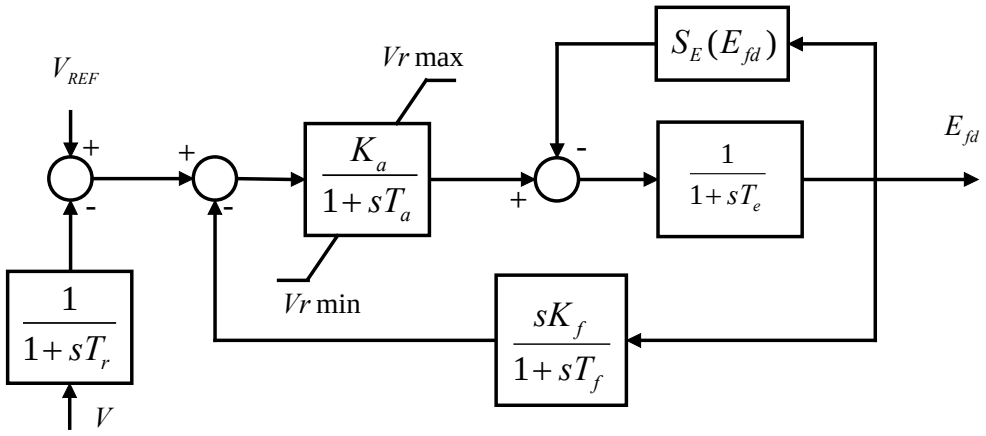

Fig. A3. 3 Exciter model adopted for 14-bus system

Note: $S_E(E_{fd}) = A_e(e^{B_e|E_{fd}|} - 1)$

Table A3. 15 Turbine governor data of 14-bus system

	Ω_{ref}	R	T_{max}	T_{min}	T_s	T_c	T_s	T_4	T_5
1	1	0.02	1.2	0.3	0.1	0.45	0.0	12	50
2	1	0.02	1.2	0.3	0.1	0.45	0.0	12	50

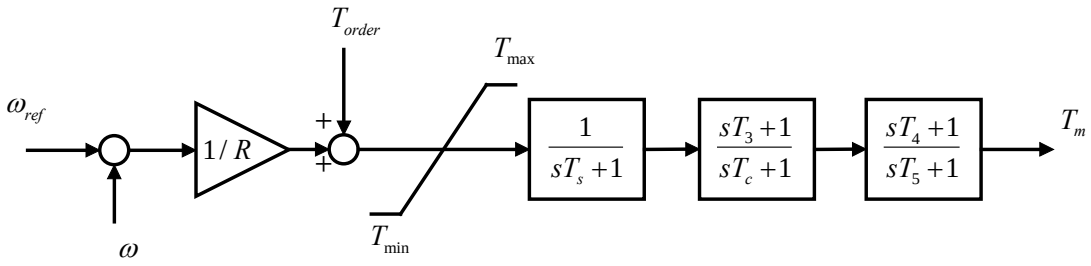

Fig. A3. 4 Turbine governor model adopted for 14-bus system

Reference

Aboreshaid, S., & Billinton, R. (1999). Probabilistic evaluation of voltage stability. *IEEE Transactions on Power Systems, 14*(1), 342-348.

Aboreshaid, S., Billinton, R., & Fotuhi-Firuzabad, M. (1996). Probabilistic transient stability studies using the method of bisection [power systems]. *IEEE Transactions on Power Systems, 11*(4), 1990-1995.

Aboul-Ela, M. E., Sallam, A. A., McCalley, J. D., & Fouad, A. A. (1996). Damping controller design for power system oscillations using global signals. *IEEE Transactions on Power Systems, 11*(2), 767-773.

Ajjarapu, V. (2006). Computational techniques for voltage stability assessment and control [electronic resource]. New York, NY :: Springer.

Ajjarapu, V., & Christy, C. (1992). The continuation power flow: a tool for steady state voltage stability analysis. *Power Systems, IEEE Transactions on, 7*(1), 416-423.

Ajjarapu, V., Lau, P. L., & Battula, S. (1994). An optimal reactive power planning strategy against voltage collapse. *IEEE Transactions on Power Systems, 9*(2), 906-917.

Alvarado, F., Dobson, I., & Yi, H. (1994). Computation of closest bifurcations in power systems. *IEEE Transactions on Power Systems, 9*(2), 918-928.

Amjady, N. (2004). A framework of reliability assessment with consideration effect of transient and voltage stabilities. *IEEE Transactions on Power Systems, 19*(2), 1005-1014.

Anders, G. J. (1990). Probability concepts in electric power systems. New York :: Wiley.

Arya, L. D., Titare, L. S., & Kothari, D. P. (2007). Probabilistic assessment and preventive control of voltage security margins using artificial neural network. *International Journal of Electrical Power & Energy Systems, 29*(2), 99-105.

Bao, L., Duan, X., & He, Y. (2000). Analysis of voltage collapse mechanisms in state space. *IEE P roceedings-Generation, T ransmission and D istribution, 147*(6), 395-400.

Bartoszyński, R. (1996). Probability and statistical inference New York :: Wiley.

Bedoya, D. B., Castro, C. A., & da Silva, L. C. P. (2008). A method for computing minimum voltage stability margins of power systems, *IET Generation, Transmission & Distribution* (Vol. 2, pp. 676-689).

Begovic, M., Fulton, D., Gonzalez, M. R., Goossens, J., Guro, E. A., Haas, R. W., et al. (1995). Summary of "System protection and voltage stability". *IEEE Transactions on Power Delivery, 10*(2), 631-638.

Begovic, M. M., & Phadke, A. G. (1990). Dynamic simulation of voltage collapse. *IEEE Transactions on Power Systems 5*(4), 1529-1534.

Begovic, M. M., & Phadke, A. G. (1992). Control of voltage stability using sensitivity analysis. *IEEE Transactions on Power Systems, 7*, 114-123.

Bian, X. (2006). Probabilistic robust damping controller designs for FACTS devices and PSS. Hong Kong :: Dept. of Electrical Engineering, The Hong Kong Polytechnic University.

Billinton, R., & Aboreshaid, S. (1998). Voltage stability considerations in composite power system reliability evaluation. *IEEE Transactions on Power Systems, 13*(2), 655-660.

Borghetti, A., Caldon, R., Mari, A., & Nucci, C. A. (1997). On dynamic load models for voltage stability studies. *IEEE Transactions on Power Systems, 12* (1), 293-303.

Burchett, R. C., & Heydt, G. T. (1978). Probabilistic Methods For Power System Dynamic Stability Studies. *IEEE Transactions on Power Apparatus and Systems, PAS-97*(3), 695-702.

Byongjun, L., & Ajjarapu, V. (1995). A piecewise global small-disturbance voltage-stability analysis of structure-preserving power system models. *IEEE Transactions on Power Systems, 10*(4), 1963-1971.

Canizares, C. A., & Alvarado, F. L. (1993). Point of collapse and continuation methods for large AC/DC systems. *IEEE Transactions on Power Systems, 8*(1), 1-8.

Chaudhuri, B., & Pal, B. C. (2004). Robust damping of multiple swing modes employing global stabilizing signals with a TCSC. *IEEE Transactions on Power Systems, 19*(1), 499-506.

Chen, Y.-L. (1996). Weak bus-oriented optimal multi-objective VAr planning. *IEEE Transactions on Power Systems, 11*(4), 1885-1890.

Chen, Y.-L., Chang, C.-W., & Liu, C.-C. (1995). Efficient methods for identifying weak nodes in electrical power networks. *IEE Proceedings: Generation, Transmission and Distribution, 142*(3), 317-322.

Chiang, H.-D., Flueck, A. J., Shah, K. S., & Balu, N. (1995). CPFLOW: a practical tool for tracing power system steady-state stationary behavior due to load and generation variations. *IEEE Transactions on Power Systems, 10*(2), 623-634.

Chiang, H.-D., & Jean-Jumeau, R. (1995). A more efficient formulation for computation of the maximum loading points in electric power systems. *IEEE Transactions on Power Systems, 10*(2), 635-646.

Chung, C. Y., Wang, K. W., Cheung, C. K., Tse, C. T., & David, A. K. (1998). Machine and load modeling in large scale power industries. Paper presented at the Dynamic Modeling Control Applications for Industry Workshop, 1998. IEEE Industry Applications 1998.

Chung, C. Y., Wang, K. W., Tse, C. T., Bian, X. Y., & David, A. K. (2003). Probabilistic Eigenvalue Sensitivity Analysis and PSS Design in Multimachine Systems. *IEEE Transactions on Power Systems, 18*(4), 1439-1445.

Chung, C. Y., Wang, K. W., Tse, C. T., & Niu, R. (2002). Power-system stabilizer (PSS) design by probabilistic sensitivity indexes (PSIs). *IEEE Transactions on Power Systems, 17*(3), 688-693.

Cover, T. M. (1991). Elements of information theory, New York :: Wiley.

Cutsem, T. V. (1998). Voltage stability of electric power systems. Boston, Mass. :: Kluwer Academic Publishers.

Dahlgren, R. W. (1994). Dynamic mechanisms of power system instability. Paper presented at the Northcon/94 Conference Record.

De Marco, C., & Bergen, A. (1987). A security measure for random load disturbances in nonlinear power system models. *IEEE Transactions on Circuits and Systems, 34*(12), 1546-1557.

de Mello, F. P., & Feltes, J. W. (1996). Voltage oscillatory instability caused by induction motor loads. *IEEE Transactions on Power Systems, 11*(3), 1279-1285.

Dobson, I. (1992). An iterative method to compute a closest saddle node or Hopf bifurcation instability in multidimensional parameter space. Paper presented at 1992 IEEE International Symposium on Circuits and Systems, 1992. the Proceedings ISCAS '92.

Dobson, I., & Lu, L. (1993). New methods for computing a closest saddle node bifurcation and worst case load power margin for voltage collapse. *IEEE Transactions on Power Systems, 8*(3), 905-913.

El-Kateb, M. M., Abdelkader, S., & Kandil, M. S. (1997). Linear indicator for voltage collapse in power systems. *IEE P roceedings-Generation, Transmission and Distribution,144*(2), 139-146.

Farsangi, M. M., Nezamabadi-pour, H., Yong-Hua, S., & Lee, K. Y. (2007). Placement of SVCs and Selection of Stabilizing Signals in Power Systems. *IEEE Transactions on Power Systems, 22*(3), 1061-1071.

Gao, B., Morison, G. K., & Kundur, P. (1992). Voltage stability evaluation using modal analysis. *IEEE Transactions on Power Systems, 7*(4), 1529-1542.

Haesen, E., Bastiaensen, C., Driesen, J., & Belmans, R. (2009). A Probabilistic Formulation of Load Margins in Power Systems With Stochastic Generation. *IEEE Transactions on Power Systems, 24*(2), 951-958.

Hatziargyriou, N. D., & Karakatsanis, T. S. (1998). Probabilistic load flow for assessment of voltage instability. *IEE Proceedings-Generation, Transmission and Distribution,145*(2), 196-202.

Hogg, R. V. (1983). Probability and statistical inference (2nd ed. ed.). New York : London :: Macmillan ; Collier Macmillan.

Hong, Y.-H., Pan, C.-T., & Lin, W.-W. (1997). Fast calculation of a voltage stability index of power systems. *IEEE Transactions on Power Systems, 12*(4), 1555-1560.

Hwachang, S., Byongjun, L., Sae-Hyuk, K., & Ajjarapu, V. (2003). Reactive reserve-based contingency constrained optimal power flow (RCCOPF) for enhancement of voltage stability margins. *IEEE T ransactions on Power Systems, 18*(4), 1538-1546.

Iba, K., Suzuki, H., Egawa, M., & Watanabe, T. (1990). A method for finding a pair of multiple load flow solutions in bulk power systems. *IEEE Transactions on Power Systems, 5*(2), 582-591.

Iba, K., Suzuki, H., Egawa, M., & Watanabe, T. (1991). Calculation of critical loading condition with nose curve using homotopy continuation method. *IEEE Transactions on Power Systems, 6*(2), 584-593.

Indulkar, C. S., & Viswanathan, B. (1983). Deterministic and Probabilistic Approach to Voltage Stability of Series-Compensated EHV Transmission Lines. *IEEE T ransactions on P ower A pparatus and Sy stems, PAS-102*(7), 2317-2322.

Irisarri, G. D., Wang, X., Tong, J., & Mokhtari, S. (1997). Maximum loadability of power systems using interior point nonlinear optimization method. *IEEE Transactions on Power Systems, 12*(1), 162-172.

Karlsson, D., & Hill, D. J. (1994). Modelling and identification of nonlinear dynamic loads in power systems. *IEEE Transactions on Power Systems, 9*(1), 157-166.

Kataoka, Y. (2003). A probabilistic nodal loading model and worst case solutions for electric power system voltage stability assessment. *IEEE Transactions on Power Systems, 18*(4), 1507-1514.

Kessel, P., & Glavitsch, H. (1986). Estimating the Voltage Stability of a Power System. *IEEE Transactions on Power Delivery, 1*(3), 346-354.

Kundur, P. (1994). *Power system stability and control*. New York :: McGraw-Hill.

Kundur, P., Paserba, J., Ajjarapu, V., Andersson, G., Bose, A., Canizares, C., et al. (2004). Definition and classification of power system stability IEEE/CIGRE joint task force on stability terms and definitions. *IEEE Transactions on Power Systems, 19*(3), 1387-1401.

Lee, B. H., & Lee, K. Y. (1993). Dynamic and static voltage stability enhancement of power systems. *IEEE Transactions on Power Systems, 8*(1), 231-238.

Li, S. H., & Chiang, H. D. (2008). Nonlinear predictors and hybrid corrector for fast continuation power flow. *IET Generation, Transmission & Distribution, 2*(3), 341-354.

Liu, C.-W., Chang, C.-S., Jiang, J. A., & Yeh, G. H. (2005). Toward a CPFLOW-based algorithm to compute all the type-1 load-flow solutions in electric power systems. *IEEE Transactions on Circuits and Sy stems I : R egular Papers, 52*(3), 625-630.

Liu, M., Cheng, J., & Cheng, Y. (1999). Dynamic voltage stability analysis of parallel AC/DC power systems. *Dianli X itong Z idonghua/Automation of Electric Power Systems, 23*(16), 27-30.

Lof, P. A., Andersson, G., & Hill, D. J. (1993). Voltage stability indices for stressed power systems. *IEEE Transactions on Power Systems, 8*(1), 326-335.

Lof, P. A., Smed, T., Andersson, G., & Hill, D. J. (1992). Fast calculation of a voltage stability index. *IEEE Transactions on Power Systems, 7*(1), 54-64.

Lu, J., Liu, C.-W., & Thorp, J. S. (1995). New methods for computing a saddle-node bifurcation point for voltage stability analysis. *IEEE Transactions on Power Systems, 10*(2), 978-989.

Ma, W., & Thorp, J. S. (1993). An efficient algorithm to locate all the load flow solutions. *IEEE Transactions on Power Systems, 8*(3), 1077-1083.

Makarov, Y. V., Maslennikov, V. A., & Hill, D. J. (1996). Revealing loads having the biggest influence on power system small disturbance stability. *IEEE Transactions on Power Systems, 11*(4), 2018-2023.

Menezes, T. V., da Silva, L. C. P., Affonso, C. M., & da Costa, V. F. (2004). MVAR management on the pre-dispatch problem for improving voltage stability

margin, *IEE Proceedings- Generation, Transmission and D istribution,* Vol. 151, pp. 665-672.

Mohammad-Djafari, A. A Matlab Program to Calculate the Maximum Entropy Distributions,2001. from http://publicationslist.org/djafari

Momoh, J. A., Makarov, Y. V., & Mittelstadt, W. (1999). A framework of voltage stability assessment in power system reliability analysis. *IEEE Transactions on Power Systems, 14*(2), 484-491.

Mori, H., & Iizuka, F. (1998). An efficient method for calculating power flow solutions and the closest bifurcation point using mathematical programming. Paper presented at ISCAS '98. the Proceedings of the 1998 IEEE International Symposium on Circuits and Systems, 1998.

Mori, H., & Yamada, S. (2002). Continuation power flow with the nonlinear predictor of the Lagrange's polynomial interpolation formula. Paper presented at the Transmission and Distribution Conference and Exhibition 2002: Asia Pacific. IEEE/PES.

Morison, G. K., Gao, B., & Kundur, P. (1993). Voltage stability analysis using static and dynamic approaches. *IEEE Transactions on Power Systems, 8*(3), 1159-1171.

Musirin, I., & Rahman, T. K. A. (2002). Estimating maximum loadability for weak bus identification using FVSI. *IEEE Power Engineering Review, 22*(11), 50-52.

Nagao, T., Tanaka, K., & Takenaka, K. (1997). Development of static and simulation programs for voltage stability studies of bulk power system. *IEEE Transactions on Power Systems, 12*(1), 273-281.

Nam, H. K., Song, C. G., Kim, D. J., Moon, Y. H., & Lee, K. Y. (1999). *A n ew efficient u nified s trategy to c ompute v oltage c ollapse point and v oltage stability e nhancement b y ge neration s hift.* Paper presented at the Power Engineering Society 1999 Winter Meeting, IEEE.

Nwankpa, C. O., & Hassan, R. M. (1993). A stochastic based voltage collapse indicator. *IEEE Transactions on Power Systems, 8*(3), 1187-1194.

Obadina, O. O., & Berg, G. J. (1988). Determination of voltage stability limit in multimachine power systems. *IEEE Transactions on Power Systems, 3*(4), 1545-1554.

Obadina, O. O., & Berg, G. J. (1990). Identifying electrically weak and strong segments of a power system from a voltage stability viewpoint. *IEE Proceedings, Part C : Generation, Transmission and Distribution, 137* (3), 205-212.

Pai, M. A., Sauer, P. W., Lesieutre, B. C., & Adapa, R. (1995). Structural stability in power systems-effect of load models. *IEEE Transactions on Power Systems, 10*(2), 609-615.

Palmer, E. W., & Ledwich, G. (1996). Optimal placement of angle transducers in power systems. *IEEE Transactions on Power Systems, 11*(2), 788-793.

Papoulis, A. (2002). Probability, random variables, and stochastic processes (4th ed. ed.). New York ; Boston :: McGraw-Hill.

Parker, C. J., Morrison, I. F., & Sutanto, D. (1996). Application of an optimisation method for determining the reactive margin from voltage collapse in reactive power planning. *IEEE Transactions on Power Systems, 11*(3), 1473-1481.

Radman, G., Pama, A., Powell, J., & Gao, D. (2007). Dynamic Voltage Stability Improvement using coordinated control of dynamic VAR-sources. Paper presented at the Bulk Power System Dynamics and Control - VII. Revitalizing Operational Reliability, 2007 iREP Symposium.

Rajagopalan, C., Lesieutre, B. C., Sauer, P. W., & Pai, M. A. (1992). Dynamic aspects of voltage/power characteristics [multimachine power systems]. *IEEE Transactions on Power Systems, 7*(3), 990-1000.

Ross, S. M. (1993). Introduction to probability models (5th ed. ed.). Boston :: Academic Press.

Sauer, P. W., & Pai, M. A. (1990). Power system steady-state stability and the load-flow Jacobian. *IEEE Transactions on Power Systems, 5*(4), 1374-1383.

Sauer;, P. W., & Pai, M. A. (1998). Power system dynamics and stability. Upper Saddle River, N.J. :: Prentice Hall.

Schellenberg, A., Rosehart, W., & Aguado, J. A. (2006). Cumulant-based stochastic nonlinear programming for variance constrained voltage stability analysis of power systems. *IEEE Transactions on Power Systems, 21*(2), 579-585.

Sharaf, T. A. M., & Berg, G. J. (1991). Probabilistic voltage stability indexes. *IEE Proceedings-Generation, Transmission and Distribution, IEE Proceedings-C, 138*(6), 499-504.

Smon, I., Verbic, G., & Gubina, F. (2006). Local voltage-stability index using tellegen's Theorem. *IEEE Transactions on Power Systems, 21*(3), 1267-1275.

Sobierajski, M., & Fulczyk, M. (2004). Voltage stability study by p-q curve with rectangular probability distribution of bus load. Paper presented at the International Conference on Probabilistic Methods Applied to Power Systems, 2004.

Song, H., Lee, B., & Moon, Y. H. (2005). Reactive optimal power flow incorporating margin enhancement constraints with nonlinear interior point method. *IEE P roceedings-Generation, T ransmission and D istribution, 152*(6), 961-968.

Su, Y. C., Cheng, S. J., Wen, J. Y., & Zhang, J. (2006). Power system dynamic stability analysis and stability type discrimination, Proceedings of the 41st International Universities Power Engineering Conference, Piscataway, NJ, USA.

Tamura, Y., Mori, H., & Iwamoto, S. (1983). Relationship Between Voltage Instability and Multiple Load FLow Solutions in Electric Power Systems. *IEEE Transactions on P ower A pparatus and Sy stems, P AS-102*(5), 1115-1125.

Tamura, Y., Sakamoto, K., & Tayama, Y. (1988). Voltage instability proximity index (VIPI) based on multiple load flow solutions in ill-conditioned power systems. Paper presented at the Proceedings of the 27th IEEE Conference on Decision and Control, 1988.

Taylor, C. W. (1994). Power system voltage stability. New York :: McGraw-Hill.

Thukaram, D., Jenkins, L., & Visakha, K. (2006). Optimum allocation of reactive power for voltage stability improvement in AC-DC power systems. *IEE Proceedings: Generation, Transmission and Distribution, 153*(2), 237-246.

Tiranuchit, A., & Thomas, R. J. (1988). A posturing strategy against voltage instabilities in electric power systems. *IEEE Transactions on Power Systems, 3*(1), 87-93.

Tse, C. T., & Tso, S. K. (1988). Approach to the study of small-perturbation stability of multimachine systems. *IEE P roceedings, P art C : G eneration, Transmission and Distribution, 135-C*(5), 396-405.

Tse, C. T., Wang, K. W., Chung, C. Y., & Tsang, K. M. (2000). Parameter optimization of robust power system stabilizers by probabilistic approach. *IEE Proceedings: Generation, Transmission and Distribution, 147*(2), 69-75.

Tse, C. T., Wang, K. W., Chung, C. Y., & Tsang, K. M. (2001). Robust PSS design by probabilistic eigenvalue sensitivity analysis. *Electric P ower S ystems Research, 59*(1), 47-54.

Van Cutsem, T. (1991). A method to compute reactive power margins with respect to voltage collapse. *IEEE Transactions on Power Systems, 6*(1), 145-156.

Van Cutsem, T., & Mailhot, R. (1997). Validation of a fast voltage stability analysis method on the Hydro-Quebec system. *IEEE Transactions on Power Systems, 12*(1), 282-292.

Van Cutsem, T., Moisse, C., & Mailhot, R. (1999). Determination of secure operating limits with respect to voltage collapse. *IEEE T ransactions on Power Systems, 14*(1), 327-335.

Van Cutsem, T., & Vournas, C. D. (1996). Voltage stability analysis in transient and mid-term time scales. *IEEE Transactions on Power Systems, 11*(1), 146-154.

Vournas, C. D., Pai, M. A., & Sauer, P. W. (1996). The effect of automatic voltage regulation on the bifurcation evolution in power systems. *IEEE Transactions on Power Systems, 11*(4), 1683-1688.

Vu, K., Begovic, M. M., Novosel, D., & Saha, M. M. (1999). Use of local measurements to estimate voltage-stability margin. *IEEE Transactions on Power Systems, 14*(3), 1029-1035.

Wang, K. W., Tse, C. T., & Tsang, K. M. (1998). Algorithm for power system dynamic stability studies taking account the variation of load power, *Electric Power Systems Research*, 46(3), 1998, pp. 221-227.

Wang, K. W. (2000). Robust PSS design based on probabilistic approach. Hong Kong :: Dept. of Electrical Engineering, The Hong Kong Polytechnic University.

Wang, K. W., Chung, C. Y., Tse, C. T., & Tsang, K. M. (1998). Optimum location of power system stabilizers based on probabilistic analysis. Paper presented at the International Conference on Power System Technology, 1998. Proceedings. POWERCON '98.

Wang, K. W., Chung, C. Y., Tse, C. T., & Tsang, K. M. (2000a). Improved probabilistic method for power system dynamic stability studies. *IEE Proceedings-Generation, Transmission and Distribution, 147*(1), 37-43.

Wang, K. W., Chung, C. Y., Tse, C. T., & Tsang, K. M. (2000b). Improved probabilistic method for power system dynamic stability studies. *IEE Proceedings: Generation, Transmission and Distribution, 147*(1), 37-43.

Wang, K. W., Chung, C. Y., Tse, C. T., & Tsang, K. M. (2000c). Multimachine eigenvalue sensitivities of power system parameters. *IEEE Transactions on Power Systems, 15*(2), 741-747.

Wang, K. W., Chung, C. Y., Tse, C. T., & Tsang, K. M. (2001). Probabilistic eigenvalue sensitivity indices for robust PSS site selection. *IEE Proceedings-Generation, Transmission and Distribution, 148*(6), 603-609.

Wang, K. W., Tse, C. T., & Tsang, K. M. (1998). Algorithm for power system dynamic stability studies taking account of the variation of load power. *Electric Power Systems Research, 46*(3), 221-227.

Wen, X., & Ajjarapu, V. (2006). Application of a novel eigenvalue trajectory tracing method to identify both oscillatory stability margin and damping margin. *IEEE Transactions on Power Systems, 21*(2), 817-824.

Xu, W., & Mansour, Y. (1994). Voltage stability analysis using generic dynamic load models. *IEEE Transactions on Power Systems, 9*(1), 479-493.

Yorino, N., Harada, S., & Cheng, H. (1997). A method to approximate a closest loadability limit using multiple load flow solutions. *IEEE Transactions on Power Systems, 12*(1), 424-429.

Yu, Y.-n. (1983). *Electric power system dynamics*. New York :: Academic Press.

Zarate, L. A. L., Castro, C. A., Ramos, J. L. M., & Ramos, E. R. (2006). Fast computation of voltage stability security margins using nonlinear programming techniques. *IEEE Transactions on Power Systems, 21*(1), 19-27.

Zellner, A., & Highfield, R. A. (1988). Calculation of maximum entropy distributions and approximation of marginalposterior distributions. *Journal of Econometrics, 37*(2), 195-209.

Zeng, Y. G., Berizzi, G., & Marannino, P. (1997). *Voltage s tability a nalysis considering dynamic load model.* Paper presented at the Fourth International Conference on Advances in Power System Control, Operation and Management, 1997. APSCOM-97. (Conf. Publ. No. 450).

Zhou, Y., & Ajjarapu, V. (2005). A Fast Algorithm for Identification and Tracing of Voltage and Oscillatory Stability Margin Boundaries. *Proceedings of t he IEEE, 93*(5), 934-946.